

**THE ACTIVATION VOLUME
FOR DIFFUSION
IN AMORPHOUS Pd₄₀Ni₄₀P₂₀
-A FREE VOLUME TREATMENT-**

Gerard Ruitenberg

**Coordinator: Prof. Dr. Ir. A. van den Beukel
Supervisor: Dr. Ir. J. Sietsma**

**Delft UT
Delft, 28 February 1997**

CONTENTS

	Preface	1
I	Introduction	2
II	The Amorphous Structure and Diffusion	4
	2.1 historical retrospect	4
	2.2 production techniques	4
	2.3 why applications remained limited up to date	5
	2.4 investigating diffusion in amorphous metals	5
	2.5 how to detect amorphicity	5
	2.6 the radial distribution function	6
	2.7 the equilibrium structure	7
	2.8 defects	7
	2.9 vibrational modes	8
III	Theory of Diffusion	10
	3.1 Boltzmann Statistics	10
	3.2 migration and formation	11
	3.3 the Keyes relation	12
	3.4 free volume theory	13
IV	Determining the Pressure Dependence of Free Volume	16
	4.1 introduction	16
	4.2 how to determine x at the end of a pressure anneal	17
	4.3 experimental	17
	4.4 results	18
	4.5 discussion	19
V	The Implications for the Diffusion Process	21
	5.1 the results concerning diffusion put together	21
	5.2 checking the Keyes relation	21
	5.3 discussing the defect size	22
	5.4 which entities are diffusing?	23
	5.5 conclusions	23
VI	The Concentration Distribution of Collective Defects	24
	6.1 introduction	24
	6.2 an exact expression for $c_n(z_c)$ in integral form	25
	6.3 an exact expression for $c_n(z_c)$ as a summation	26
	6.4 the Taylor approximation	27
	6.5 characteristics of the exact solution	27
	6.6 the Gaussian approximation of $c_n(z_c)$	29
	6.7 discussion	29
	References	31

PREFACE

This master thesis is a report of the work that I have done as a student of Materials Science at Delft University of Technology, in the Physical Materials Science group of Prof.Dr.Ir. A. Van den Beukel. The project was supervised by Dr.Ir. J. Sietsma.

The DSC measurements I have performed at the "Max-Planck-Institut für Metallforschung, Institut für Werkstoffwissenschaft" in Stuttgart, Germany. The measurements were supervised by Prof.Dr. F. Sommer.

The pressure anneals on one of the two Pd₄₀Ni₄₀P₂₀ batches were performed by Dipl.Ing. P. Klugkist, under supervision of Prof.Dr. F. Faupel and Dr. K. Rätzke at the University of Kiel, Germany.

There are several ways of putting the results of our research in a scientific context. From a minimalistic point of view, we have made it plausible that the equilibrium structure of Pd₄₀Ni₄₀P₂₀ depends on pressure. And for scientists who do not believe in free volume theory, this is the only interesting result from our research. What we shall do here, is to take some earlier results from free volume theory and make a few assumptions to be able to work with them. We then obtain our numerical result and take the remarkable internal consistency of the theory as a justification for our approach. All this is entirely in the spirit of the way we work at this laboratory.

I INTRODUCTION

The reason for measuring the activation volume of diffusion is that we hope it will teach us something about the mechanism of diffusion in amorphous metals. The measurements are performed on amorphous $\text{Pd}_{40}\text{Ni}_{40}\text{P}_{20}$, which is a 80-20 metal-metalloid system. This alloy has over the past decennium served as a model system. It was chosen because its amorphous state can reach meta-stable equilibrium.

There are still some important unsolved problems concerning the mechanism of diffusion in amorphous metals. In particular, there is still some controversy over the question whether diffusion occurs via a single-atom hopping process or via some cooperative mechanism. The latter possibility seems increasingly probable as research continues. The strongest indication for cooperative diffusion is given by the results of the isotope effect measurements. Rätzke et al. [1] showed that typically 10-30 atoms participate in diffusion in the well-relaxed state. The measurements were performed for Co-diffusion in amorphous $\text{Co}_{77}\text{Fe}_2\text{Nb}_{14}\text{B}_7$.

Besides distinguishing between a single-atom and a cooperative mechanism for diffusion, there is yet another classification to be made. When diffusion is mediated through defects, the mechanism is called indirect (e.g. vacancy diffusion in a crystal), whereas the mechanism is called direct when diffusion occurs without the presence of a defect (e.g. diffusion in a liquid at temperatures not too close to the melting point). Up to now, there is no direct experimental evidence for the existence of diffusion defects. The question whether the mechanism of diffusion in amorphous metals is direct or indirect is not yet answered and often not even asked.

The ultimate goal we are trying to achieve is to understand the mechanism of diffusion in amorphous metals and to find an expression for the diffusivity that matches the experimental diffusion data qualitatively. This report is set up in such a way as to emphasize the importance of the results with respect to the goal mentioned above.

In Chapter II, a few important issues are mentioned as background information. A basic idea is given of what the amorphous structure looks like, which is essential for understanding what is happening in an amorphous metal at an atomic level. Some important results obtained from experiment and computer simulation are given.

In Chapter III, all we need to know about the theoretical background is given. The analogy between the equations for diffusion in amorphous and crystalline materials is emphasized by the set-up of the chapter. This is done for the sake of clarity. Unfortunately, this clear analogy inevitably entails the danger of encouraging people to think of crystals when talking about amorphous metals. So be it.

Chapter IV is a report of the measurements that were performed in order to determine the pressure dependence of the free volume. As far as we know, this is the first time ever that this is measured. To account for the fact that this result has importance for the amorphous structure and its relaxation behavior, it is not placed within the scope of diffusion until the next chapter.

Chapter V: in this chapter, several aspects of the pressure dependence of diffusion in amorphous $\text{Pd}_{40}\text{Ni}_{40}\text{P}_{20}$ are discussed in terms of activation volumes. An assessment is made of what the results of Chapter IV, together with a previous result from our group, tell us about the mechanism of diffusion in amorphous $\text{Pd}_{40}\text{Ni}_{40}\text{P}_{20}$.

In Chapter VI, a new type of defect is defined; we shall call these defects *collective defects*. Using the free volume model introduced in Chapter III, we can calculate the concentration of these defects as a function of their size, for any given value of the average free volume. This calculation can be seen as the first step on the way of finding a quantitative description of cooperative diffusion in amorphous metals.

II THE AMORPHOUS STRUCTURE AND DIFFUSION

2.1 Historical Retrospect

The concept of an amorphous structure is nothing new. Many a modern day physicist, materials scientist or chemist would probably know that ordinary liquids, window pane glass, Wedgewood porcelain and many plastics have an amorphous structure. And when we look back at the physics community before Bragg and Von Laue entered the stage, we find that many physicists actually believed that ordinary metals and alloys had an amorphous structure. Since then, diffraction techniques have established the periodicity of the atomic structure of metals. This periodicity, or translation symmetry, has now become a key ingredient in many a physical description of metals. The notions of a vacancy, dislocation as well as Bloch's theorem are all based on the regular lattice and its periodicity.

Seen from this perspective, it is quite understandable that the discovery of amorphous metals in 1959 [2] came quite as a surprise; amorphous metals almost sounded like a contradiction in terms. Furthermore, it added to the surprise that these amorphous metals resembled their crystalline counterparts in many physical properties. This pointed out that these properties were not so much determined by the periodicity of the structure as anybody brought up with crystals would assume.

2.2 Production Techniques

The technique, that was first used to obtain metals with an amorphous structure is splat-quenching [2]; a droplet of liquid metal is splat between two surfaces and thus cooled from the melting point to room temperature in a fraction of a second.

What normally happens, when we cool the liquid below its melting point at ordinary cooling rates is that, after a certain incubation time, small crystalline nuclei start to form at a rate mainly determined by the undercooling. Some of these nuclei then grow to become crystallites. When the surfaces of the crystallites meet, a boundary is formed. This process is finished when all liquid has crystallized, leaving behind a polycrystal consisting of crystalline grains, separated by so-called grain boundaries. The size of the grains decreases with increasing cooling rate. For metals that can be made amorphous, there exists an experimentally attainable critical cooling rate above which no crystallites are formed and the liquid structure is quenched-in, so to speak. These metals can be cooled from their melting points to a temperature at which atomic mobility is too low to form nuclei, in a time shorter than the nucleation time. It is emphasized, that the structure of an amorphous metal is not just that of a polycrystal with very small grains.

The technique that is nowadays most commonly used for making amorphous metals is melt spinning. Although similar to splat-quenching from a physical point of view, the method is experimentally rather more elegant. The technique makes use of a copper wheel (typical diameter 200 mm), rotating at high speed (typical surface speed: 40 ms^{-1}). In a small crucible above the wheel, metal is melted with induction heating and a continuous stream of liquid metal flows on the wheel. The metal then rapidly solidifies (achievable cooling rates up to 10^6 Ks^{-1}) and is thrown off the wheel in the form of a thin ribbon (typically 2-20 mm wide and 10-40 μm thick). One of the advantages of the technique is, that it is continuous in principle.

From a theoretical point of view, the solid state amorphisation reaction (discovered in 1975) [3], is interesting too. It was found that, under certain conditions, crystalline metal films could transform into a homogeneous amorphous structure by solid state diffusion.

Other techniques that can produce amorphous materials are ball milling, vapour deposition and particle or laser irradiation.

2.3 Why Applications Remained Limited up to Date

Shortly after their discovery, when the good news about some of their properties got through, amorphous metals were thought to have a very promising career as an engineering material. Amorphous alloys have, however, always remained very costly. Furthermore, synthesis of amorphous bulk material has only recently become possible. And unfortunately, the alloys that have critical cooling rates low enough to allow the synthesis of bulk material are even more expensive.

2.4 Investigating Diffusion in Amorphous Metals

Amorphous metals seem to be more interesting for research than for practical application. Amongst the most intriguing aspects of amorphous metals are: their atomic structure itself in a thermodynamical context, their phonon spectrum, their specific heat at cryogenic temperatures and the implications of the fact that some of them display superconductivity.

Together with creep, viscous flow and structural relaxation, diffusion is one of the processes of which the atomic mechanism is still under investigation. And despite many years of rather intensive research, progress is made only slowly. From a practical point of view, problems first arise due to the experimental difficulties that one faces when measuring a diffusion coefficient: the process is very slow and the uncertainty in the measurements relatively high. Furthermore, the importance of many previous results has been shown to be somewhat limited, since the effect of structural relaxation was not accounted for in the early days of research.

The main reason for measuring the pressure dependence of diffusion is that we hope that the activation volume will tell us something about the mechanism of diffusion. What it exactly tells us is not really obvious, when it comes to amorphous metals. Hence, we have attempted to explain this very carefully (see Chapters III and V).

Now, before developing the theoretical background needed for a proper understanding of what we are trying to measure, we shall first have a close look at the amorphous structure. The reason for this is that some notions or arguments later to be used may be better appreciated when one has some feeling for the amorphous structure.

2.5 How to Detect Amorphicity

Suppose we have a sample of some alloy; how do we know it is (still) amorphous? A rather obvious method is to directly check if long range order exists within the atomic structure of the sample, using X-ray diffraction. And so it is done in practice: the Debije-Scherrer technique is the most commonly used method for checking whether a metallic structure is

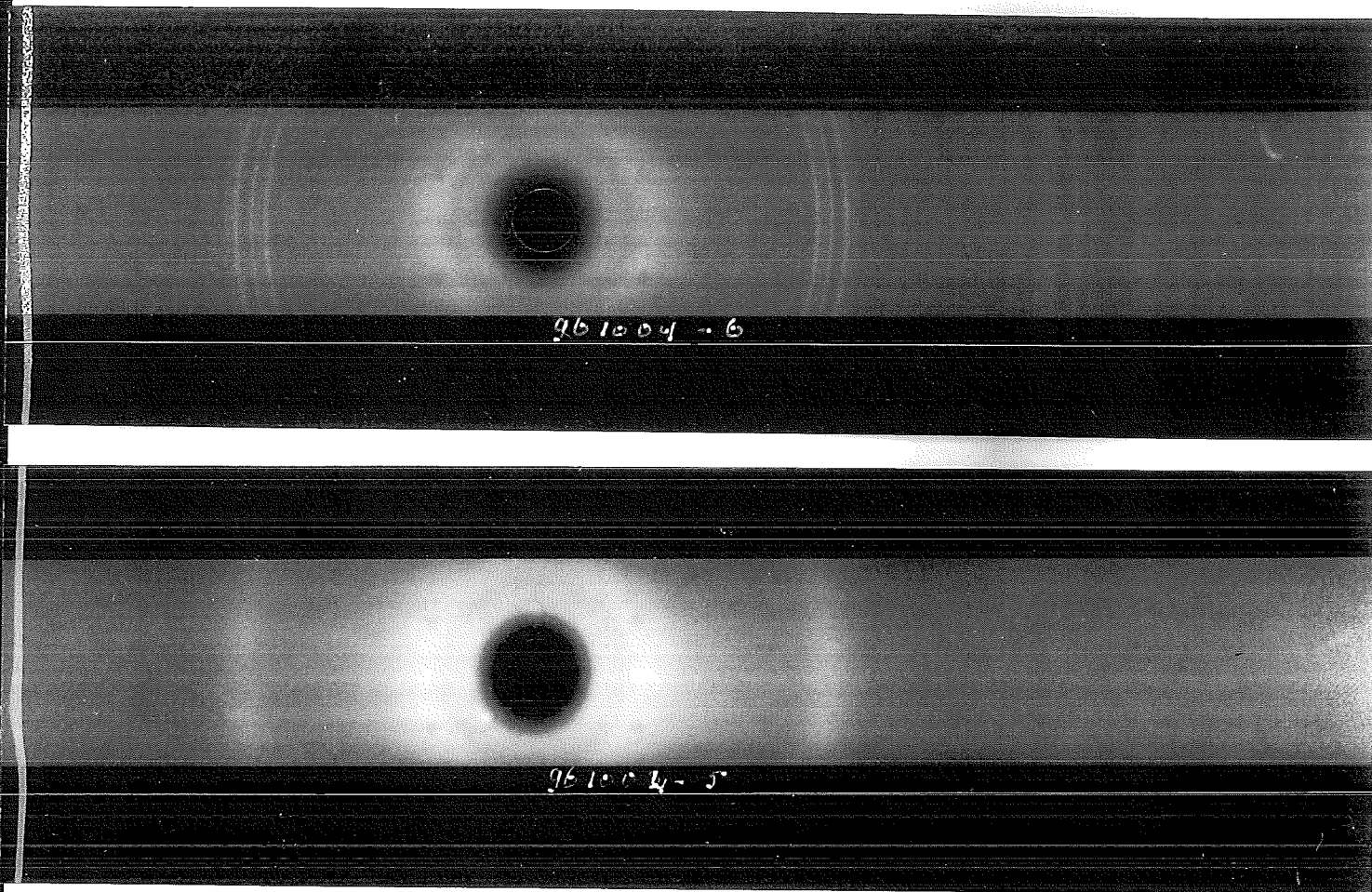


Figure 1: Debye-Scherrer recordings of: a) crystalline and b) amorphous Pd₄₀Ni₄₀P₂₀.

amorphous. In figure 1, two of such recordings are shown: one for crystalline and one for amorphous Pd₄₀Ni₄₀P₂₀. The sharp lines in figure 1 a) indicate the presence of a crystalline phase. With this technique, a crystalline phase can only be detected when it makes up at least 5% of the structure. Note, that there may be several crystalline phases present, each adding a set of lines to the pattern.

When diffraction patterns would be made of a crystallising amorphous structure, the patterns would resemble figure 1 b) at the start of crystallisation and figure 1 a) when the process has finished. Of course, any intermediary pattern can occur, depending on the fraction of the material that has crystallised.

For a polycrystalline material, a decreasing grain size broadens the diffraction lines only slightly. Hence, in practice, all diffraction patterns with a crystalline fraction exceeding 5% show lines as sharp as in figure 1 a).

Crystallisation of an amorphous alloy normally starts at the surface of the sample. Hence, we can use surface techniques such as glancing-angle X-ray diffraction to see whether or not our amorphous sample has crystallised.

2.6 The Radial Distribution Function

The importance of diffraction with respect to the amorphous structure goes far beyond checking whether or not crystallization has occurred. From a diffraction pattern, we can quantify the short range order that exists in the structure and present it in the form of a radial distribution function (sometimes also called the "pair correlation function"), denoted RDF. We will show how this is done for a monatomic structure (Ge, for instance, can be made amorphous), by presenting the essential ideas without mathematical rigour (for a rather more detailed treatment see [4]).

From a diffraction pattern, we obtain the intensity I of the scattered radiation as a function of K , the magnitude of the difference between the wave vectors of the incoming and outgoing beams, \mathbf{k} and \mathbf{k}' : $K \equiv |\mathbf{k} - \mathbf{k}'|$.

We represent the intensity in a normalised form, as a *structure factor*, defined by:

$$S(K) \equiv I(K) / Nf^2 \quad (1)$$

for a monatomic structure containing N atoms. The atomic form factor f , is a measure of the scattering power of the atom under view.

Now, we define the radial distribution function $g(r)$ as:

$$g(r) \equiv \rho(r) / \rho_0 \quad (2)$$

where $\rho(r)$ is the average density of all spherical shells of thickness dr at radius r around the N atoms in the structure; ρ_0 is the macroscopic density of the sample. Hence, $g(r)$ is a statistical measure for the number of atoms we find at a distance r from the centre of certain atom, picked at random.

From diffraction theory it can be shown for an isotropic material that $S(K)$ depends on $g(r)$ in the following manner:

$$S(K) = 1 + 4\pi\rho_0 \int_0^{\infty} (g(r) - 1) r^2 \frac{\sin(Kr)}{Kr} dr \quad (3)$$

Or, reversely, using the Fourier integral theorem, we can write:

$$g(r) = 1 + \frac{1}{2\pi^2\rho_0 r} \int (S(K) - 1) K \sin(Kr) dK \quad (4)$$

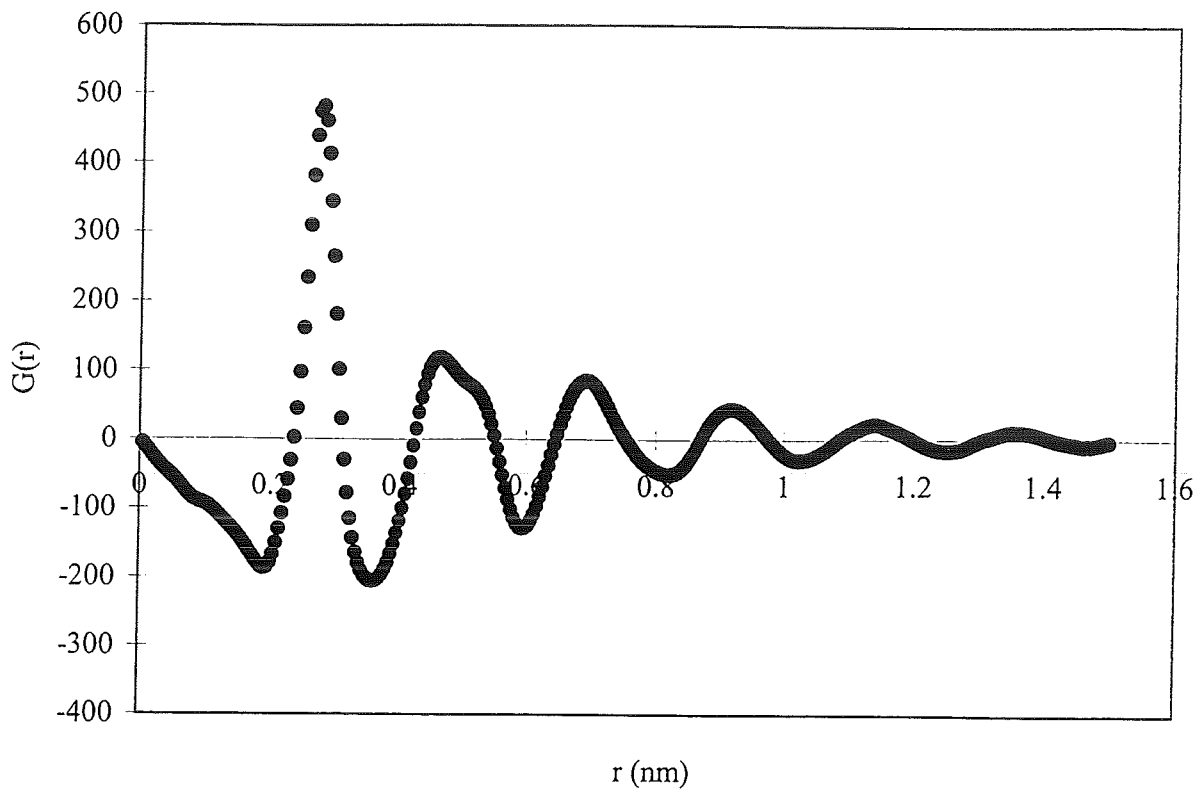


Figure 2: Reduced Radial Distribution Function of amorphous $\text{Pd}_{40}\text{Ni}_{40}\text{P}_{20}$, taken from [5].

Here, we have the expression for the RDF as a function of the experimentally accessible structure factor. Common diffraction techniques for determining the structure factor are X-ray and neutron diffraction. In figure 2, an example of an RDF is shown for Pd₄₀Ni₄₀P₂₀. The topological short range order (TSRO) is visualised very neatly in this representation. Note that an RDF only provides us with statistical information about the average atom; this is a reflection of the statistical nature of TSRO in an amorphous metal.

If one is interested in the *chemical* short range order (CSRO) of the elements of some alloy, one could select any pair of chemical elements and look at their radial distribution function (in the case of Pd₄₀Ni₄₀P₂₀, one of the things this would tell us, is that P atoms only have Ni and Pd atoms as nearest neighbours). In this work, we will not look at CSRO.

The validity of the derivation can easily be adjusted to cover crystals by incorporating the diffraction condition $\mathbf{k}-\mathbf{k}'=\mathbf{G}$ (which is completely equivalent to the Bragg condition and the Von Laue equations), with \mathbf{G} the reciprocal lattice vector. With the diffraction condition, the translation symmetry of the crystal enters the scene. The presence of a translation symmetry means that all atoms in the structure have a sparsely defined coordination of nearest neighbours. As a result, the RDF for crystals does not just give statistical information about the average atom, but uniquely tells us the integer number of atoms that we will find at very sharply defined values for r . At 0 K, the RDF for a single-crystal would consist of delta function peaks, broadened at higher temperatures by the thermal vibration only. Since, for a crystal, the unit cell directly finds its way into the structure factor (see ref. [4]), the radial distribution functions are, as a description of the crystal, completely equivalent to the unit cell with its periodic lattice.

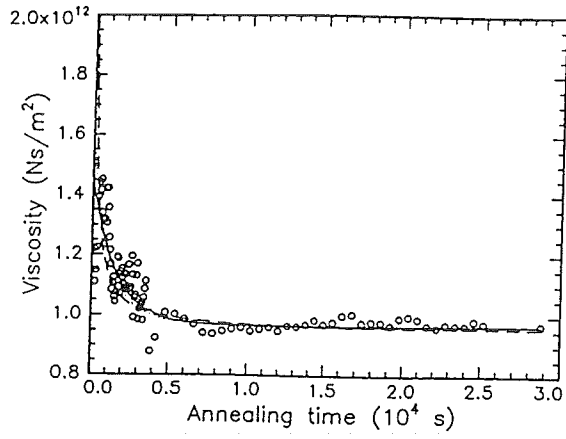
The change in perspective is brought about by the Fourier transform, when we translate our information from reciprocal space to a radial view of real space.

2.7 The Equilibrium Structure

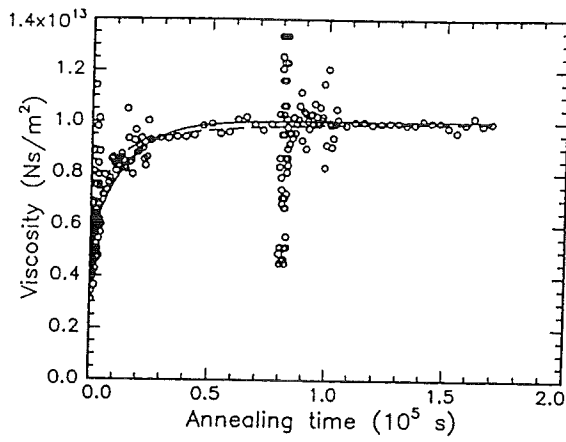
After preparation, the structure of most amorphous metals is kinetically stable at room temperature. That is to say, atomic migration is negligible on any time scale of interest. Only very few amorphous alloys have been shown to reach a meta-stable equilibrium with respect to temperature. The equilibrium is *meta*-stable, because the crystal is the thermodynamically *stable* structure. Throughout the rest of the text we shall simply refer to this structure as the "equilibrium structure", bearing in mind that this equilibrium is meta-stable. If at all, the equilibrium is reached only in a temperature range of some tens of degrees at most. To be sure that a structure has reached its equilibrium at a certain temperature, one should check that the equilibrium is *reversible*, for any equilibrium should be. If the equilibrium depends on temperature, this can be done by verifying that the state of the structure can be reached from both sides on the temperature scale. Several parameters would, in principle, qualify as a measure for the state of the structure as a function of time and temperature. In figure 3, the viscosity is used to illustrate that Pd₄₀Ni₄₀P₂₀ can reach equilibrium at 563 K.

Since the equilibrium is thermodynamic in nature, and depends on the intensive state variable T , one might expect the equilibrium also to depend on the ambient pressure p , for the ambient pressure is an intensive state variable too. This, we investigated and it turned out that the equilibrium structure indeed depends on pressure like it does on temperature (the results can be found in Chapter IV).

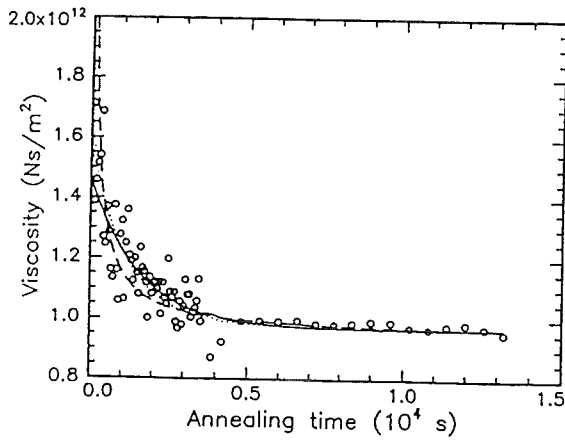
2.8 Defects



(a)



(b)



(c)

Figure 3: The viscosity of amorphous $\text{Pd}_{40}\text{Ni}_{40}\text{P}_{20}$ during temperature cycling between 553 and 563 K. (a) Annealing at 563 K after pre-annealing to equilibrium at 553 K. (b) Subsequent annealing at 553 K. (c) Subsequent annealing at 563 K [6].

2.8.1 Can a vacancy be defined?

The amorphous structure is a surprisingly dense structure, with a mass density comparable to that of crystals. Hence, one might wonder if a vacancy can be defined in this structure. In the absence of a regular lattice, the only starting point seems to be the relatively well-defined number of nearest neighbours that the atoms have. So, what would happen if we were to take one atom from the structure? Would this artificially created "vacancy" be stable? Computer simulations at about 10 K [7] have indicated that the "vacancy" is absorbed in the structure after several jumps. From the finite lifetime of the vacancy, Limoge argued that vacancies might naturally exist in the amorphous structure. We, on the other hand, do not think that the evidence is very conclusive.

But where did the artificially created vacancy go? Is it really gone, in the sense that the macroscopic volume of the sample decreased by one atomic volume after these few jumps? It seems more probable that it just spread out over its neighbours. Hence, we must be aware of the possibility that defects in the amorphous structure are localised at a group of atoms. Note, that such a site of loose packing could be seen as a localized area of low density.

2.8.2 Looking for defects

The obvious method for detecting open spaces in the structure is positron annihilation, because it has been successful in detecting vacancies and determining their concentration. The technique has been used in the past to detect defects (see e.g. [8]), but did not give us any conclusive evidence for their existence.

Recently, a relatively novel technique, the Reverse Monte Carlo (RMC) method, has yielded a remarkable result concerning defects. The RMC method is derived from the standard Monte Carlo (MC) method, which involves random movement of atoms in a box. In an MC simulation, one assumes potential curves for the atoms; the change in the potential energy then determines the probability with which the movement is accepted. In a RMC simulation, not the potential energy of the system is minimized, but the parameter χ^2 , a measure for the deviation of some physical property of the structure from the experimental value (see [9] for a detailed explanation of RMC).

This RMC method was used to construct an amorphous structure for $\text{Pd}_{52}\text{Ni}_{32}\text{P}_{16}$, fitted to an experimentally determined RDF [10]. When looking for open spaces between the atoms, "holes" were found, surrounded by about ten atoms and approximately 5.4 \AA^3 in size. It is argued that these holes may be connected to diffusion [10].

2.9 Vibrational Modes

The vibrational spectrum of the amorphous structure has been investigated using computer simulations. Starting with a structure made with RMC, Molecular Dynamics (MD) is used to analyse the phonon spectrum. Some of the modes of vibration were found to be *localized* and *cooperative*. This vibration could sometimes be seen to result in a "chain-jump" [11,12]. The jump can be said to start sometimes at the first and sometimes at the last atom. The chain does not endlessly travel through the structure in procession; the cooperative mode is lost after the jump.

Very recently, another type of localised cooperative mode was discovered [13]. Some ten atoms, rather spherically arranged, were found to vibrate at a very low frequency. The vibration is *not* simple harmonic (see figure 4). By giving the atoms participating in the

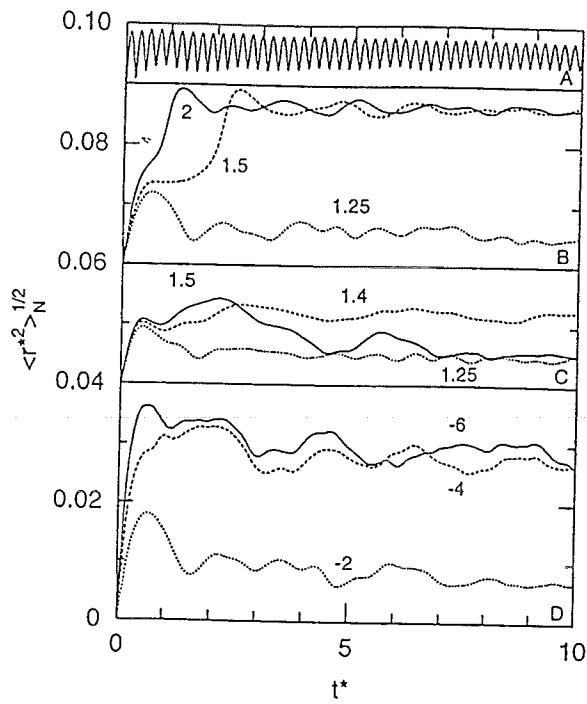


Figure 4: Root mean square displacement of all atoms versus time for the launching of four vibrational modes. A) is a non-localised mode; B), C) and D) are all localized modes. Note that only A) is simple harmonic in good approximation [13].

vibration a "push", at a certain time, in the direction in which they were just moving, the atoms were shown to rearrange (i.e. the equilibrium position around which the atoms vibrate, changes permanently) when the strength of the push exceeded a certain critical value. The mode is kept when the push is not strong enough to initiate a rearrangement, while (as in the case of the chain-jump) the mode is lost after the jump. Hence, the jump is irreversible. The potential energy of the system before and after the jump is kept the same.

It is noted that these simulations correspond to temperatures of the order of 10 K. Hence, it is not at all clear what implications these results have for the mechanism of diffusion at room temperature or near the glass transition temperature. Both the results indicate, however, that diffusion in amorphous metals is probably collective.

III THEORY OF DIFFUSION

3.1 Boltzmann Statistics

For some atomic processes to occur, an energy barrier must be surpassed. For a single event in such a process to take place, the participating atom(s) must have an energy higher than this energy barrier. The distribution of the thermal energies of the atoms in a crystal is given, in good approximation, by the Boltzmann distribution. Thus, we can calculate the fraction of atoms with a thermal energy higher than some critical value. When the energy barrier itself does not depend on temperature (which is normally the case), this fraction is given by:

$$\exp\left(-\frac{\Delta E}{k_B T}\right), \quad (5)$$

where ΔE is the height of the energy barrier and k_B is the Boltzmann constant. These fractions are called Boltzmann factors.

3.1.1 The activation enthalpy

Measured at ambient pressure, the temperature dependence of the diffusivity D is, for crystals, normally found to be Arrhenian over the entire experimentally accessible temperature range. This kind of temperature dependence is given by an Arrhenius equation:

$$D(T) = D_1 \exp\left(-\frac{\Delta H}{k_B T}\right), \quad (6)$$

where D_1 and ΔH are, by definition, constant with respect to temperature. Since it appears in a Boltzmann factor, ΔH must be interpreted as an activation enthalpy for the diffusion process (enthalpy, because ΔH is an energy defined at constant pressure). When $\ln D$ is plotted as a function of $1/k_B T$, the activation enthalpy is equal to the negative slope of this line:

$$\Delta H = -\left[\frac{\partial \ln D}{\partial (1/k_B T)}\right]_p. \quad (7)$$

3.1.2 The activation volume

We now have characterised the mechanism of diffusion by its activation enthalpy ΔH . The mechanism can also be characterised by an activation *volume*, ΔV . It is derived in Appendix A that the activation volume related to the diffusion process is approximated by

$$\Delta V = -k_B T \left[\frac{\partial \ln D}{\partial p}\right]_T, \quad (8)$$

where p is the hydrostatic pressure, defined to be positive. The expression is accurate if the jump distance and the attempt frequency do not depend on pressure. For crystals, these conditions are fulfilled and eqn. (8) gives a good approximation of ΔV . When ΔV is found to be independent of pressure, we can integrate eqn. (8) to obtain the pressure dependence of the diffusivity:

$$D(p) = D_2 \exp\left(-\frac{p\Delta V}{k_B T}\right), \quad (9)$$

where D_2 is independent of pressure. Again, the exponential factor is a Boltzmann factor. For ambient pressure, $\Delta H \ll p\Delta V$, so we may take a result for ΔH that is found at ambient pressure as an approximation for the value at zero pressure, thus putting the pressure dependence into eqn. (9).

3.1.3 The general expression for thermally activated diffusion

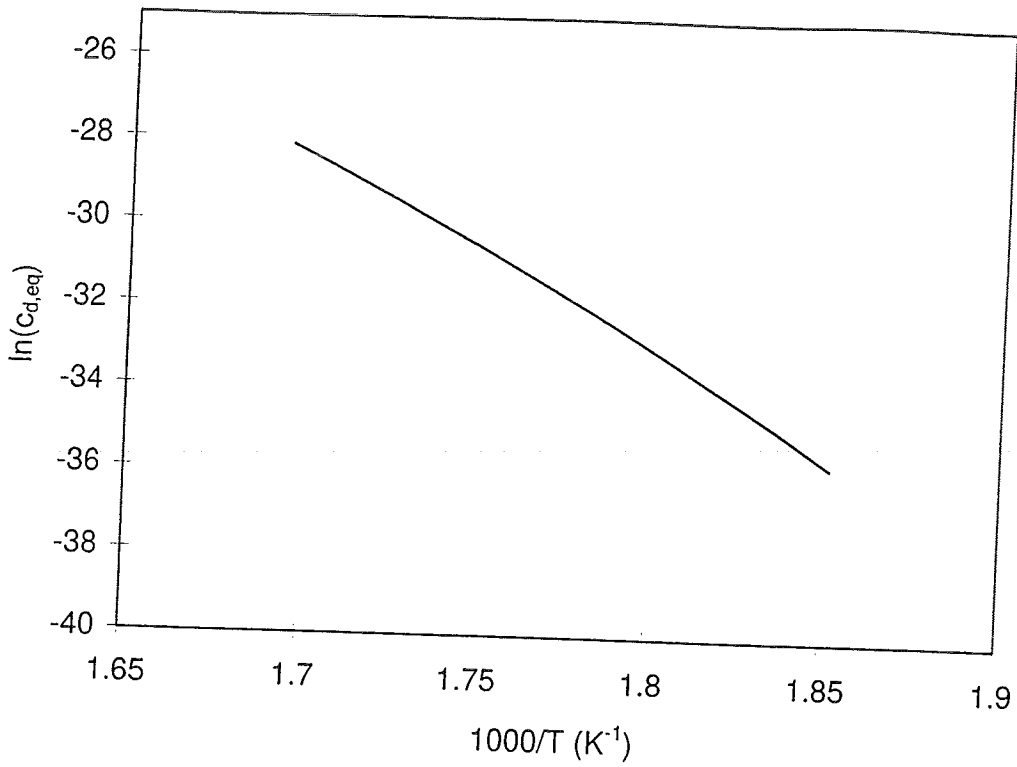


Figure 5: Arrhenius plot of the equilibrium defect concentration in amorphous $Pd_{40}Ni_{40}P_{20}$ for the temperature range over which this material can be shown to reach equilibrium.

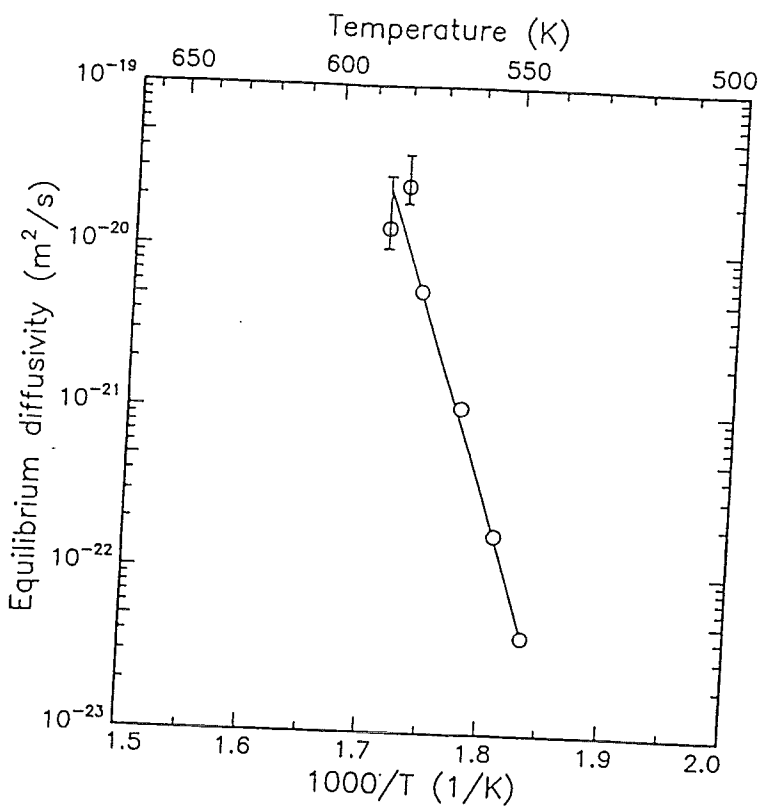


Figure 6: The temperature dependence of the diffusivity of Au in amorphous $Pd_{40}Ni_{40}P_{20}$ in equilibrium [21].

The last parameter to characterise the mechanism of diffusion in the same way as do ΔH and ΔV , is the activation entropy ΔS . The activation entropy enters the Boltzmann factor as $-T\Delta S$. Putting all this together, we get the general expression for thermally activated diffusion:

$$D(p,T) = D_o \exp\left(\frac{\Delta S}{k_B}\right) \exp\left(-\frac{\Delta H}{k_B T}\right) \exp\left(-\frac{p\Delta V}{k_B T}\right). \quad (10)$$

For ambient pressure, $p\Delta V \ll k_B T$ and therefore, the last Boltzmann factor is normally omitted. For crystals it can be shown that $-T\Delta S \ll \Delta H$, so the entropy contribution to the activation energy is negligible.

The pre-exponential factor can be shown to be equal to:

$$D_o = ab\lambda^2 v \quad (11)$$

where a is a geometrical factor, b is a correlation factor, λ is the jump distance and v is the attempt frequency. In principle, λ and v may depend on temperature and pressure, but this can be shown to be a higher order effect, at least for crystals.

3.2 Migration and Formation

For any indirect mechanism of diffusion, the formation as well as the migration of a defect play a role. Hence, the terms ΔS , ΔH and ΔV can all be split according to this criterium. Disregarding the activation entropy, we have for the activation enthalpy:

$$\Delta H = \Delta H_F + \Delta H_M \quad (12)$$

where ΔH_F is the increase of the enthalpy upon the formation of a defect and ΔH_M is the height of the enthalpy barrier for the diffusion step. Hence, we could define a rate factor k :

$$k(T) \equiv v \exp\left(-\frac{\Delta H_M}{k_B T}\right) \quad (13)$$

as a measure of the number of successful jumps per unit time at ambient pressure. The vacancy concentration c_v at ambient pressure is equal to:

$$c_{vac}(T) = \exp\left(-\frac{\Delta H_F}{k_B T}\right). \quad (14)$$

Similarly, we have for the activation volume

$$\Delta V = \Delta V_F + \Delta V_M \quad (15)$$

where ΔV_F corresponds to the change in volume of the system upon the creation of a defect. This is illustrated in figure 7 a) for vacancy diffusion in a crystal. Note that ΔV_F would be negative for an interstitial-type of defect. Now consider the configuration of all atoms participating in a diffusion event, at the moment when the enthalpy of the configuration is at the height of the enthalpy barrier (see figure 7). Then, ΔV_M is the difference in volume of this configuration and the configuration before the jump (i.e. when the configuration is at its enthalpy minimum). This is illustrated in figure 7 b), again for vacancy diffusion in a crystal. Similarly to eqn.s (13) and (14), we have for the rate constant under pressure:

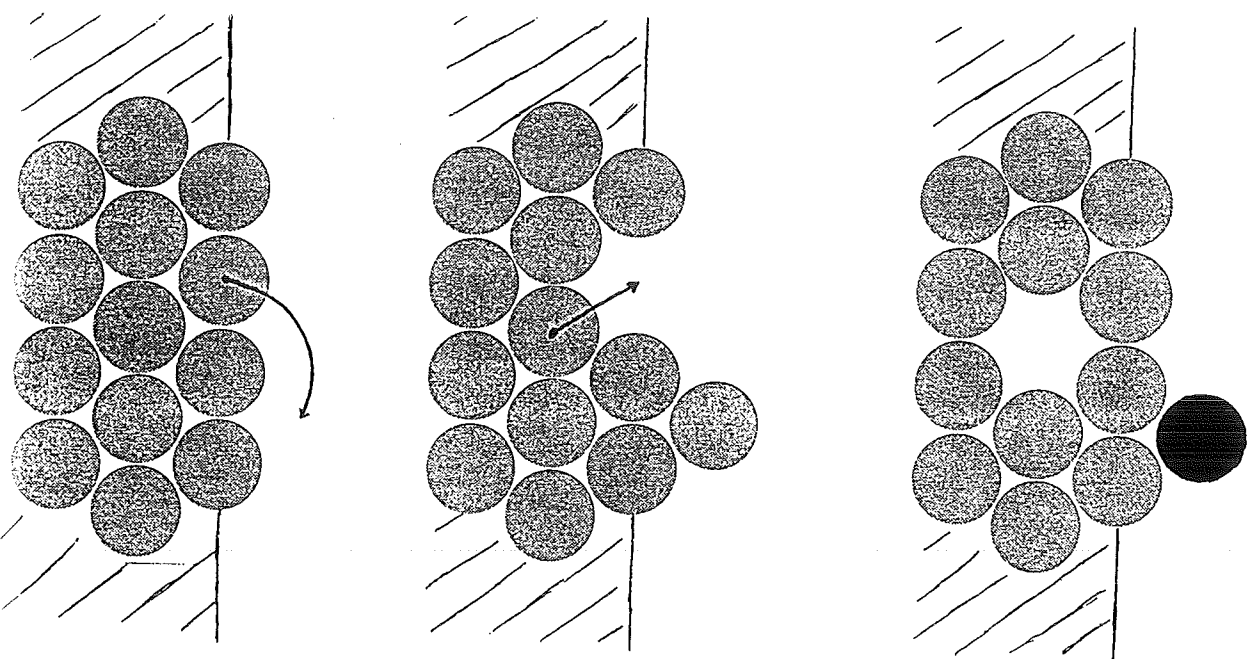
$$k(p,T) = v \exp\left(-\frac{\Delta H_M}{k_B T}\right) \exp\left(-\frac{p\Delta V}{k_B T}\right) \quad (16)$$

and for the equilibrium vacancy concentration under pressure:

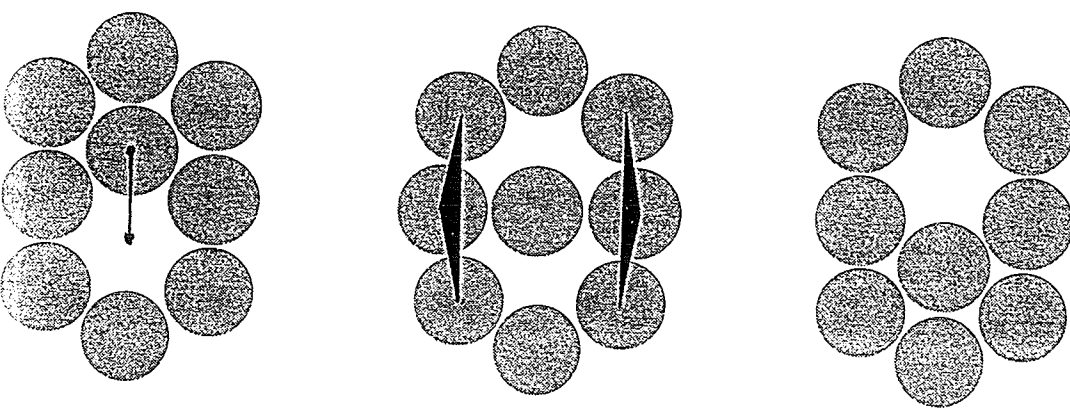
$$c_{vac}(p,T) = \exp\left(-\frac{\Delta H_F}{k_B T}\right) \exp\left(-\frac{p\Delta V_F}{k_B T}\right). \quad (17)$$

Like for ΔH and ΔV , we have for the activation entropy:

$$\Delta S = \Delta S_F + \Delta S_M \quad (18)$$



a)



b)

Figure 7: Schematic representation of the activation volumes for a) formation and b) migration.

but since we can not determine ΔS from the dependence of the diffusivity on some state variable, it can not be investigated.

3.3 The Keyes Relation

Since ΔH and ΔV characterise the same diffusion process, we would expect them to be correlated somehow. The relationship was first acknowledged by Keyes, some forty years ago.

3.3.1 The migration process

The relation was first derived for interstitial diffusion of solute atoms in a crystal. The concentration of the solute atoms does not depend on temperature and pressure; the derivation applies to the migration process. Keyes took the strain energy during the migration step as a starting point and assumed macroscopic elastic properties to be valid at an atomic level [14]. The derivation yields:

$$\Delta V_M = \kappa_M \chi \Delta H_M \quad (19)$$

where χ is the compressibility of the material and κ is a dimensionless proportionality factor; κ is a material constant.

3.3.2 The formation process

Although derived for the migration process only, this equation was experimentally shown also to be valid for vacancy diffusion in crystals, which, together with eqn.s (12) and (15) gives us the empirical result:

$$\Delta V_F = \kappa_F \chi \Delta H_F \quad (20)$$

Later, using a very simple energetic model with the Mie potential as the interatomic pair potential, Keyes gave a derivation for this result [14]. The proportionality constant κ was shown to be of the same order of magnitude as for the migration process.

From a more detailed derivation of eqn. (19), see [15], the similarity of eqn.s (19) and (20) can be understood, by recognizing that it is the same anharmonicity of the atomic interactions that lies at the basis of both relations.

3.3.3 The Grüneisen parameter

Stemming from the anharmonic theory for crystal vibrations, the Grüneisen parameter γ_k expresses the change of the angular frequency ω of a mode with respect to the specific volume (see, for instance, [17]):

$$\gamma_k \equiv - \frac{\partial \ln \omega(k)}{\partial \ln V_m} \quad (21)$$

The overall Grüneisen parameter γ is defined as the average of γ_k , with contribution of each mode to the specific heat as a weight factor:

$$\gamma \equiv \frac{\sum_k \gamma_k c_V(k)}{\sum_k c_V(k)} \quad (22)$$

This overall Grüneisen parameter can be expressed as:

$$\gamma = \frac{V_m \alpha_V}{\chi C_V} \quad (23)$$

and is only very weakly dependent on temperature. Note, however, that the molar volume V_m [$\text{m}^3 \text{mol}^{-1}$], the thermal volume expansion coefficient α_V [K^{-1}], the compressibility χ [Pa^{-1}]

and the specific heat at constant volume C_V [$\text{Jmol}^{-1}\text{K}^{-1}$], are all much more strongly dependent on temperature. Hence, they should all be determined at the same temperature to be able to calculate γ .

It can be shown that, for crystals, the proportionality factor κ is a function of the overall Grüneisen parameter only [16]:

$$\kappa = 2\gamma - \frac{2}{3} \quad (24)$$

From experimental results, it was observed [18] that the proportionality factor κ seems to be determined by the packing density of the structure only. Roughly, κ seems to be around 2 for bcc materials and 5.5 for fcc materials. For Hf diffusion in amorphous Ni-Zr, a value for κ also of around 5.5 was found, conforming that amorphous Ni-Zr has a dense packing [18]. But to which extent is it justified to use eqn.s (19) and (20) for diffusion in amorphous metals? As long as migration and formation are thermally activated processes, the equations seem to hold at first sight. There is, however, a serious reservation to be made about directly applying eqn. (24) to amorphous metals. To illustrate why this might go wrong, let us consider a hypothetical case. Suppose, we have a cooperative mechanism of diffusion, based on the existence of the low-frequency localised mode, with wave vector \mathbf{k} , mentioned in section 2.9. For this case, it is much more likely that γ_k is the parameter of interest and not γ .

3.4 Free Volume Theory

3.4.1 The probability distribution function

As Boltzmann statistics can be used to calculate a vacancy concentration in a crystal from its formation enthalpy (eqn. (14)), we can use free volume theory to calculate a defect concentration in an amorphous structure from its "volume".

In free volume theory, every atom is ascribed a volume v' , defined, for instance, as the volume of the Voronoï cell (a Voronoï cell is constructed like the Wigner-Seitz cell in a crystal). If the volume of this cell exceeds a certain value v_c , the remaining volume is called *free volume*:

$$v_f = v' - v_c \quad (25)$$

Assuming the redistribution of free volume over the atoms to take place without changing the Helmholtz free energy, Cohen and Turnbull [19] calculated the distribution function $P(v_f)$ of the free volume. This calculation is essentially statistic in nature and gives us the probability of finding an atom with a free volume between v_f and $v_f + dv_f$ to be:

$$P(v_f)dv_f = \frac{\varepsilon}{\langle v_f \rangle} \exp\left(-\varepsilon \frac{v_f}{\langle v_f \rangle}\right) dv_f \quad (26)$$

where $\langle v_f \rangle$ is the average free volume and ε is an overlap factor, whose value lies between 0.5 and 1.

3.4.2 The concentration of defects

Atomic mobility is now assumed only to take place at those sites in the structure where the free volume of a certain atom is larger than some critical value v^* . Such an atom can be seen to be a defect. Looking at diffusion as a form of atomic mobility, we can calculate the concentration of diffusion defects c_d :

$$c_d = \int_{v^*}^{\infty} P(v_f)dv_f = \exp\left(-\varepsilon \frac{v^*}{\langle v_f \rangle}\right) \quad (27)$$

For convenience, we now define the reduced free volume x as:

$$x \equiv \frac{\langle V_f \rangle}{\varepsilon v^*} \quad (28)$$

and hence, we have for the defect concentration:

$$c_d = \exp\left(-\frac{1}{x}\right) \quad (29)$$

It is noted, that the value of v^* (and thus of the defect concentration) may be different for other types of atomic mobility.

3.4.3 Fulcher-Vogel temperature dependence

The reduced free volume in the equilibrium structure is found to be given by:

$$x_{eq} = \frac{T - T_o}{B_T} \quad (30)$$

where T_o [K] and B_T [K] are constant. Hence, the defect concentration in equilibrium is given by:

$$c_{d,eq} = \exp\left(-\frac{B_T}{T - T_o}\right) \quad (31)$$

Note, that this temperature dependence is not Arrhenian; it is called a Fulcher-Vogel type of temperature dependence.

The defects mentioned in the previous section are *diffusion defects* and not *flow defects*. The concentrations of these two types of defects are connected by the relation $c_f = c_d^2$ [20]. This distinction between diffusion and flow defects was not made in the original free volume model [19]. Throughout the rest of this report we will only be considering diffusion defects.

3.4.4 The effective activation enthalpy of formation

The temperature range over which the amorphous structure can be shown to reach equilibrium is some tens of K at most (for Pd₄₀Ni₄₀P₂₀, the range is about 50 K, see figure 6). Together with the relatively large uncertainty in a measurement of the diffusivity at temperatures near T_g , it is rather difficult to determine from experiment, whether the temperature dependence is Arrhenian or of a Fulcher-Vogel type. To illustrate this, the defect concentration in Pd₄₀Ni₄₀P₂₀ (eqn. (31)) is represented in an Arrhenius plot, over the range of temperatures where equilibrium can be reached: see figure 5. For practical purposes, we will now define an effective formation enthalpy at some T^{eff} , e.g. the midpoint of the equilibrium temperature range. Using eqn. (31), we have:

$$\begin{aligned} \Delta H_F^{\text{eff}} &\equiv -\frac{\partial \ln c_{d,eq}}{\partial(1/k_B T)} = -\frac{\partial \ln c_{d,eq}}{\partial T} \frac{\partial T}{\partial(1/k_B T)} = -\frac{\partial}{\partial T} \left(-\frac{B_T}{T - T_o} \right) \left(\frac{\partial}{\partial T} \frac{1}{k_B T} \right)^{-1} \\ &= -\frac{B_T}{(T - T_o)^2} \left(\frac{-1}{k_B T^2} \right)^{-1} = k_B B_T \left(\frac{T}{T - T_o} \right)^2 \quad \text{at some } T = T^{\text{eff}} \end{aligned} \quad (32)$$

Throughout the rest of the text, we will drop the superscript "eff" for convenience.

3.4.5 The effective activation volume of formation

In analogy to the formation enthalpy for thermally activated diffusion, we can define an effective value for the volume of formation as:

$$\Delta V_F^{\text{eff}} \equiv -k_B T \left(\frac{\partial \ln c_{d,eq}}{\partial p} \right) = -k_B T \left(\frac{1}{x_{eq}^2} \frac{\partial x_{eq}}{\partial p} \right) \quad \text{at some } p = p^{\text{eff}}. \quad (33)$$

Again, we will drop the superscript "eff" from now on. It is noted that this effective ΔV_F does not necessarily correspond to the volume of a defect. However, ΔV_F is still the increase of the volume of the system upon the formation of a defect. This paradox can best be explained by a simple (but artificial) example. Consider the atom with the largest free volume v_f that is still smaller than v^* (hence it is, by definition, not a defect). We now increase the free volume of *each* atom in the structure, until the atom under view has a free volume $v_f > v^*$. Thus, we have created a defect, but the formation volume ΔV_F is not necessarily equal to v^* , the volume of a defect.

To determine ΔV_F , we need to know the pressure dependence of the free volume in equilibrium. We have determined this for $\text{Pd}_{40}\text{Ni}_{40}\text{P}_{20}$: how this is done, is described in the next chapter.

3.4.6 Free volume on its way to equilibrium

The differential equation that describes the change of the defect concentration on its way to equilibrium is [21]:

$$\frac{\partial c_d}{\partial t} = -k_r' c_d (c_d^2 - c_{d,eq}^2) \quad (34)$$

where the rate factor is given by

$$k_r'(p, T) = v_r \exp\left(-\frac{Q_r}{k_B T}\right) \exp\left(-\frac{p \Delta V_M}{k_B T}\right) \quad (35)$$

and the defect concentration in equilibrium is given by:

$$c_{d,eq}(p, T) = \exp\left(-\frac{\Delta H_F}{k_B T}\right) \exp\left(-\frac{p \Delta V_F}{k_B T}\right) \quad (36)$$

which are expressions similar to eqn.s (16) and (17), with ΔH_F and ΔV_F now given by eqn.s (32) and (33): they are effective values.

IV DETERMINING THE PRESSURE DEPENDENCE OF FREE VOLUME

4.1 Introduction

The temperature dependence of the free volume has been the subject of extensive study over the years. The pressure dependence, on the other hand, had not been examined before. Some five years before it was experimentally determined, Spaepen and Turnbull [22] estimated the pressure dependence of the free volume. They assumed, that the reduction of the equilibrium free volume with pressure is simply given by the compressibility of the bulk. In terms of the reduced free volume, this gives:

$$\frac{\partial x_{eq}}{\partial p} = -\frac{\chi}{\epsilon V^*} \Omega \quad (37)$$

where Ω is the atomic volume. However, this estimation soon proved to be too simple [23]. Limoge showed [24], that assuming a linear decrease of the free volume with pressure (as is eqn. (37)) results in a zero free volume, and hence a diverging activation volume, at experimentally accessible values of the pressure.

He further pointed out that this divergence may result from an assumption made in the free volume model itself. The hypothesis that free volume can be redistributed without change in enthalpy introduces inconsistencies with all pressure related quantities [24].

In the spirit of the free volume theory, Van den Beukel derived [25] that the dependence of the free volume with pressure should not be linear, but of the form:

$$x_{eq}(p, T) = x_{eq}(T) \exp(-c' p) \quad (38)$$

where c' is a positive constant. The derivation can be found in Appendix B. This pressure dependence does not give rise to a diverging activation volume.

Under the condition that $p \ll 1/c'$, we can approximate eqn. (38) by

$$x_{eq}(p, T) = x_{eq}(T)(1 - c' p) \quad (39)$$

which is a linear pressure dependence. To emphasize the analogy between the temperature dependence expressed by eqn. (30) and the pressure dependence expressed by eqn. (39) we define $p_o^{-1} \equiv c'$ and $B_p^{-1} \equiv c' x_{eq}(T)$ and we get

$$x_{eq}(p) = \frac{p_o - p}{B_p} \quad (40)$$

where p_o [GPa] and B_p [GPa] are constant with respect to pressure.

We have aimed to determine the pressure dependence of the free volume in amorphous $Pd_{40}Ni_{40}P_{20}$ at 563 K. To do so, amorphous $Pd_{40}Ni_{40}P_{20}$ samples were first annealed 563 K at different pressures. Then, the glass transition peak was measured for every sample by means of Differential Scanning Calorimetry (DSC). The height of the glass transition peak can be related to the amount of free volume at the beginning of the DSC measurement [26,27], which is equal to the amount of free volume at the end of the pressure anneal. We then know for every sample at which pressure it has been annealed and what the corresponding amount of free volume is. In this way, the pressure dependence of the free volume was established. The implications for the diffusion process are discussed in Chapter V.

Pd40Ni40P20-SF2-SR40-ESP37-23.06

Mass = 11.238 mg
 Heating Rate = 40.00 K/min
 Tmin = 320.0 K

Molweight = 73.466 g/mol
 Cooling Rate = 40.00 K/min
 Tmax = 630.0 K

Saphir Mass = 33.958 mg
 Range = 10.0 mcal/s

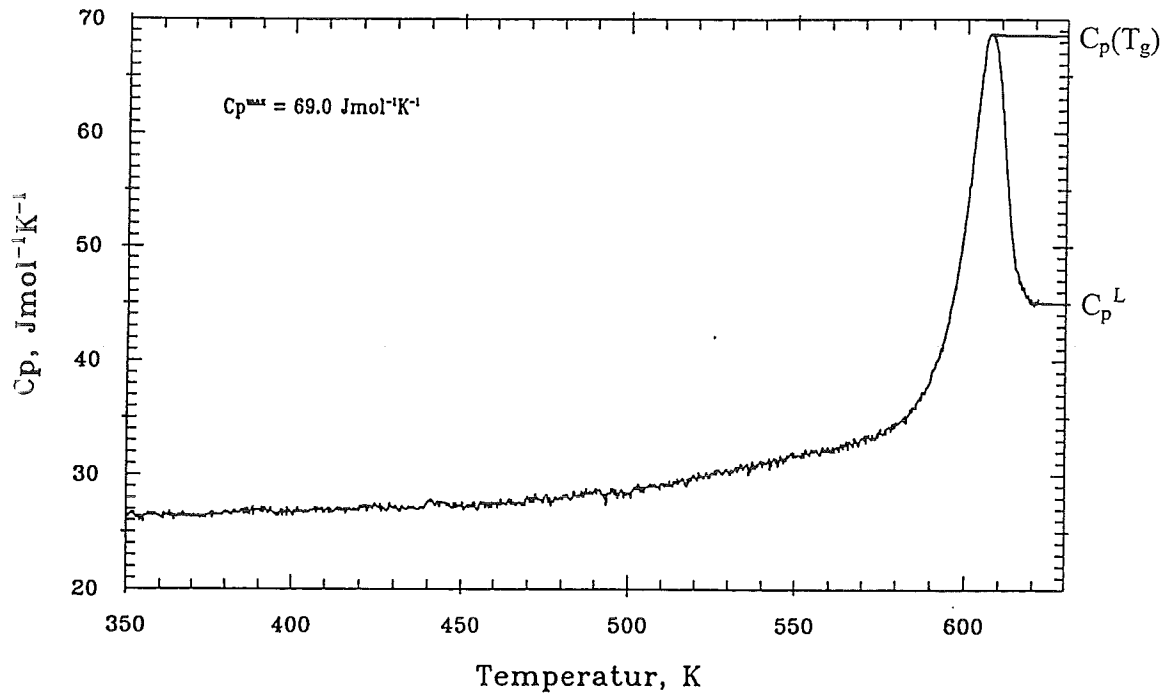


Figure 8: Specific heat as a function of temperature for amorphous Pd₄₀Ni₄₀P₂₀, recorded with a heating rate of 40 Kmin⁻¹. C_p(T_g) and C_p^L are indicated.

Pressure Generator 1GPa

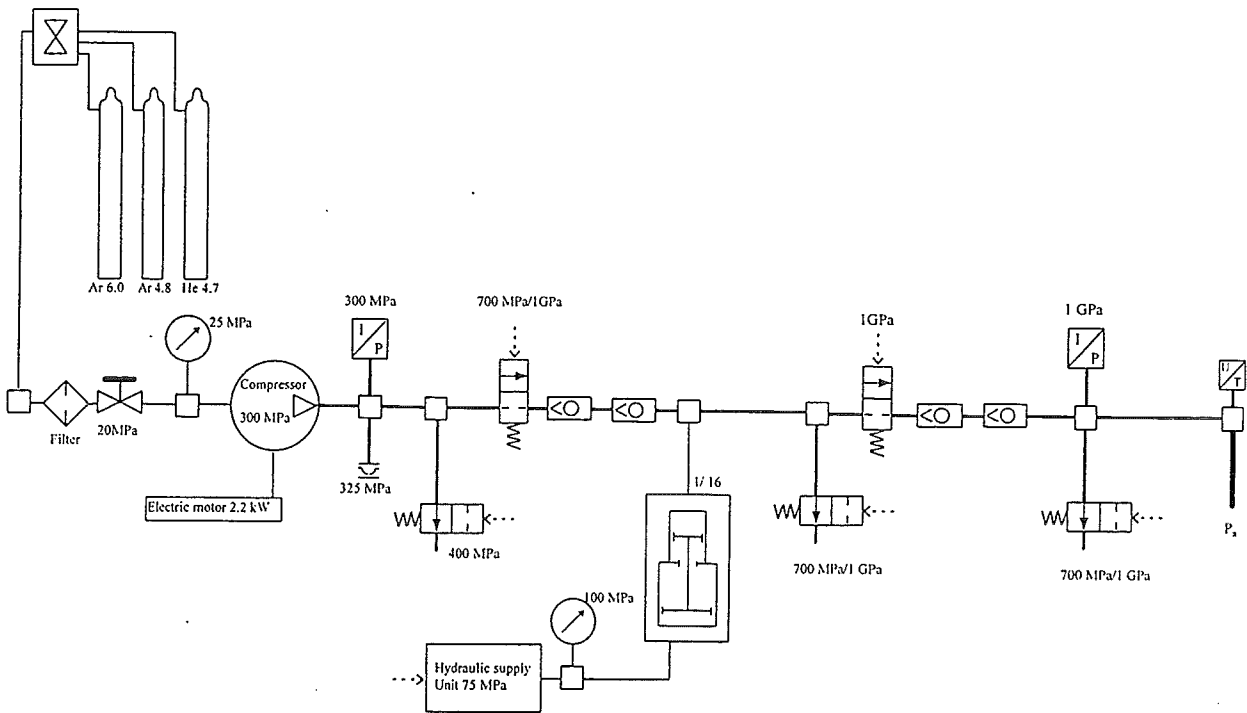


Figure 9: Schematic representation of the pressure equipment used for the pressure anneals.

4.2 How to determine x at the end of a pressure anneal

When a sample has been annealed under pressure during the time planned, it is cooled, as fast as the experimental conditions allow, to a temperature where the structure has become kinetically stable. Thus, we hope to have quenched-in the amount of free volume at the end of the pressure anneal. This amount of free volume can be determined using Differential Scanning Calorimetry (DSC) [26].

In a DSC experiment, the apparent specific heat is dynamically measured as a function of temperature. The glass-liquid transition gives rise to a peak in this dynamic $C_p(T)$ curve. We here define the glass-liquid transition temperature T_g as the temperature at which C_p has a maximum. We also define ΔC_p as:

$$\Delta C_p \equiv C_p(T_g) - C_p^L \quad (41)$$

where C_p^L is the specific heat of the undercooled liquid; see figure 8. The height of the glass transition peak, expressed as ΔC_p , was shown by Tuinstra et al. [27] only to depend on the amount of free volume at the start of the experiment (which, in the present experiment, should be equal to the amount of free volume at the end of the pressure anneal).

It was shown in reference [26] that integrating eqn. (34) under the conditions of a DSC experiment gives a glass transition peak that is in good agreement with the experiment. This agreement is even better when the thermal lag of the DSC apparatus is taken into account: this was done by Tuinstra et al., using a simple R-C model [27]. In this work, we will use the values for R and C that Tuinstra determined for Pd₄₀Ni₄₀P₂₀-measurements on a Perkin Elmer DSC-7.

Using the free volume of the samples at the beginning of the DSC scan as a fit parameter, ΔC_p was fitted to the experimentally obtained value.

4.3 Experimental

The measurements under review were performed on two different batches of amorphous Pd₄₀Ni₄₀P₂₀. The two batches were annealed under pressure in two different pressure chambers, but measured with the same DSC apparatus. Details of the two batches will be given separately.

4.3.1 Annealing under pressure

Batch 1. The samples from this batch have been used to determine the pressure dependence of the diffusivity by Duine in 1992 [28]. Prior to the annealing treatment, the samples have been equilibrated at 563 K for 2h45min at ambient pressure. Then, Au atoms were implanted to a dose of $0.8 \cdot 10^{15}$ at/cm², using a Van der Graaff implanter. Finally, the samples were annealed at 563.0 ± 0.1 K for 12.0 ± 0.1 h at several pressures up to 0.75 GPa. The samples were cooled down in approximately 20 min. Au concentration profiles before and after diffusion were measured with Rutherford Backscattering Spectrometry (RBS). The samples have since been stored at room temperature, at which atomic migration is negligible, and therefore the free volume was assumed to be unchanged after a period of four years.

Batch 2. The samples of this batch have been annealed under pressure in the laboratory of Prof. F. Faupel (see preface). No diffusion measurements have been performed on this batch. Also, they have not been equilibrated before the pressure anneal. Instead, the as-quenched samples were directly annealed at 563 ± 1 K for 12.0 ± 0.1 h at pressures up to 0.84 GPa. Although cooling was considerably slower here (it took approximately 30 min for the

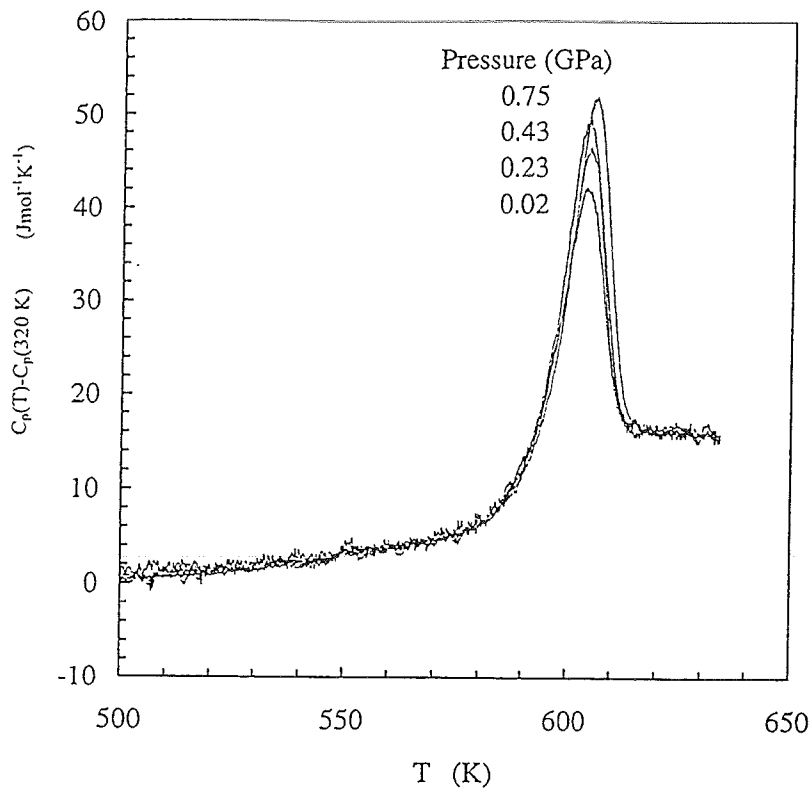


Figure 10: DSC traces of the measurements of the pressure samples of batch 1. The pressures at which the samples were annealed are indicated.

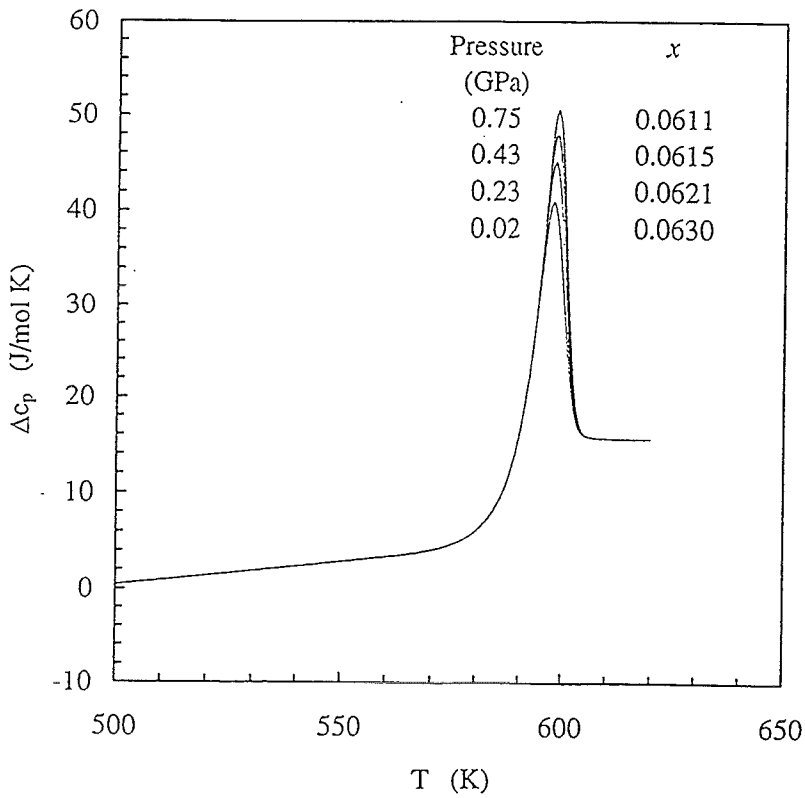


Figure 11: Reproduction of the peak heights of the glass transition peak, ΔC_p , using the free volume x at the beginning of the experiment as a fit parameter.

temperature to decrease 200 K), integrating eqn. (34) for the conditions of cooling after the pressure anneal showed that the systematic error thus introduced was small compared to the uncertainty in the DSC measurements.

In figure 9, a schematic representation of the pressure equipment used for batch 2 is given. The temperature of the samples (measured with a thermocouple contacting the sample) and the pressure in the pressure chamber are given as a function of annealing time in Appendix C.

4.3.2 Differential Scanning Calorimetry

The DSC measurements were performed on a modified Perkin-Elmer DSC-2, in an argon atmosphere, as described in reference [29]. In every DSC scan, the sample was heated from 320 K to 640 K, with a heating rate of 40 K/min.

Batch 1. For this batch, only *one* DSC measurement was made for each pressure. The samples weighed typically 10 mg. We much rather would have made several measurements with samples weighing approximately 20 mg each, but this was not possible since there was not enough material left from the diffusion measurements (see section 4.3.1).

Batch 2. In this case, three DSC scans were made for each pressure; the mass of the samples was typically 20 mg for each scan.

The preparations and the test measurements that needed to be made were very time consuming; it took the author approximately four months to learn how to make DSC measurements that reproduced sufficiently. Normally, a high reproducibility is achieved by using a high sample mass. However, this was not possible for batch 1 since we had to measure the samples on which the diffusion measurements had been performed and there was not much material left. To optimize the reproducibility, the following measures were taken:

- 1) The samples and the sample pans were handled with tweezers and layd down on a clean sheet of paper (never on the table; no tissue-paper!) to keep them free from grease and dust.
- 2) The sample pans were placed exactly in the middle of the measure and reference cell.
- 3) The samples were cut into small pieces with a surface area of typically 3 mm² to be assured of a good heat contact at all times of the experiment; it was noted after one of the test measurements that the ribbon was buckled after the experiment, resulting in an inferior heat contact.
- 4) The apparatus was not touched during a measurement.

4.4 Results

For both batches, the experimentally determined values of ΔC_p are shown in table 1. The corresponding values of the free volume at the beginning of the experiment are also given. For batch 1, the measured DSC scans are shown in figure 10. The DSC curves were corrected for a linear baseline drift: the values of the specific heat at the beginning and at the end of the DSC scan were made to fit the values found in an isothermal experiment. These values are $C_p(320\text{ K})=23.8\text{ Jmol}^{-1}\text{K}^{-1}$ and $C_p(630\text{ K})=42.0\text{ Jmol}^{-1}\text{K}^{-1}$ [30]. Note that this measure does not affect the height of the glass transition peak ΔC_p . The original DSC traces of the measurements on the samples of both the batches can be found in Appendix D. For batch 1 the calculated reproductions of the DSC curves are shown in figure 11. The values of the free volume x at the beginning of the DSC experiment are indicated.

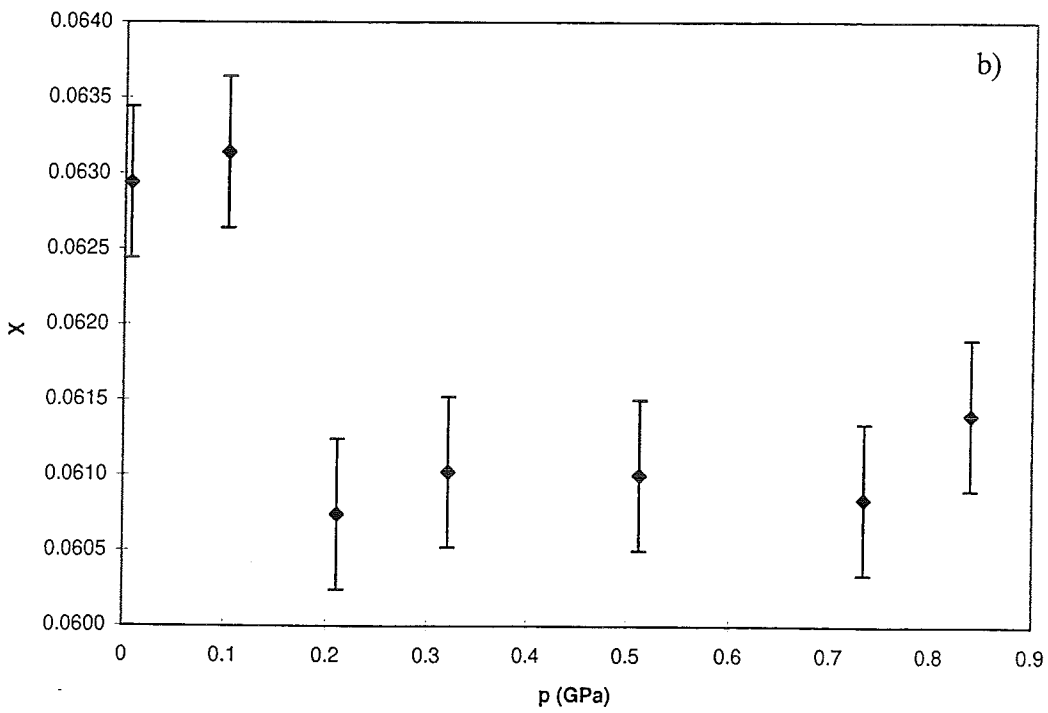
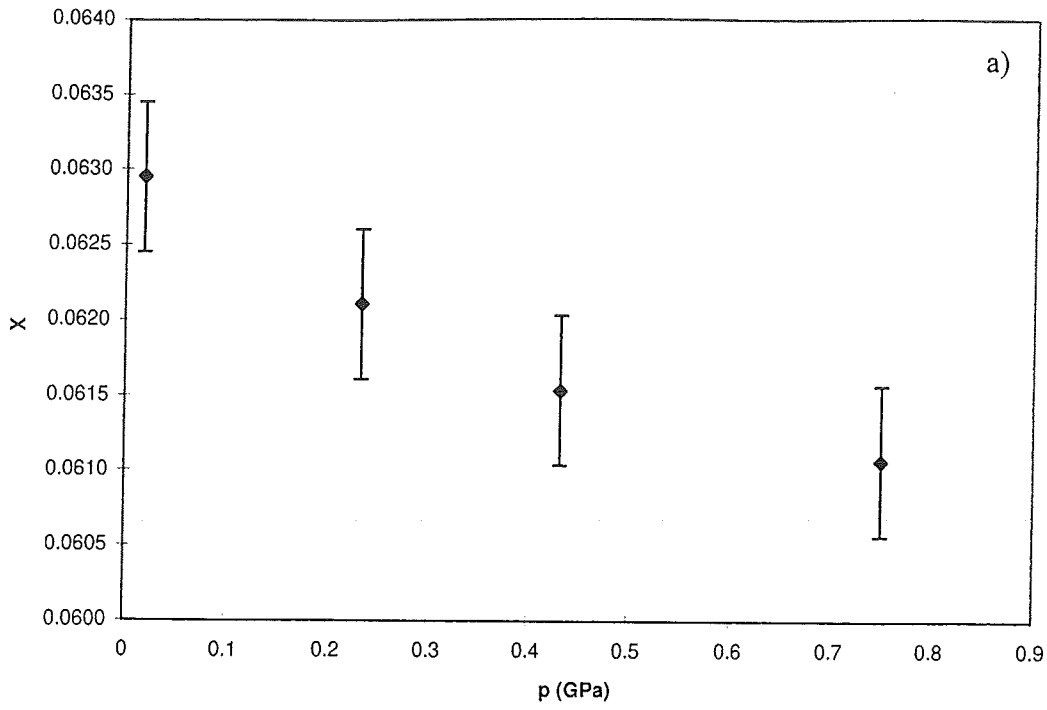


Figure 12: Results of the measurements of the free volume as a function of pressure for:
a) batch 1 and b) batch 2.

For both batches the values of x are shown as a function of pressure in table 1 and in figure 12. The error bars correspond to the error in the DSC measurements only. The error introduced by the pressure anneal is not known. The size of the error bars is estimated by the author on the basis of his experience with the DSC apparatus used.

4.5 Discussion

As can be seen from the DSC curves in figure 13, the glass transition temperatures are different for both batches. We find $T_g=(605\pm 1)$ K for batch 1 and $T_g=(612\pm 1)$ K for batch 2. It has been shown by Tuinstra et al. [27] that T_g does not depend strongly on the amount of free volume at the beginning of the experiment. The difference in T_g indicates that the equilibrium defect concentration in batch 2 is higher than that in batch 1, that the kinetics are slower, or both. For practical reasons, we assume the difference to be due to slower kinetics only and hence we use a different activation energy in the rate factor (see eqn. (35)). For batch 1 $T_g=605$ K and we use $Q_f=1.65$ eV/at as did Tuinstra for his DSC measurements on the same batch. For batch 2 $T_g=612$ K and we need to use $Q_f=1.72$ eV/at to account for this shift in T_g . The values for T_g and Q_f are also shown in table 2.

Eqn. (34) can be integrated under the conditions of the pressure anneal. From previous measurements [27] we know that $v_f=3.365\cdot 10^{25}$ s⁻¹, $B_T=3300$ K and $T_o=355$ K. As described in section 4.3, the annealing time was 12 h and the annealing temperature 563 K. The migration volume in eqn. (35) and the formation volume in eqn. (36) are not known. We use them to fit the experimental data of figure 12. This is done in the following manner:

- 1) First, ΔV_F is estimated using eqn. (33) for $p^{\text{eff}}=0$ and a guess is made of the numerical value of ΔV_M .
- 2) For different values of the ambient pressure ($p=0.1, 0.2, \dots, 0.9$ GPa), eqn. (34) is integrated numerically under the conditions of the pressure anneal as mentioned above. As a result, a defect concentration is obtained as a function of pressure.
- 3) Using eqn. (29) the free volume is calculated from the defect concentration. Thus, the free volume is obtained as a function of pressure.
- 4) The result is compared with the experimental data of figure 12. If the fit does not look good, the numerical values of ΔV_F and ΔV_M are changed and the procedure is repeated from point 2). This procedure is repeated until an agreeable fit is obtained. The best fit can be found in figure 14 for both batches.

Batch 1. For this batch, the value found for the formation volume is:

$$\Delta V_F=(6\pm 2) \text{ \AA}^3.$$

The migration volume could not be determined in this manner because all physically realistic values of ΔV_M yielded the same fit.

The pressure dependence of the free volume is generally due to the pressure dependence of the *equilibrium* free volume and to the pressure dependence of the *kinetics* of the free volume on its way to equilibrium. The parameter that describes the pressure dependence of the kinetics is ΔV_M . Since the value of ΔV_M and thus the kinetics do not seem to influence the pressure dependence of the free volume in batch 1, we assume that the samples of batch 1 were in equilibrium at the end of the pressure anneal. The pressure dependence of the free volume in the samples of batch 1 can well be represented by a linear relation, at least for pressures up to 0.75 GPa (see figure 14 a)). Hence, we have for the pressure constants of equation (40):

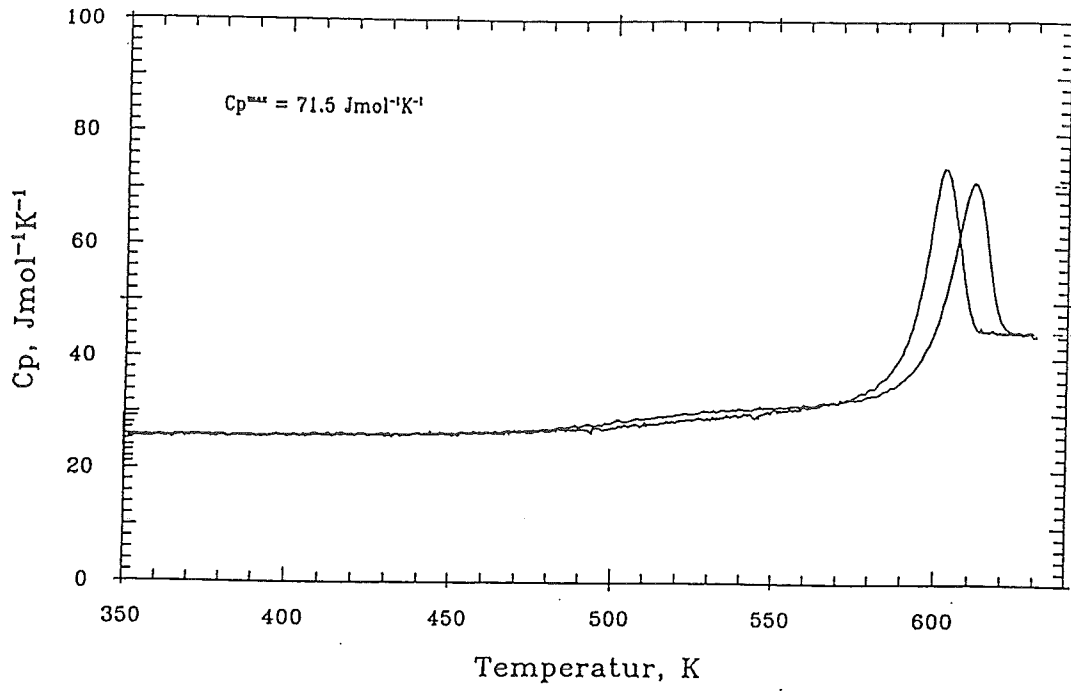


Figure 13: Illustration of the difference in the glass transition temperature for batch 1 ($T_g=605$ K) and batch 2 ($T_g=612$ K).

Table 1: Values of the peak height ΔC_p and the free volume x at the beginning of the DSC scan for the different annealing pressures of a) batch 1 and b) batch 2.

a)	p (GPa)	0.02	0.23	0.43	0.75
	ΔC_p (Jmol ⁻¹ K ⁻¹)	26.36	29.09	31.82	35.91
	x	0.06295	0.06210	0.06153	0.06106

b)	p(GPa)	0.006	0.10	0.21	0.32	0.51	0.73	0.84
	ΔC_p (Jmol ⁻¹ K ⁻¹)	26.24	25.34	37.59	35.98	36.20	37.04	33.94
	x	0.06294	0.06314	0.06074	0.06102	0.06100	0.06084	0.06140

$$p_0=22.2 \text{ GPa and}$$

$$B_p=353 \text{ GPa.}$$

The errors in p_0 and B_p are not indicated because the error in $x_{eq}(0 \text{ GPa})=p_0/B_p$ at 563 K is very small, while the error in the slope $\partial x_{eq}/\partial p$ is considerably larger.

Putting the result $\partial x_{eq}/\partial p=-1/B_p$ into eqn. (33) necessarily gives us back the result $\Delta V_F=6 \text{ \AA}^3$.

Batch 2. The values for the formation and migration volumes for this batch are:

$$\Delta V_F=(12\pm 4) \text{ \AA}^3 \text{ and}$$

$$\Delta V_M=(7\pm 3) \text{ \AA}^3.$$

The curvature in the solid line in figure 15 b) is due to the fact that batch 2 did not reach equilibrium under high pressures. This is due to two reasons. Firstly, the samples of batch 2 were in the as-quenched state at the beginning of the pressure anneal; they had not been pre-annealed at 563 K and ambient pressure like the samples of batch 1 (see section 4.3.1). Since the amount of free volume in the as-quenched state is much higher ($x_{aq}=0.082$) than the equilibrium amount of free volume at 563 K ($x_{eq}(563 \text{ K})=0.063$), it takes much longer to reach the pressure dependent equilibrium from the as-quenched state. Secondly, the larger value of the activation energy in the rate factor (see above) makes the approach to equilibrium markedly slower. Equilibrium is still reached at lower pressures. Apparently, the $p\Delta V_M$ term only becomes important at pressures above, say, 0.3 GPa. Using $\Delta V_M=0$ or a very large annealing time in our calculation would yield the dashed line representing equilibrium in figure 14 b). The equilibrium line for batch 2 is markedly steeper. The numerical values of the pressure constants (see eqn. (40)) at 563 K are for batch 2:

$$p_0=10.5 \text{ GPa and}$$

$$B_p=167 \text{ GPa.}$$

The errors for p_0 and B_p are not given for the reason mentioned when discussing batch 1. Why the best fit of the equilibrium line is so much steeper we do not know. Neither do we know why the scatter of the measurements on batch 2 is so much larger than that on batch 1 (especially the difference between the points at $p=0.10 \text{ GPa}$ and $p=0.21 \text{ GPa}$ is rather striking).

It is acknowledged that the fit of eqn. (34) to the experimental data of batch 2 is not satisfactory at all. One should bear this in mind when judging the importance of the results obtained from this batch. Despite the poor agreement of the calculated curve with the measured points, the values found for ΔV_F and ΔV_M seem to be physically realistic.

It is also acknowledged that the exponential dependence of the equilibrium free volume on pressure given by eqn. (38) could have been used instead of eqn. (40). However, this would yield quite the same result; as the exponential decreases towards $x=0$ at very high pressures, eqn. (40) is a good first order approximation of the exponential in the experimentally accessible range of pressures. The curvature of the solid line in figure 14 b) can not be described with eqn. (38), because the exponential decreases towards $x=0$ and not towards a value of the free volume around $x=0.0605$.

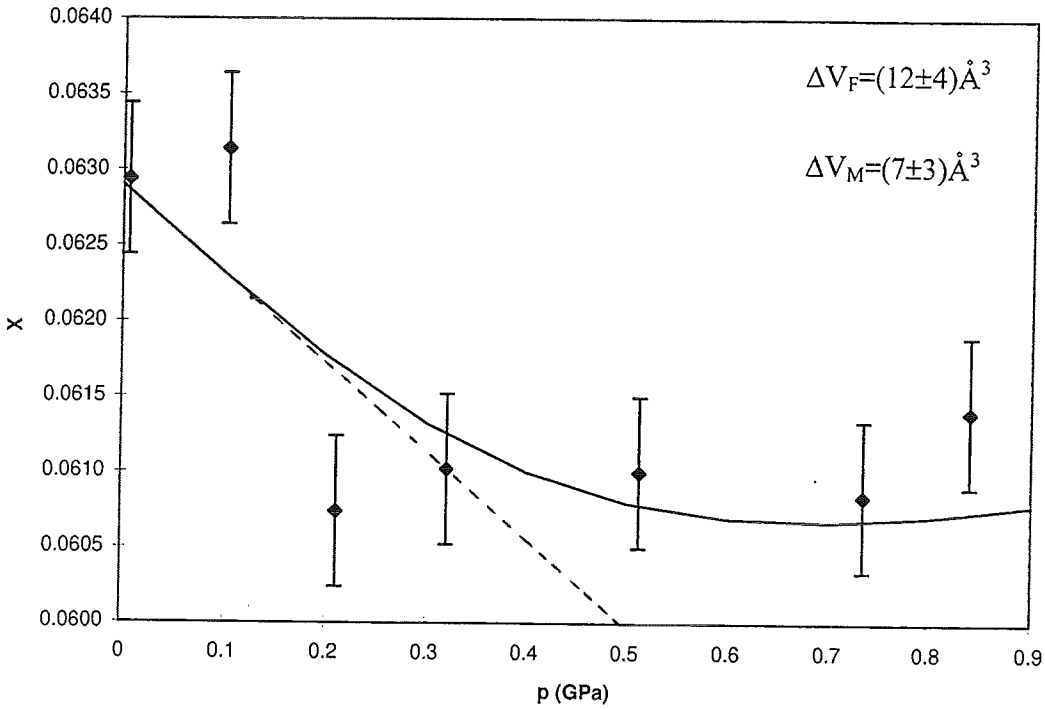
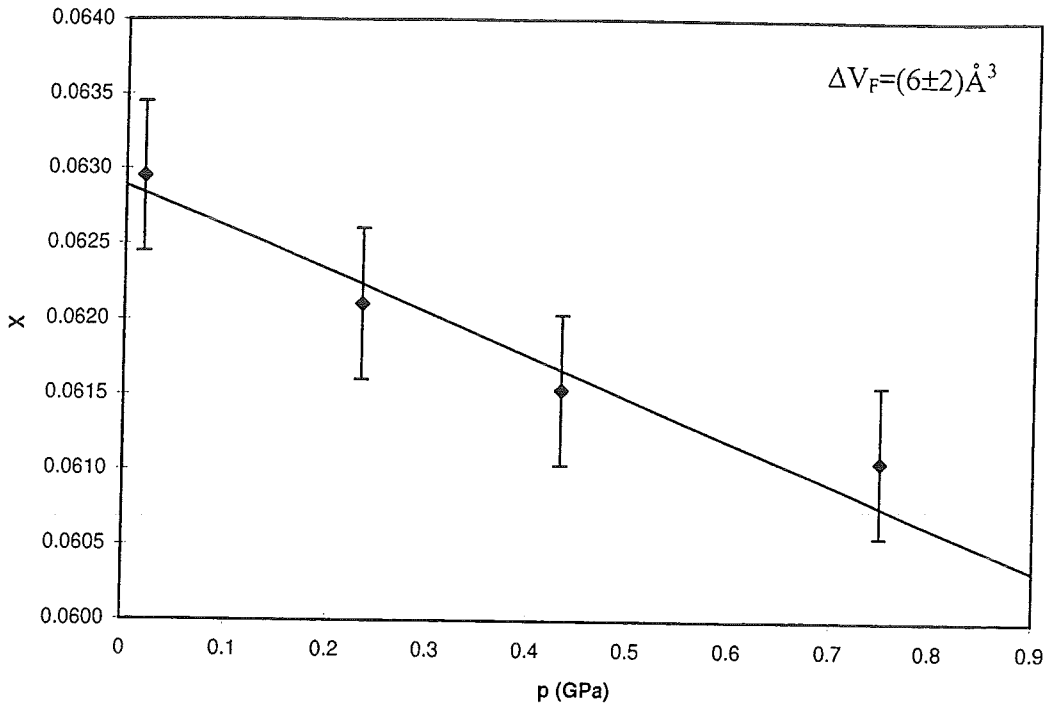


Figure 14: Results of the measurements of the free volume as a function of pressure for: a) batch 1 and b) batch 2 (after figure 12). The solid lines are fits to eqn. (38). The dashed line in b) is the tangent of the solid line at $p=0$.

V THE IMPLICATIONS FOR THE DIFFUSION PROCESS

5.1 The Results Concerning Diffusion Put Together

Batch 1. On this batch Duine [28,31] has performed a set of measurements of the diffusivity of Au as a function of temperature and pressure. For the activation enthalpy was found

$$\Delta H = 4.3 \text{ eV.}$$

Using $B_T = 3300 \text{ K}$ and $T_0 = 355 \text{ K}$ [27] we can calculate the formation enthalpy from eqn. (32). This gives:

$$\Delta H_F = 2.1 \text{ eV.}$$

Eqn. (12) then yields for the migration enthalpy:

$$\Delta H_M = 2.2 \text{ eV.}$$

The errors in ΔH , B_T and T_0 were not given by Duine. When necessary, we will estimate the relative errors in ΔH_F and ΔH_M to be 10%, which seems to be a realistic choice.

For the activation volume was found (see figure 15):

$$\Delta V = (11 \pm 4) \text{ \AA}^3.$$

As can be found in section 4.5 we have found for the formation volume $\Delta V_F = (6 \pm 2) \text{ \AA}^3$ for batch 1. Eqn. (15) then yields for the migration volume:

$$\Delta V_M = (5 \pm 4) \text{ \AA}^3.$$

The activation enthalpies and volumes that we now know for batches 1 and 2 are put together in table 3.

5.2 Checking the Keyes Relation

5.2.1 The proportionality constant

Batch 1. Using eqn. (20), we obtain for the process of formation of a defect:

$$\kappa_F = (3.1 \pm 1.4)$$

From eqn. (19), we get for the process of migration of a defect:

$$\kappa_M = (2.5 \pm 2.0).$$

The necessary data are taken from tables 3 and 4; the relative errors in ΔH_F and ΔH_M are taken to be 10% (see section 5.1). These results tell us that we have split ΔH in ΔH_F and ΔH_M from the temperature dependence of D and c_d in the same way as we have split ΔV in ΔV_F and ΔV_M from the pressure dependence of D and c_d . This result means that the way we use the free volume model to quantitatively describe the diffusion process, as a function of both temperature and pressure, is internally consistent.

Batch 2. Since we assumed that for this batch the equilibrium free volume as a function of temperature is the same as for batch 1, the values of ΔH_F are the same; see eqn. (32). The fact that we find different values for ΔV_F for both batches indicates that this assumption is wrong. The best one could do to mend this is to assume that κ , rather than ΔH_F , is the same for both batches. However, there is not much to be gained from this approach and we did not pursue it because of the practical difficulties involved.

Since we do not know ΔV_M for this batch, we can not check the Keyes relation for the migration process either.

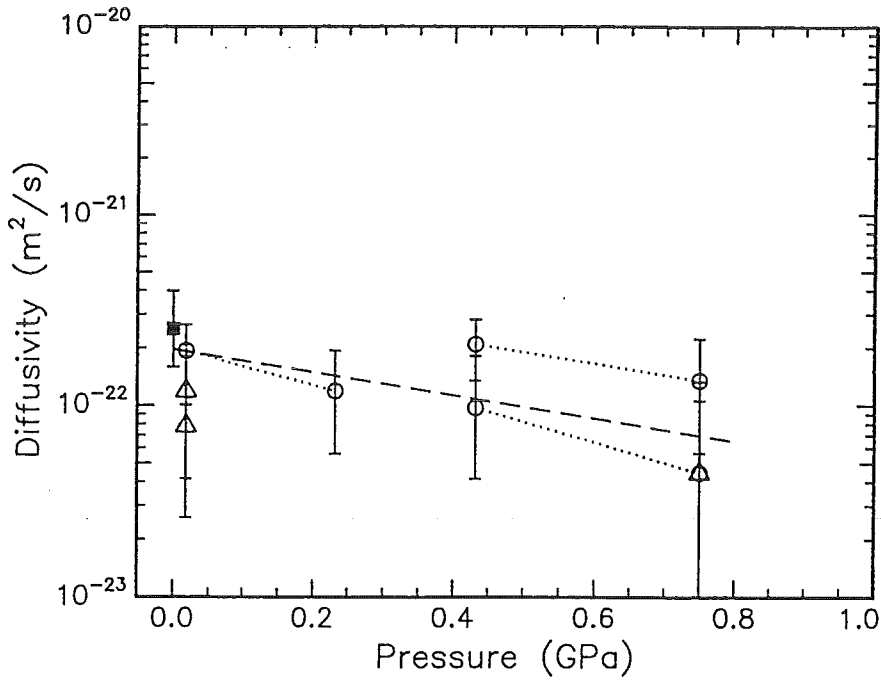


Figure 15: The pressure dependence of the diffusivity of Au in amorphous Pd₄₀Ni₄₀P₂₀ at T=563 K. The dotted lines connect data that have been taken on a single sample [28].

Table 2: Overview of some important temperature and pressure related parameters for amorphous Pd₄₀Ni₄₀P₂₀.

	T _g (K)	Q (eV)	T _o (K)	B _T (K)	p _o (GPa)	B _p (GPa)
a)	605±1	1.65	355	3300	22.2	353
b)	612±1	1.72	355	3300	10.5	167

Table 3: Overview of the activation enthalpies and volumes for amorphous Pd₄₀Ni₄₀P₂₀.

	ΔH (eV)	ΔH _F (eV)	ΔH _M (eV)	ΔV (Å ³)	ΔV _F (Å ³)	ΔV _M (Å ³)
a)	4.3	2.1	2.2	11±4	6±2	5±4
b)	----	2.1	----	-----	12±4	7±3

Table 4: Overview of some physical properties of amorphous Pd₄₀Ni₄₀P₂₀ at room temperature. The values of C_v and χ are taken from Appendix E.

M (gmol ⁻¹)	ρ [8] (kgm ⁻³)	V _m (m ³ mol ⁻¹)	α _v [31] (K ⁻¹)	C _v (Jmol ⁻¹ K ⁻¹)	χ (m ² N ⁻¹)	γ
72.236	9.4·10 ³	7.7·10 ⁻⁶	4.5·10 ⁻⁵	22.5±1.0	(5.7±1.3)10 ⁻¹²	2.7±0.7

Table 5: The proportionality factor κ, determined for batch 1.

κ _F	κ _M	κ
3.1±1.4	2.5±2.0	4.7±1.4

5.2.2 The Grüneisen parameter

We now check the validity of eqn. (24) for amorphous Pd₄₀Ni₄₀P₂₀. Using the parameters from table 4, γ can be calculated from eqn. (23), yielding:

$$\gamma=(2.7\pm 0.7)$$

at room temperature. The error in γ is calculated by assuming a 5% error in the values of the parameters shown in table 4, hence the error in γ is only a rough estimation. Since the temperature dependence of γ is small in general, we expect its value to hold at 563 K as well. Eqn. (24) then gives us:

$$\kappa=(4.7\pm 1.4)$$

which is of the same order of magnitude as we have found experimentally for κ_F and κ_M : see table 4.

It is noted that, in an amorphous structure, the distribution of frequencies around a defect could be distinctly different from the average distribution. The occurrence of cooperative localised modes found in computer simulations is an indication that this is indeed the case. If so, the *overall* Grüneisen parameter calculated from eqn. (22) might not be the parameter of interest.

5.3 Discussing the Defect Size

The average atomic volume Ω of Pd₄₀Ni₄₀P₂₀ is:

$$\Omega=16\text{\AA}^3.$$

Hence, the typical volume of the holes mentioned in section 2.4 is, expressed in terms of Ω is:

$$v_{\text{hole}}=0.3\Omega$$

which is of the same order of magnitude as the activation volume of formation:

$$\Delta V_F=0.4\Omega \quad \text{for batch 1 and}$$

$$\Delta V_F=0.8\Omega \quad \text{for batch 2.}$$

Relating eqn. (33) to eqn. (37), we can write for the minimal amount of free volume present at a defect:

$$v^* = k_B T \frac{\chi}{\varepsilon \chi_{eq}^2} \frac{\Omega}{\Delta V_F} \quad (42)$$

Taking $\varepsilon=1$, and using eqn. (30), this gives us for $p^{\text{eff}}=0$ and $T^{\text{eff}}=563$ K:

$$v^*=2.2\Omega \quad \text{for batch 1 and}$$

$$v^*=4.4\Omega \quad \text{for batch 2.}$$

which seems to be too high to be physically feasible, confirming that eqn. (37) is not a good guess.

In our free volume model, v^* is the minimal amount of free volume present at a defect. As we mentioned in section 3.2, ΔV_F corresponds to the change in volume of the structure when a defect is formed. Hence, we would expect v^* and ΔV_F to be correlated. It is derived in Appendix F that at atmospheric pressure and 563 K we should have:

$$v^*=3 \cdot 10^{-5} \Delta V_F.$$

which seems to give a value for v^* that is much too low. We have little idea about why our free volume model predicts a value for v^* that is so physically unrealistic. Perhaps it has something to do with the notion of the formation of defects. We have assumed that only atoms with a free volume $v_f > v^*$ are defects and that only those participate in diffusion. Now, consider again an atom that is nearly a defect. Not only is it unlikely that such an atom has no contribution to diffusion, but we can make it a defect by adding the slightest amount of free

volume. To say that a defect is thus created might just have more consequences than we can oversee.

5.4 Which Entities Are Diffusing?

The values of ΔH , ΔH_M , ΔV and ΔV_M for batch 1 (see table 3) correspond to the diffusion of Au in $\text{Pd}_{40}\text{Ni}_{40}\text{P}_{20}$. The other values for the activation enthalpies and volumes correspond to the diffusion of defects in $\text{Pd}_{40}\text{Ni}_{40}\text{P}_{20}$. Au is an element similar to Pd with respect to atomic size and mass. Therefore, we expect the values we have measured for Au diffusion to be valid for the diffusion of Pd atoms as well. How exactly the diffusion of defects relates to self-diffusion is not obvious. The only reason why we do not treat them separately is that we can not compare them but for one case: $\Delta V_M^{\text{Au}}=(5\pm 4) \text{ \AA}^3$ for batch 1 and $\Delta V_M^{\text{Def}}=(7\pm 3) \text{ \AA}^3$ for batch 2. All we can say is that the order of magnitude is the same.

5.5 Conclusions

The equilibrium value of the free volume in amorphous $\text{Pd}_{40}\text{Ni}_{40}\text{P}_{20}$ has been shown to decrease with pressure.

Whether this dependence is linear or not, we can not conclude from our measurements.

The measurements on the two batches that have been investigated do not show the same results. Both the kinetics and the equilibrium properties seem to be different. Most strikingly, the glass transition temperatures differ 7 K.

The activation volume for the formation of a defect is positive. Taking the result of the two batches together, we have: $\Delta V_F=(0.6\pm 0.3) \Omega$.

The activation volume for migration is not zero. Again, taking the two batches together, we have: $\Delta V_M=(0.4\pm 0.3) \Omega$.

These results suggest that the defects that govern diffusion are sites of loose packing (i.e. diffusion is indirect). However, the sites are not necessarily open spaces between the atoms of volume ΔV_F . Hence, the results do not directly support a vacancy-like mechanism for diffusion.

The relation of Keyes was checked and found to be valid within the (rather large) uncertainty limits.

Two estimates of the minimal free volume present at a defect differ some six orders of magnitude. This gross inconsistency indicates that there is something wrong with our free volume model or with the way we use it.

Whether the mechanism of diffusion is cooperative or single-atom can not be determined from the measurements we have performed.

VI THE CONCENTRATION DISTRIBUTION OF COLLECTIVE DEFECTS

6.1 Introduction

6.1.1 Why define a collective defect?

Measurements of the isotope effect have indicated that the mechanism of diffusion in amorphous metals is most probably collective; ten to thirty atoms seem to be involved in the diffusion process. On the other hand, we have assumed that diffusion is governed by sites in the structure where the free volume of an atom satisfies the condition $v_f > v^*$. We then have calculated the concentration of such defects using a free volume model. Finally, we have simply taken the expression for the diffusivity for crystals and replaced the vacancy concentration by the concentration of defects that we have calculated.

In principle, the approach is not inconsistent with the experimental observation. And what we are doing is not just calculating a vacancy concentration with a liquid model. Nevertheless, the approach is not very amorphous and this stimulated the author to define a type of defect that is more collective in nature. The same free volume model was used to calculate the defect concentrations.

6.1.2 Introducing an alternative notation

Starting from eqn. (26), we define

$$z \equiv \varepsilon \frac{v_f}{\langle v_f \rangle} \quad (43)$$

in order to be able to write the free volume distribution function in a more convenient form for calculation:

$$P(z)dz = e^{-z} dz . \quad (44)$$

Next, we define:

$$z_c \equiv \varepsilon \frac{v^*}{\langle v_f \rangle} \quad (45)$$

and hence, we have for $c_1(z_c)$, the probability of one atom having a free volume $z \geq z_c$:

$$c_1(z_c) = e^{-z_c} , \quad (46)$$

which is completely equivalent with eqn. (29). Introducing a new terminology, we say that eqn. (46) gives us the concentration of defects of order 1, since we have looked at the probability of *one* atom having a free volume $z \geq z_c$.

6.1.3 Definition of a collective defect of order n

Let us consider an amorphous structure. We label all atoms that satisfy the condition $z > z_c$ with $n=1$; they are the first order defects defined in the previous section. We now ask the question: how many *pairs* of the remaining atoms have a free volume of *together* that exceeds z_c ? These pairs must satisfy:

$$z_1 + z_2 \geq z_c . \quad (47)$$

We label all the atoms that satisfy this condition with $n=2$; they form second order defects. As with defects of order 1, their concentration is defined as the number of defects divided by the number of atoms. In this way, we continue until all atoms are labeled. Note that it is inherent to the approach that every atom in the structure is part of some defect of some order n .

6.1.4 What we aimed for and what we achieved

The original idea was to define a collective defect of order n as a group of n neighbouring atoms with the sum of their free volumes exceeding a critical value z_c . The critical value was taken to be independent of n . This assumption seemed physically plausible to us. Our approach immediately rose two questions:

- 1) Regarding multiple counting: should we allow one particular atom to be part of two (or more) defects at the same time? and
- 2) Regarding the geometry of a defect of order $n > 2$: do we have to account for the fact that defects of the same order can have different shapes?

We decided *not* to allow multiple counting. The reason for this decision is illustrated by an example: consider two groups of atoms, different in size, but with the same total amount of free volume, exceeding z_c . We expect that the smaller group of the two is more likely to give a contribution to diffusion than the larger group, because the packing of the group is more loose. For this reason we decided, as a first order approximation, that any atom can only be part of *one* defect at a time, namely the smallest group of neighbouring atoms (of which the atom that we are considering is part) that has a free volume exceeding z_c .

Finding the answer to question 2) was postponed until later. It was acknowledged that we could first calculate the probability for a group of n atoms to have a free volume exceeding z_c (without multiple counting) and worry about the possible shapes of this group later. The results of this calculation are shown in sections 6.2-6.6. However, this calculation turned out to be so time-consuming that when it was finished we did not have enough time left to consider the possible shapes of a group of n atoms.

Along the way we realised that in our definition of a defect of order n (see section 6.1.3) we had not required the n atoms to be neighbours. Obviously, we should have. The problem is that we do not directly know how. It is expected that the average number of nearest neighbours will enter the calculation here. As a consolation we note that it can be done later; the approach described in sections 6.2-6.6 is not affected.

It is emphasized that the concentration distribution that we are about to calculate should later be modified on the two points mentioned in the last two paragraphs.

6.2 An Exact Expression for $c_n(z_c)$ in Integral Form

We shall now calculate the concentration distribution $c_n(z_c)$ of collective defects. Consider a group of n atoms in a structure of N atoms with $n \ll N$. Now order this group according to their amount of free volume:

$$z_1 > z_2 > \dots > z_n. \quad (48)$$

Now define S_i as the largest sum of the free volumes of a selection of i atoms from the group of n atoms that we are considering:

$$\begin{aligned} S_1 &\equiv z_1 \\ S_2 &\equiv z_1 + z_2 \\ &\cdot \\ &\cdot \\ S_n &\equiv \sum_{i=1}^n z_i \end{aligned} \quad (49)$$

There are two conditions that must be satisfied for this group to qualify as a defect of order n . First, we must have:

$$S_n \geq z_c. \quad (50)$$

But this is not enough: there may still be an atom in this group for which $z_i \geq z_c$, and we have already counted these atoms as being first order defects. Since we did not allow an atom to be part of two defects at the same time, we must beware for this multiple counting. We must recognize that any selection of $n-1$ atoms or less poses a condition. However, the condition for the *largest sum* of $n-1$ atoms

$$S_{n-1} = S_n - z_n < z_c \quad (51)$$

is the strongest and it covers all others. Alternatively, we can write:

$$S_n - z_c < z_n < S_n / n \quad (52)$$

where the last inequality expresses that z_n is the smallest of all z_i 's.

We have expressed all conditions in terms of the sum S_n of the free volumes of the n atoms in the defect and of the atom with the least free volume, z_n .

We now calculate the probability that S_n lies between λ and $\lambda+d\lambda$ and, at the same time, that z_n lies between μ and $\mu+d\mu$. This probability is given by:

$$n \int d\mu e^{-\mu} \int dz_1 \int dz_2 \cdots \int dz_{n-1} \exp(-S_{n-1}). \quad (53)$$

The factor n in eqn. (53) accounts for the fact that we have defined z_n to be the smallest of all z_i (see eqn. (48)). Incorporating the boundary conditions imposed by eqn.s (50) and (52) into eqn. (53) gives us the concentration distribution we are looking for. This calculation can be found in Appendix F. The final result can be expressed in a relatively simple form:

$$c_n(z_c) = \frac{1}{(n-1)(n-1)!} \exp\left(-\frac{n}{n-1}z_c\right) \int_0^{z_c} dv \exp\left(\frac{v}{n-1}\right) v^{n-1} \quad (54)$$

which is an exact result.

This integral could be solved numerically, but we did not try.

6.3 An Exact Expression for $c_n(z_c)$ as a Sommmation

Eqn. (54) can also be solved analytically. In a straightforward calculation, it is shown in Appendix G, that this leads to:

$$c_n(z_c) = (n-1)^{n-1} e^{-z_c} (-1)^n \left\{ \exp\left(-\frac{z_c}{n-1}\right) - \sum_{i=0}^{n-1} \frac{1}{i!} \left(-\frac{z_c}{n-1}\right)^i \right\}. \quad (55)$$

This equation is of a rather peculiar form. The expression between braces consists of an exponent subtracted with its Taylor approximation of order $n-1$; the expression is positive when n is even and negative when n is odd. The term $(-1)^n$ makes $c_n(z_c)$ positive for all n . Of course, since $c_n(z_c)$ is a concentration, it should be.

We can calculate eqn. (55) with an ordinary spreadsheet programme, but only for relatively small n . The reason for this is that most computer programmes use a Taylor approximation for the exponential itself; this will instantly give $c_n(z_c)=0$ when the Taylor approximation that the programme uses is of the same order as the defect of which we are trying to calculate the concentration.

When we replace the exponential in eqn. (55) by its Taylor expansion around zero, we get:

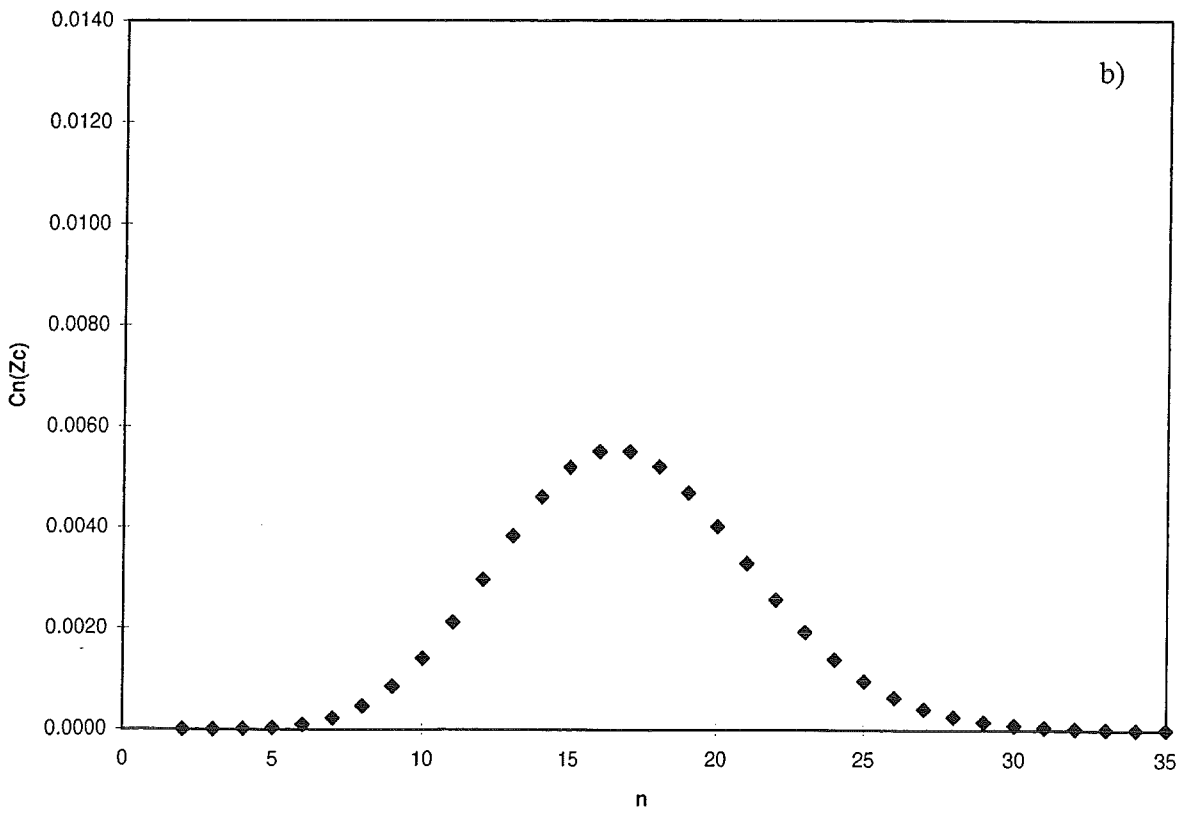
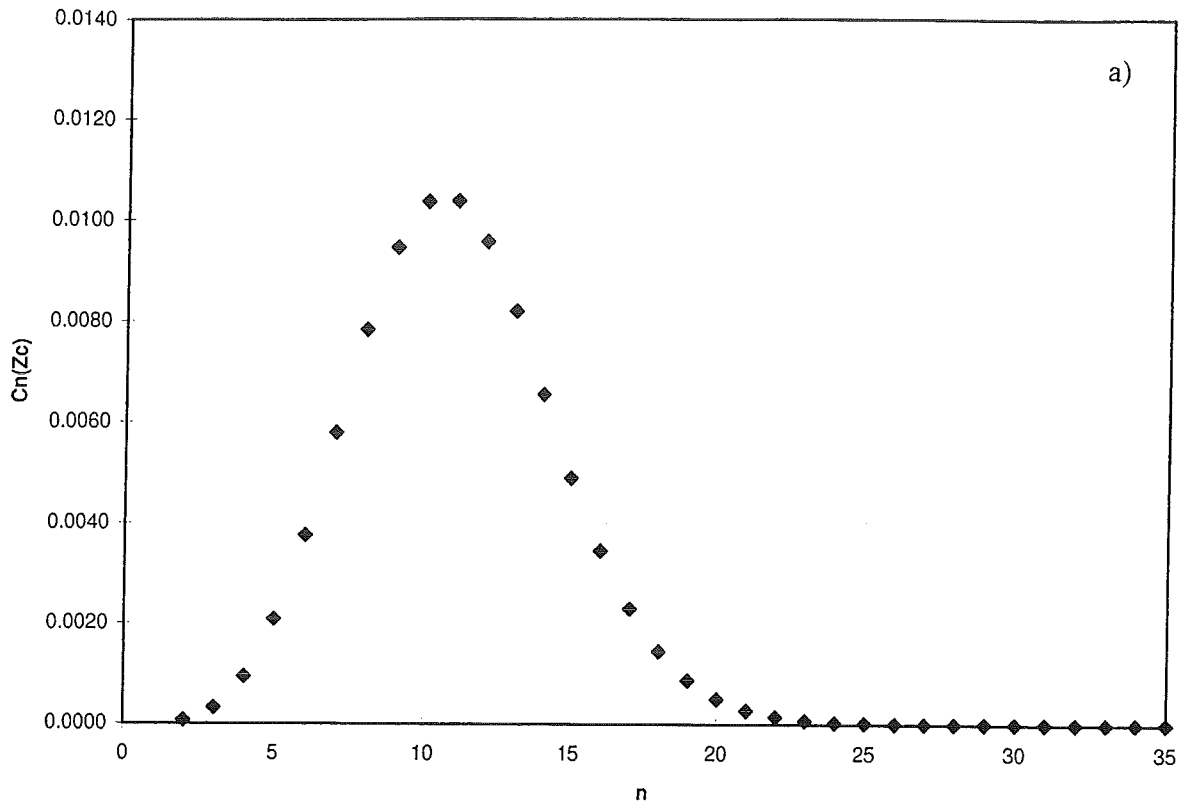


Figure 16: Plot of the exact solution of a) $c_n(12)$ and b) $c_n(18)$.

$$c_n(z_c) = (n-1)^{n-1} e^{-z_c} (-1)^n \left\{ \sum_{i=n}^{\infty} \frac{1}{i!} \left(-\frac{z_c}{n-1} \right)^i \right\}. \quad (56)$$

This expression can also be calculated using a spreadsheet programme, but this is not very practical for small n ; since the Taylor approximation is taken around zero, we need a lot of terms for an accurate result.

In figure 16 we have calculated $c_n(z_c)$ with eqn. (55) for $n < 6$ and we used eqn. (56) for $n \geq 6$ for two values of z_c ; $z_c = 12$ corresponds to the free volume in the as-quenched state of amorphous $\text{Pd}_{40}\text{Ni}_{40}\text{P}_{20}$ and $z_c = 18$ corresponds to the equilibrium state at 540 K, the lower limit of the equilibrium temperature range. It was checked if the numerical value of $c_6(12)$ was the same when calculated from eqn. (55) and from eqn. (56); this was indeed the case.

6.4 The Tailor Approximation

Let us consider the function

$$f(z_c) = \exp\left(-\frac{z_c}{n-1}\right). \quad (57)$$

Its standard Taylor expansion of order $n-1$ around zero is given by:

$$f(z_c) = \sum_{i=0}^{n-1} \frac{1}{i!} \left(-\frac{z_c}{n-1} \right)^i + R_{n-1}(z_c) \quad (58)$$

where R_{n-1} is the Lagrangian rest, given by:

$$R_{n-1}(z_c) = \frac{1}{n!} \left[\frac{d^n f(z_c)}{dz_c^n} \right]_{\xi} z_c^n \quad (59)$$

with $\xi = \xi(n, z_c)$; ξ is defined to make eqn. (58) exact. For $f(z_c)$, we have:

$$\frac{d^n f(z_c)}{dz_c^n} = (-1)^n \frac{1}{(n-1)^n} \exp\left(-\frac{z_c}{n-1}\right) \quad (60)$$

and hence, we have for eqn. (59):

$$R_{n-1}(z_c) = (-1)^n \frac{1}{n!} \left(\frac{z_c}{n-1} \right)^n \exp\left(-\frac{\xi}{n-1}\right). \quad (61)$$

Putting eqn.s (58) and (61) into (55), we get:

$$c_n(z_c) = \frac{1}{(n-1)n!} z_c^n e^{-z_c} \exp\left(-\frac{\xi}{n-1}\right), \quad (62)$$

which is still an exact result. It can be approximated by taking $\xi = 0$, which yields:

$$c_n(z_c) = \frac{1}{(n-1)n!} z_c^n e^{-z_c}. \quad (63)$$

This approximation becomes more accurate for larger n , since we have made a Taylor expansion around zero. The accuracy of eqn. (63) is illustrated in figure 17, where eqn. (63) is compared to the exact solution of eqn. (54).

6.5 Characteristics of the Exact Solution

Perhaps the most striking feature of the concentration distribution is the clear maximum that is found for the probability of finding defects that are approximately of order

$$n = z_c. \quad (64)$$

According to this, the position of the maximum changes with the amount of free volume z_c : this is indeed the case, as is shown in figure 18.

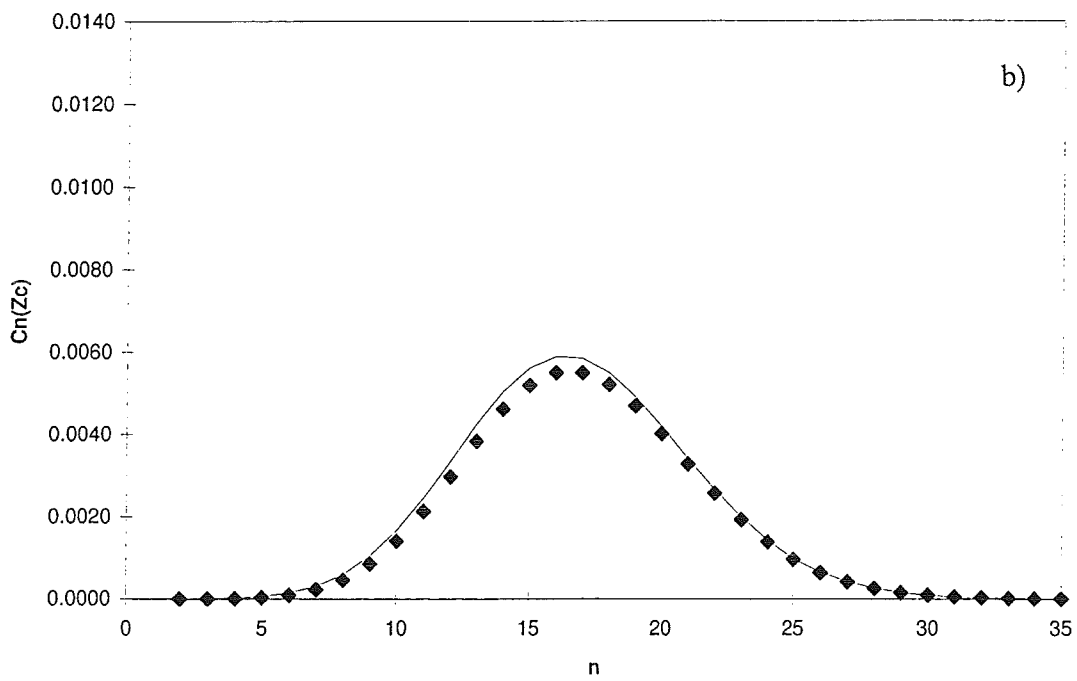
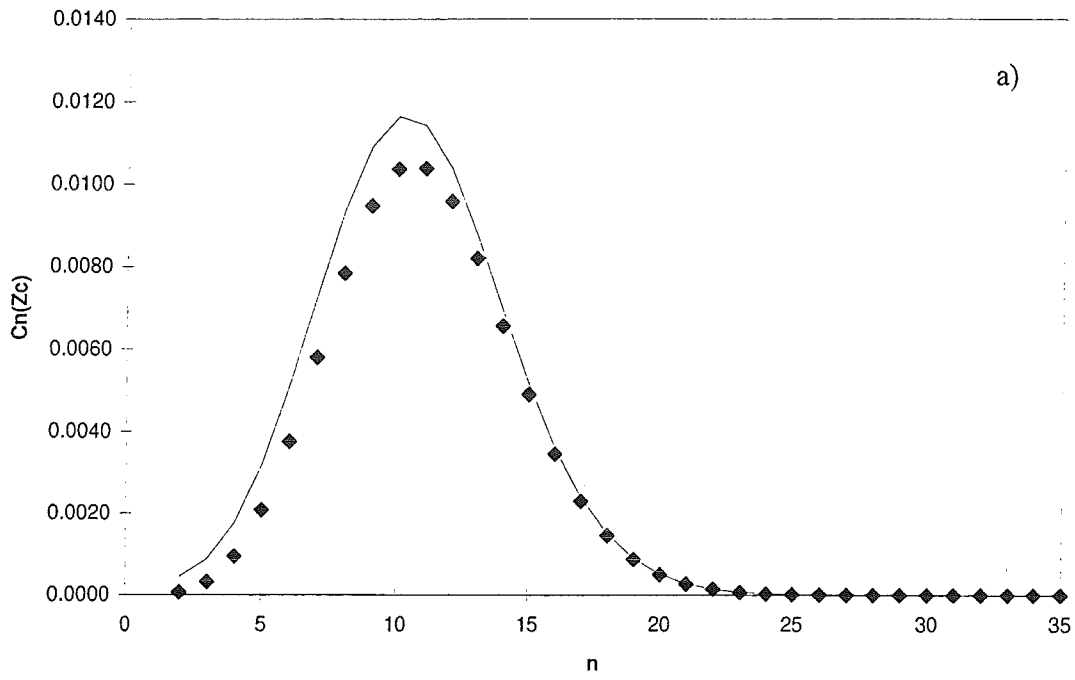


Figure 17: Plot of the Taylor approximation (solid line) of a) $c_n(12)$ and b) $c_n(18)$. The marker points represent the exact solution of figure 17.

Now why do we find a maximum? Obviously, the probability of *two* atoms having $z_1+z_2 \geq z_c$ is much bigger than *one* atom having $z_1 \geq z_c$; this is inherent to the free volume distribution itself. The reason that the probability c_n decreases for large n lies in our definition of a collective defect. This is most clear for a finite collection of atoms, as discussed in § 6.1. For increasing n , there are increasingly less atoms left to label and for some large n , we will even have $c_n=0$. In fact, we already have $c_n \approx 0$ for $n > 2z_c$.

The distribution is also surprisingly symmetrical around its maximum. The width of the peak is therefore a well-defined characteristic. In this case, the most practical definition of the width of the curve is the distance between the points of inflection. Since n is an integer, the second differential of $c_n(z_c)$ with respect to n is given by:

$$\frac{d^2 c_n(z_c)}{dn^2} = c_{n+1}(z_c) - 2c_n(z_c) + c_{n-1}(z_c). \quad (65)$$

The points of inflection are then given by:

$$\frac{d^2 c_n(z_c)}{dn^2} = 0. \quad (66)$$

For convenience, we take the Taylor approximation for $c_n(z_c)$ and put it into eqn. (65). The condition (66) then gives:

$$z_c^2 - 2n \frac{n+1}{n-1} z_c + n^2 \frac{n+1}{n-2} = 0. \quad (67)$$

If we take n as a continuous variable, eqn. (67) has two solutions, n_1 and n_2 (we define $n_1 < n_2$), for every value of z_c . The distance between the points of inflection is then given by:

$$\Delta n \equiv n_2 - n_1. \quad (68)$$

For physically realistic values of z_c , n_1 and n_2 are shown in table 6, together with Δn . In figure 18 Δn is shown as a function of z_c for the values in table 6, with a linear fit. The fit yields:

$$\Delta n = 0.253z_c + 4.074. \quad (69)$$

The concentration of *defects* of order n is $c_n(z_c)$. Since there are n atoms in a defect of order n , $nc_n(z_c)$ gives the concentration of *atoms* that are part of a defect of order n . Due to our definition of a defect, *every* atom in the structure belongs to *one* defect of a certain order n . Since the concentration of atoms must be equal to one, the concentration distribution must be normalised to:

$$\sum_{n=1}^{\infty} nc_n(z_c) = 1. \quad (70)$$

This normalisation can be used to check the correctness of an exact solution or the accuracy of an approximation.

The symmetry of the distribution around its maximum $z_c \approx n$ tells us that the average defect is of order $n \approx z_c$. Since every atom is part of a defect, the total defect concentration must be close to $1/z_c$:

$$\sum_{n=1}^{2z_c} c_n(z_c) \approx z_c^{-1} \quad (71)$$

where we have cut off the summation at $2z_c$, since $c_n(z_c)$ is effectively zero for $n \geq 2z_c$. This expression may be of more practical use than eqn. (70).

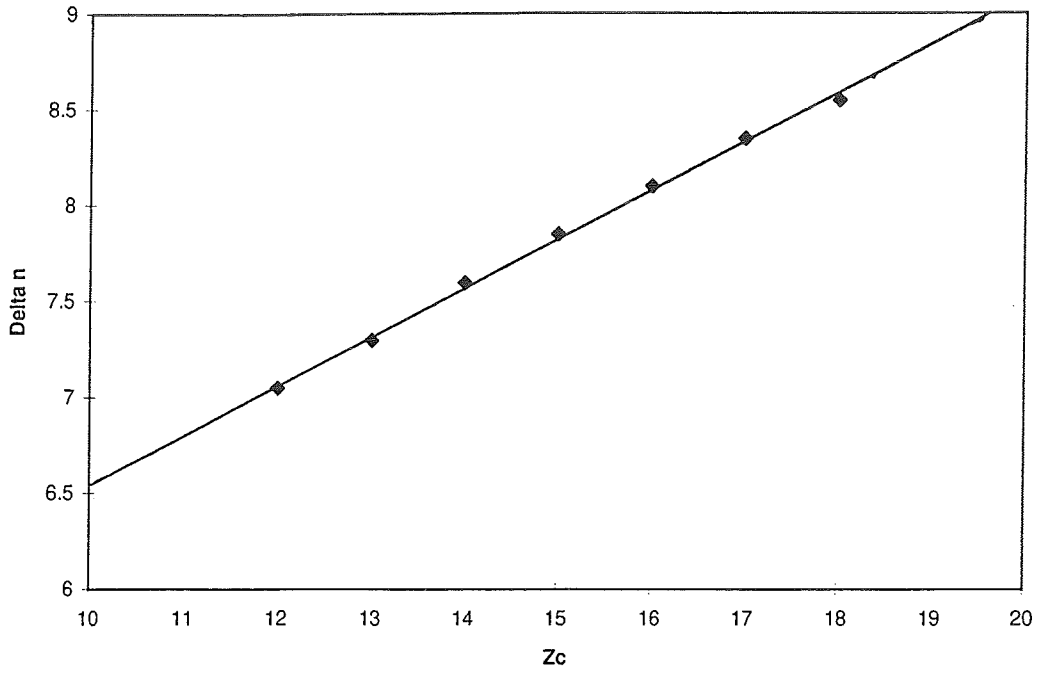


Figure 18: Plot of the peak width as a function of z_c .

Table 6: The peak width Δn as a function of z_c .

z_c	n_1	n_2	Δn
12	6.8	13.8	7.0
13	7.7	15.0	7.3
14	8.5	16.1	7.6
15	9.4	17.3	7.9
16	10.3	18.4	8.1
17	11.2	19.6	8.4
18	12.1	20.7	8.6

6.6 The Gaussian Approximation of $c_n(z_c)$

The shape of the concentration distribution rather resembles that of a Gaussian. Since a Gaussian is mathematically much more convenient to handle than our Taylor approximation, we shall try to fit a Gaussian to the exact solution. The general expression for a Gaussian concentration distribution is:

$$c_n(z_c) = \frac{A}{\sigma\sqrt{2\pi}} \exp\left[-\frac{1}{2}\left(\frac{n - \langle n \rangle}{\sigma}\right)^2\right] \quad (72)$$

where A is the normalisation constant of the Gaussian, $\langle n \rangle$ is the average order of a defect and σ is the standard deviation. A, $\langle n \rangle$ and σ are calculated for the exact solution using:

$$A \equiv \sum_{n=1}^{\infty} c_n \quad (73)$$

$$\langle n \rangle \equiv \sum_{n=1}^{\infty} n c_n \left(\sum_{n=1}^{\infty} c_n \right)^{-1} \quad (74)$$

$$\sigma = \sqrt{\langle n^2 \rangle - \langle n \rangle^2} \quad (75)$$

where we have used

$$\langle n^2 \rangle \equiv \sum_{n=1}^{\infty} n^2 c_n \left(\sum_{n=1}^{\infty} c_n \right)^{-1} \quad (76)$$

This yielded $A=0.0903$, $\langle n \rangle=11.07$ and $\sigma=3.401$. In figure 19, the Gaussian approximation is shown for these parameters compared to the exact solution of figure 17 for $z_c=12$ and $z_c=18$.

6.7 Discussion

Checking the normalisation with eqn. (70) yields:

$$\sum_{n=2}^{25} n c_n(12) = 0.99 \quad \text{for the exact solution,}$$

$$\sum_{n=2}^{25} n c_n(12) = 1.10 \quad \text{for the Taylor approximation and}$$

$$\sum_{n=2}^{25} n c_n(12) = 0.99 \quad \text{for the Gaussian approximation.}$$

Taking the sum over a wider range of values of n does not change the outcome significantly. The result indicates that the calculation that lead to the exact solution was correct and that the Taylor and Gaussian approximations seem to be accurate enough to be useful.

It is inherent to the treatment that every atom in the structure is part of a defect and every atom therefore contributes to diffusion. At first sight, this concept may seem to be unrealistic. On second thought, however, it is not necessarily wrong. Although the meaning of the word defect is indeed lost, we have no strong indication that there are atoms present in the amorphous structure whose equilibrium positions can not change at all at any certain time. One may argue that too small changes in the equilibrium position do not qualify as diffusion, but this is only a practical matter.

The key result of our calculation is that for $\text{Pd}_{40}\text{Ni}_{40}\text{P}_{20}$, defects defined by typically 5 to 20 atoms in the as-quenched state and typically 10 to 25 atoms in equilibrium at 540 K have a concentration that is much bigger than that of any other defect size. This result seems to be in

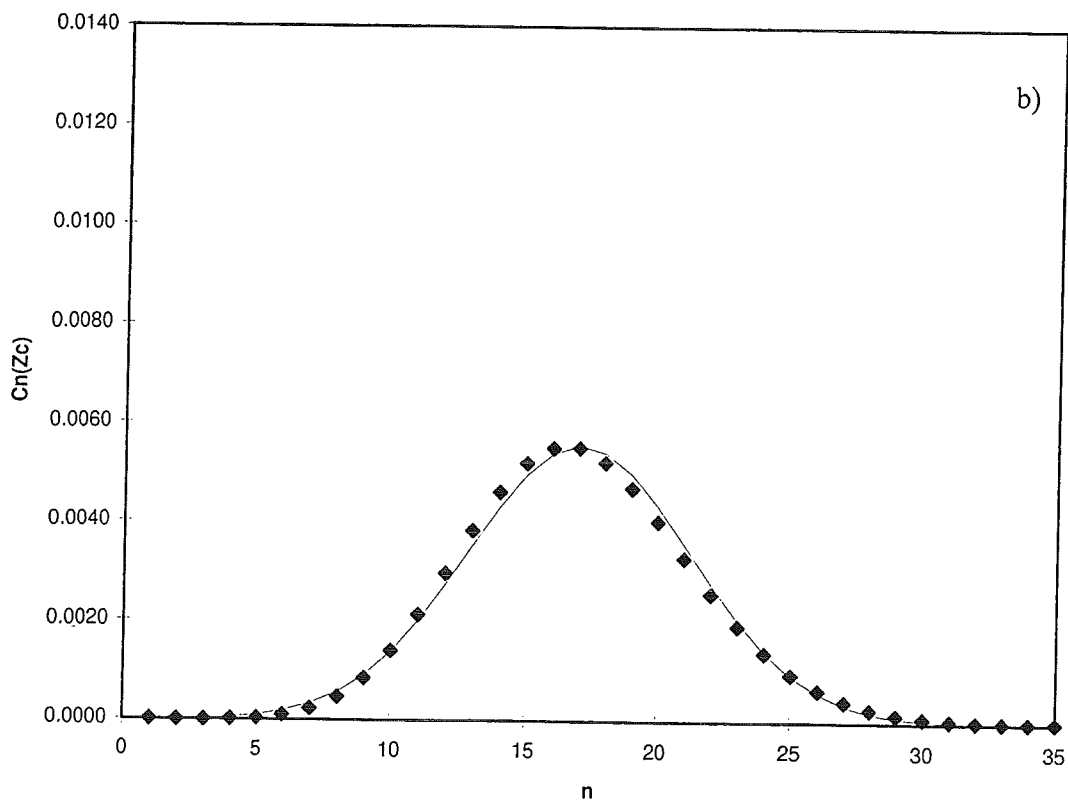
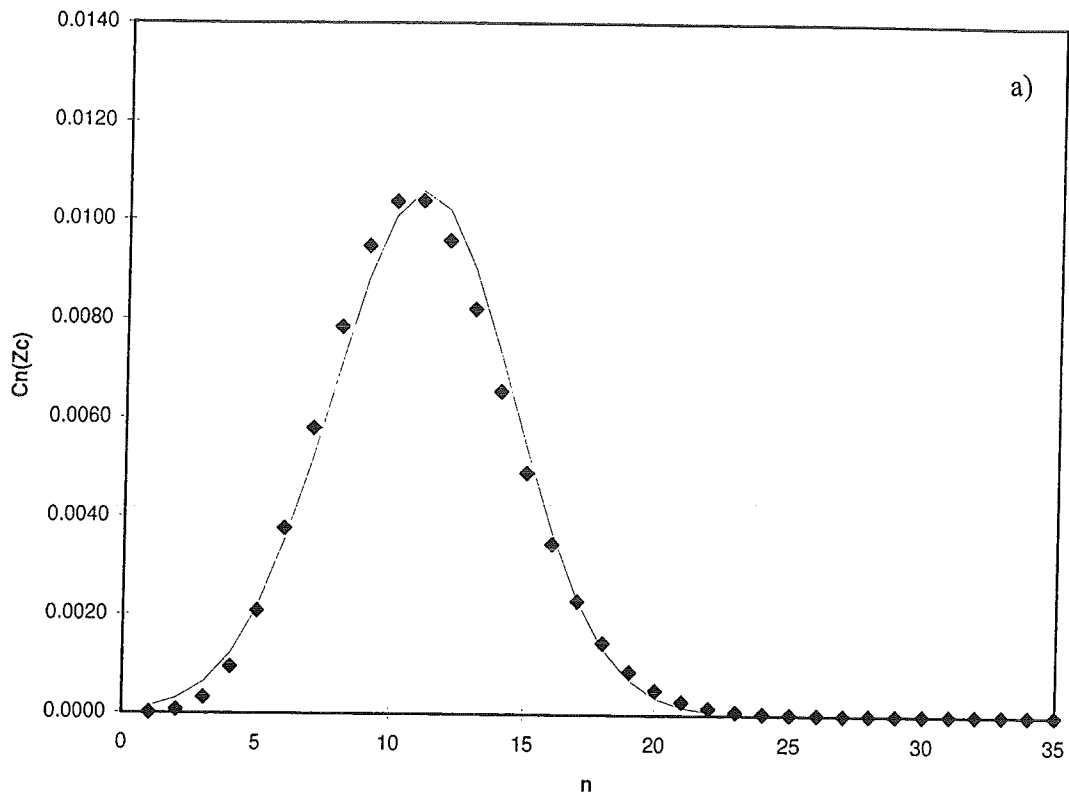


Figure 19: Plot of the Gaussian approximation (solid line) of a) $c_n(12)$ and b) $c_n(18)$. The marker points represent the exact solution of figure 17.

clear agreement with the results of the measurements of the isotope effect. It is noted, however, that the migration enthalpy, the attempt frequency and the jump distance may all depend on the order of the defect as well and these parameters determine the contribution to diffusion of the defects.

In fact, at least one of these parameters *must* have an n -dependence to make this model agree with the experimental diffusion data. For if every defect had the same contribution to diffusion, the only parameter of interest would be the *sum* of the concentrations of all the defects, which is roughly z_c^{-1} , and hence the whole calculation would collapse. And this would be inconsistent with the experimental observation, since the diffusivity does not depend linearly up on z_c^{-1} .

In the past, a Gaussian distribution of migration enthalpies has been introduced by Knuyt et al. [35]. It has not been attempted to make a qualitative model of diffusion by putting the result of the present calculation, together with a Gaussian distribution of migration enthalpies into a diffusion equation. Originally, this was the aim, but there was not enough time for even a preliminary attempt.

REFERENCES

- [1] K. Rätzke, P.W. Hüppe and F. Faupel, *Phys. Rev. Lett.* **68** (1992) p. 2347.
- [2] P. Duwez, R.W. Willens and W. Klemert, *Nature* **187** (1960) p. 869.
- [3] R.B. Schwarz and W.L. Johnson, *Phys. Rev. Lett.* **51** (1983) p. 415.
- [4] C. Kittel, *Introduction to Solid State Physics*, 6th Edition, J. Wiley & Sons (1986).
- [5] B.J. Thijsse, unpublished result (1985).
- [6] P.A. Duine, J. Sietsma and A. van den Beukel, *Acta Metall. Mater.* **40** (1992) p. 743.
- [7] J.M. Delaye and Y. Limoge, *J. Non-Cryst. Solids* **156-158** (1993) p. 982.
- [8] G.W. Koebrugge, *PhD Thesis*, Delft University of Technology, Netherlands (1991).
- [9] R.L. McGreevy and L. Pusztai, *Mol. Simul.* **1** (1988) p. 359.
- [10] J. Sietsma and B.J. Thijsse, *Phys. Rev. B* **52** (1995) p. 3248.
- [11] A. Hörner, *PhD Thesis*, Max-Planck-Institut für Metallforschung, Stuttgart (1993).
- [12] B.J. Thijsse, L.D. van Ee and J. Sietsma, *MRS Proc.* **321** (1994) p. 65.
- [13] L.D. van Ee, B.J. Thijsse and J. Sietsma, to appear in *Mat. Sci. & Eng.* (1997).
- [14] R.W. Keyes, *J. Chem. Phys.* **29** (1958) p. 467.
- [15] C.P. Flynn, *Point defects and diffusion*, Clarendon Press, Oxford (1972) p. 306
- [16] J.P. Poirier and R.C. Liebermann, *Phys. Earth Planet. Inter.* **35** (1985) p. 283.
- [17] N.W. Ashcroft and N.D. Mermin, *Solid State Physics*,
Int. Edition, Saunders College Publishing (1976).
- [18] A. Grandjean and Y. Limoge, to appear in *Acta Metall.* (1997).
- [19] D. Turnbull and M.H. Cohen, *J. Chem. Phys.* **29** (1958) p. 1049;
M.H. Cohen and D. Turnbull, *ibid.* **31** (1959) p. 1164; **34** (1961) p. 120.
- [20] A. van den Beukel, *Scripta Metall. Mater.* **22** (1988) p. 877.
- [21] P.A. Duine, *PhD Thesis*, Delft University of Technology,
Delft, The Netherlands (1994).
- [22] F. Spaepen and D. Turnbull, *Scripta Metall. Mater.* **25** (1991) p. 1563.
- [23] M.H. Cohen and D. Turnbull, *J. Chem. Phys.* **31** (1959) p. 1164.
- [24] Y. Limoge, *Scripta Metall. Mater.* **26** (1992) p. 809.
- [25] A. van den Beukel, unpublished result (1992).
- [26] A. van den Beukel and J. Sietsma, *Acta Metall. Mater.* **38** (1990) p. 383.
- [27] P. Tuinstra, P.A. Duine, J. Sietsma and A. van den Beukel,
Acta Metall. Mater. **43** (1995) p. 2815.
- [28] P.A. Duine, S.K. Wonnell and J. Sietsma, *Mat. Sci. & Eng.* **A179/A180** (1994) p. 270.
- [29] B. Zappel and F. Sommer, *Mater. Sci. & Eng.* **A179/A180** (1994) p. 283.
- [30] B. Zappel, *PhD Thesis*, Max-Planck-Institut für Metallforschung,
Stuttgart, Germany (1995).
- [31] P.A. Duine, J. Sietsma and A. van den Beukel, *Phys. Rev. B* **48** (1993) p. 6957.
- [32] H. S. Chen et al., *J. Non-Cryst. Sol.* **13** (1973/74) p. 321.
- [33] L.A. Davis, *Proc. II Int. Conf. Rapidly Quenched Metals*,
(ed. N.J. Grant and B.C. Giessen), MIT Press (1976) p. 369.
- [34] B. Golding, B.G. Bagley and F.S.L. Hsu, *Phys. Rev Lett.* **29** (1972) p. 68.
- [35] G. Knuyt, L.M. Stals and L. De Schepper, *Phil. Mag. B* **63** (1991) p. 1289.

APPENDIX A

The starting point for this derivation is the Arrhenius equation:

$$D(T) = D_0 \exp\left(-\frac{\Delta H}{k_B T}\right) \quad (\text{A.1})$$

with

$$D_0 = ab\lambda^2 v \exp\left(\frac{\Delta S}{k_B}\right) \quad (\text{A.2})$$

where a is a geometrical factor, b is a correlation factor, λ is the jump distance, v is the attempt frequency and ΔS is the activation entropy. Combining eqn.s (A.1) and (A.2) and taking the logarithm yields:

$$\ln(D) = \ln(ab\lambda^2 v) - \frac{\Delta H - T\Delta S}{k_B T} \quad (\text{A.3})$$

We now use the thermo-dynamical relations

$$G = H - TS \quad (\text{A.4})$$

and

$$V = \left(\frac{\partial G}{\partial p}\right)_T \quad (\text{A.5})$$

and putting eqn. (A.3) and eqn. (A.4) into eqn. (A.5), we get for an isothermal process:

$$\Delta V = \left(\frac{\partial(\Delta H - T\Delta S)}{\partial p}\right)_T = -k_B T \left[\left(\frac{\partial \ln D}{\partial p}\right)_T - \left(\frac{\partial \ln(ab\lambda^2 v)}{\partial p}\right)_T \right] \quad (\text{A.6})$$

Neglecting the pressure dependence of the jump distance and the attempt frequency gives:

$$\Delta V = -k_B T \left(\frac{\partial \ln D}{\partial p}\right)_T \quad (\text{A.7})$$

APPENDIX B

Derivation of Equation (38)

The bulk modulus B is defined as:

$$B^{-1} \equiv \frac{-1}{V} \frac{dV}{dp} \quad (\text{B.1})$$

Consider an amorphous structure of N atoms. The volume can be thought to consist of two contributions: the volume of the ideally amorphous structure V_{id} and the free volume $V_f = N \langle v_f \rangle$ (where $\langle v_f \rangle$ is the average free volume per atom). Hence, we have:

$$V = V_{id} + N \langle v_f \rangle \quad (\text{B.2})$$

From eqn.(B.1) and eqn.(B.2), we have:

$$B^{-1} = -\frac{1}{V} \frac{dV_{id}}{dp} - \frac{N}{V} \frac{d \langle v_f \rangle}{dp} \quad (\text{B.3})$$

for which we can write:

$$B^{-1} = B_o^{-1} - \frac{1}{\Omega} \frac{d \langle v_f \rangle}{dp} \quad (\text{B.4})$$

where we have used $V = N\Omega$ (Ω is the atomic volume) and B_o is the bulk modulus of the ideally amorphous structure.

From this equation, the dependence of the free volume on pressure can be calculated. Measurements of Young's modulus as a function of the free volume have indicated that the relation between these two quantities is linear. Assuming that this is also the case for the bulk modulus, we have:

$$B = B_o - c \langle v_f \rangle \quad (\text{B.5})$$

where c is a positive constant. Putting this into eqn.(B.4), we have for the pressure dependence of the free volume:

$$\frac{d \langle v_f \rangle}{dp} = \frac{\Omega}{B_o} \left(1 - \frac{1}{1 - (c \langle v_f \rangle / B_o)} \right) \approx \frac{\Omega}{B_o} \left(1 - \left(1 + \frac{c \langle v_f \rangle}{B_o} \right) \right) = -\frac{\Omega}{B_o^2} c \langle v_f \rangle \quad (\text{B.6})$$

The approximation holds when $B_o \gg c \langle v_f \rangle$. Defining $c' \equiv c\Omega/B_o^2$, we have in terms of the reduced free volume x :

$$\frac{dx}{dp} = -c' x \quad (\text{B.7})$$

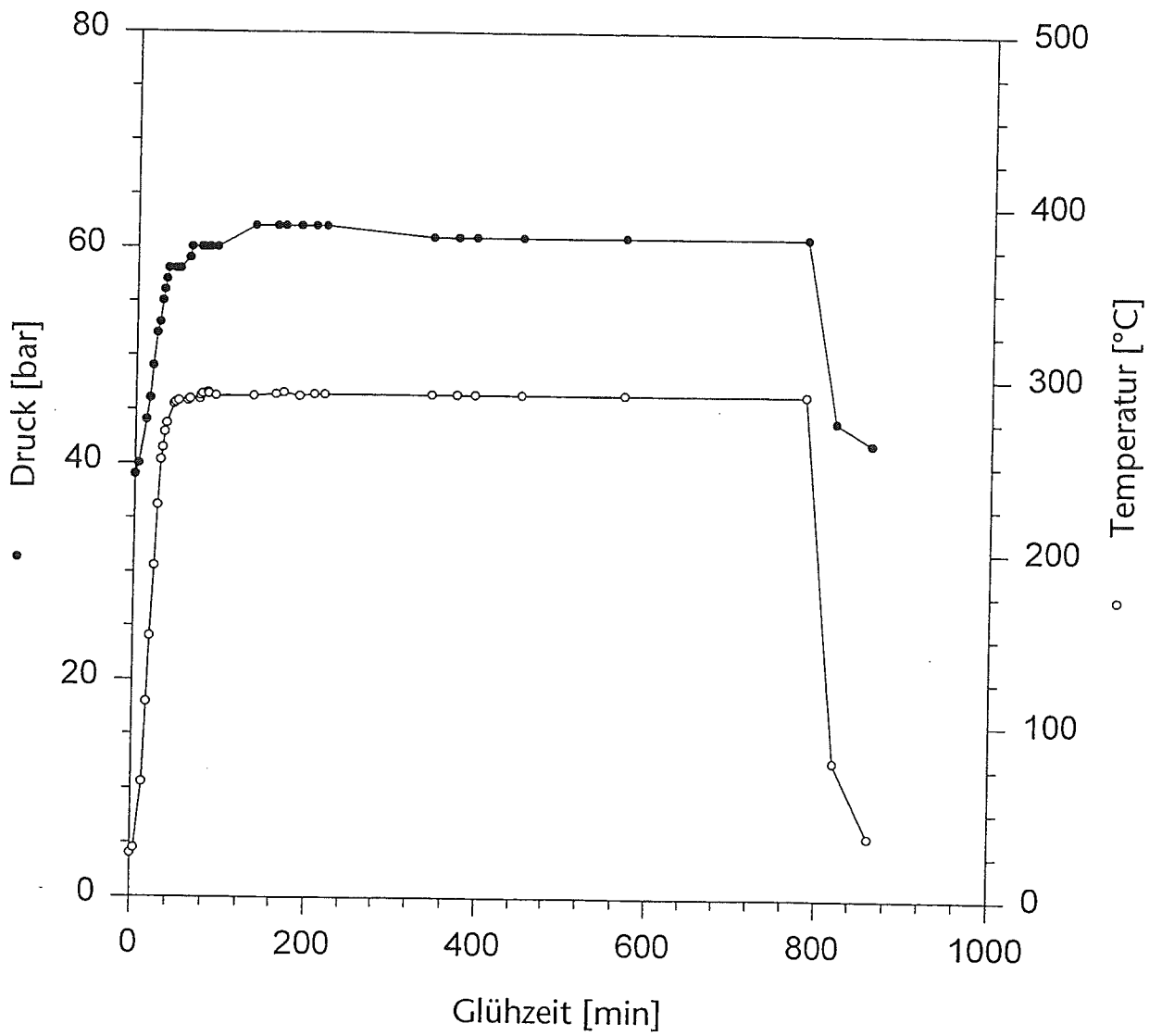
which we can integrate to give:

$$x(p, T) = x(0, T) \exp(-c' p) \quad (\text{B.8})$$

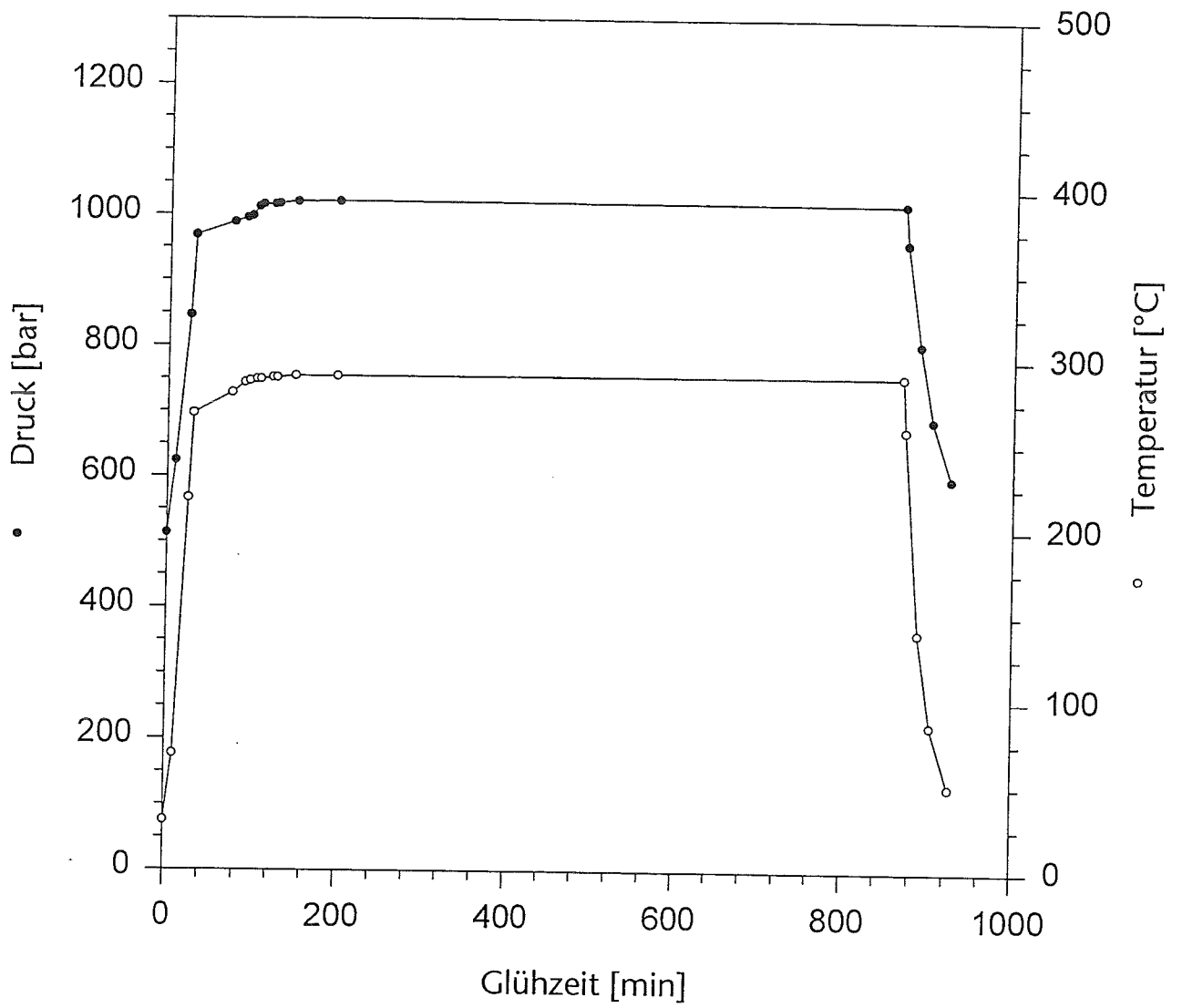
APPENDIX C

The Temperature and Pressure as a Function of Time during the Pressure Anneals

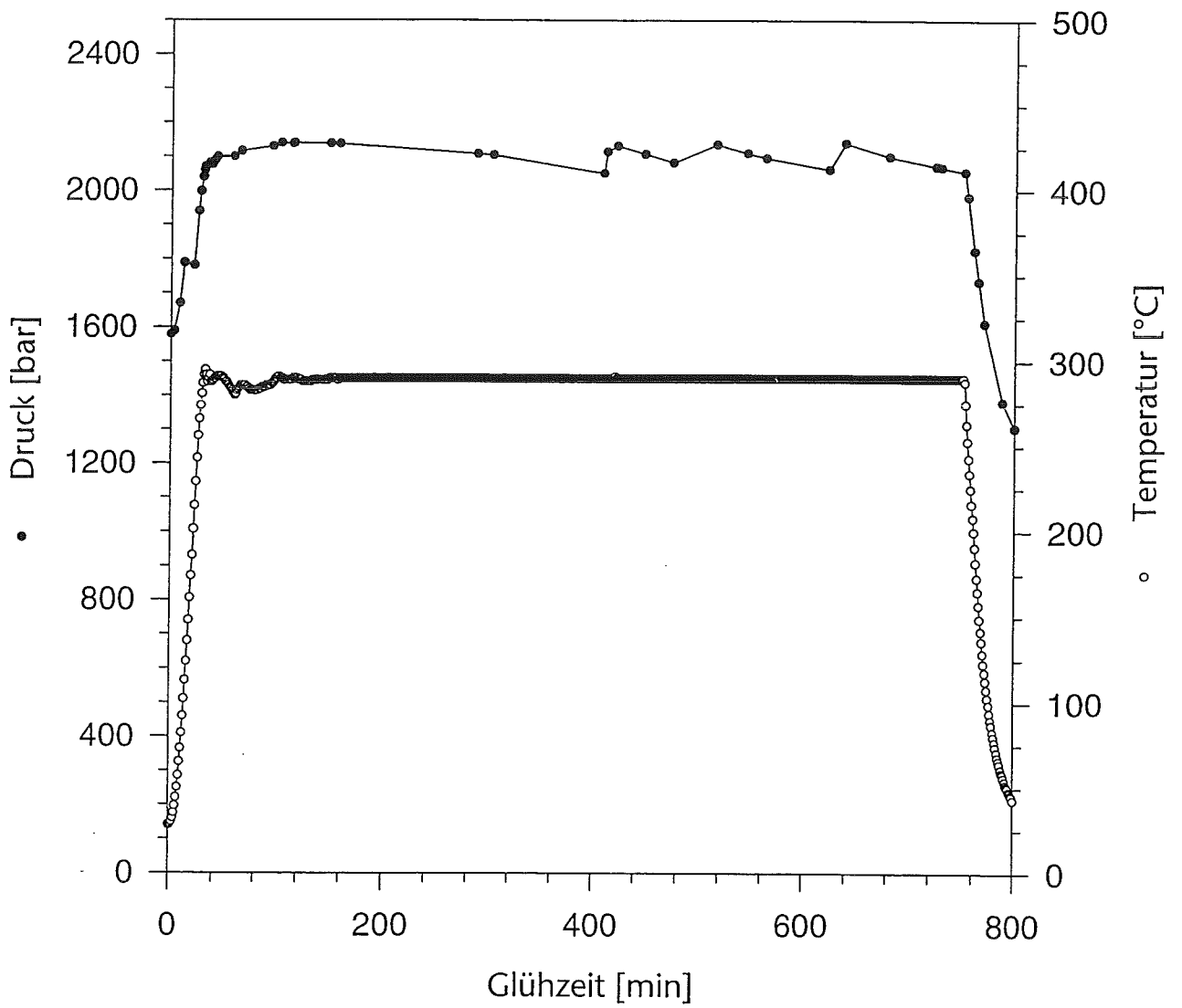
p=0.006 GPa



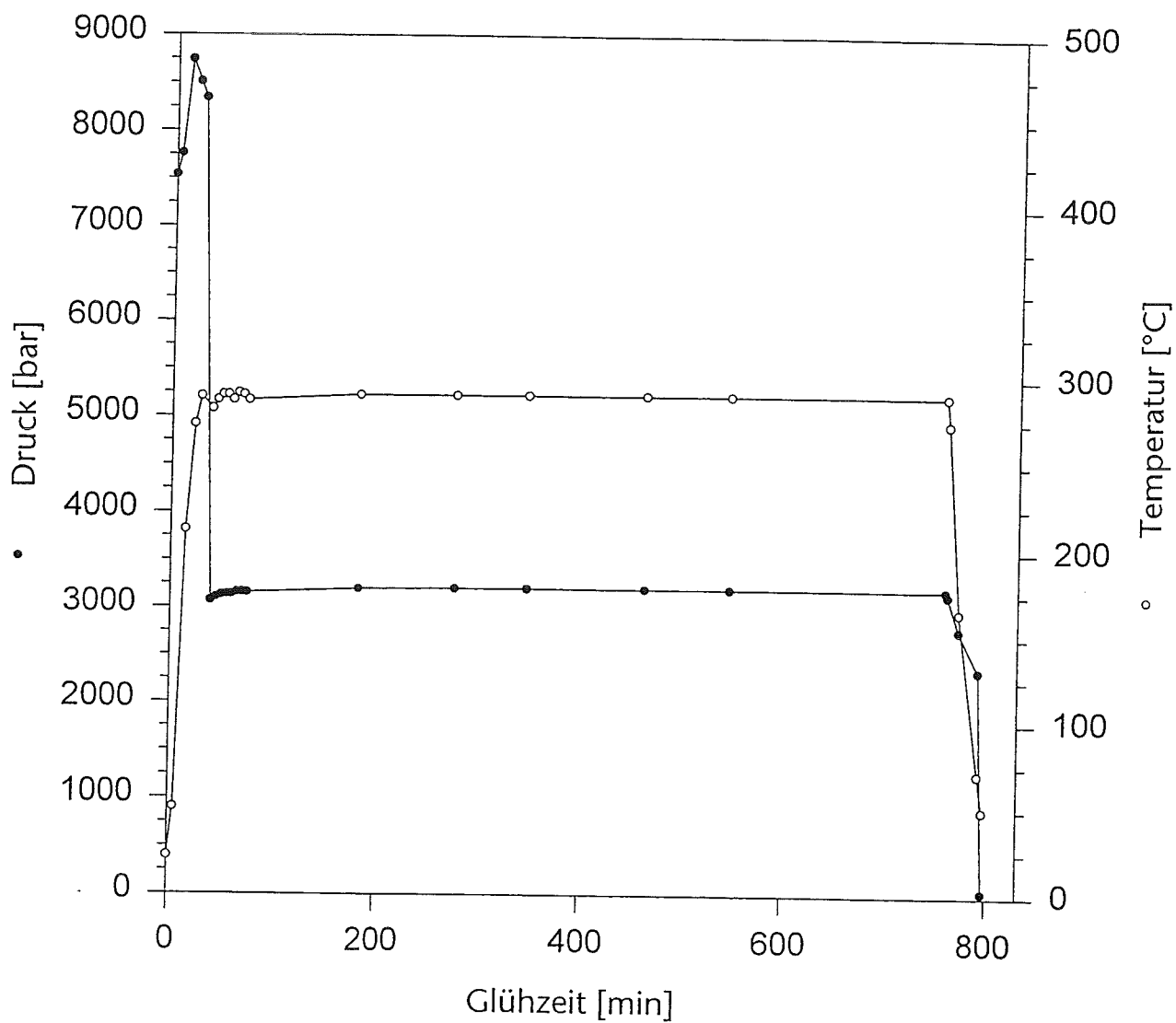
p=0.10 GPa



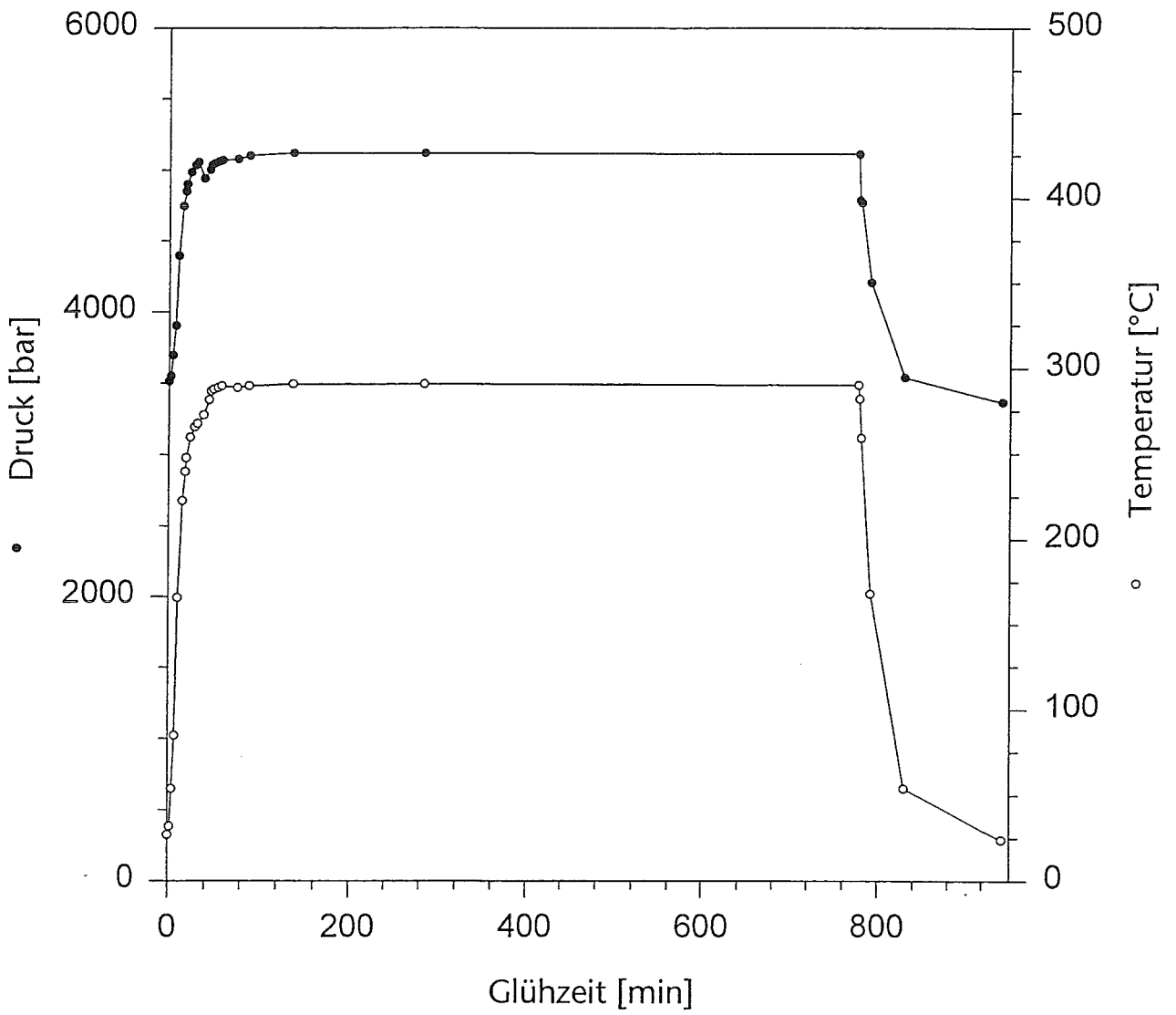
p=0.21 GPa



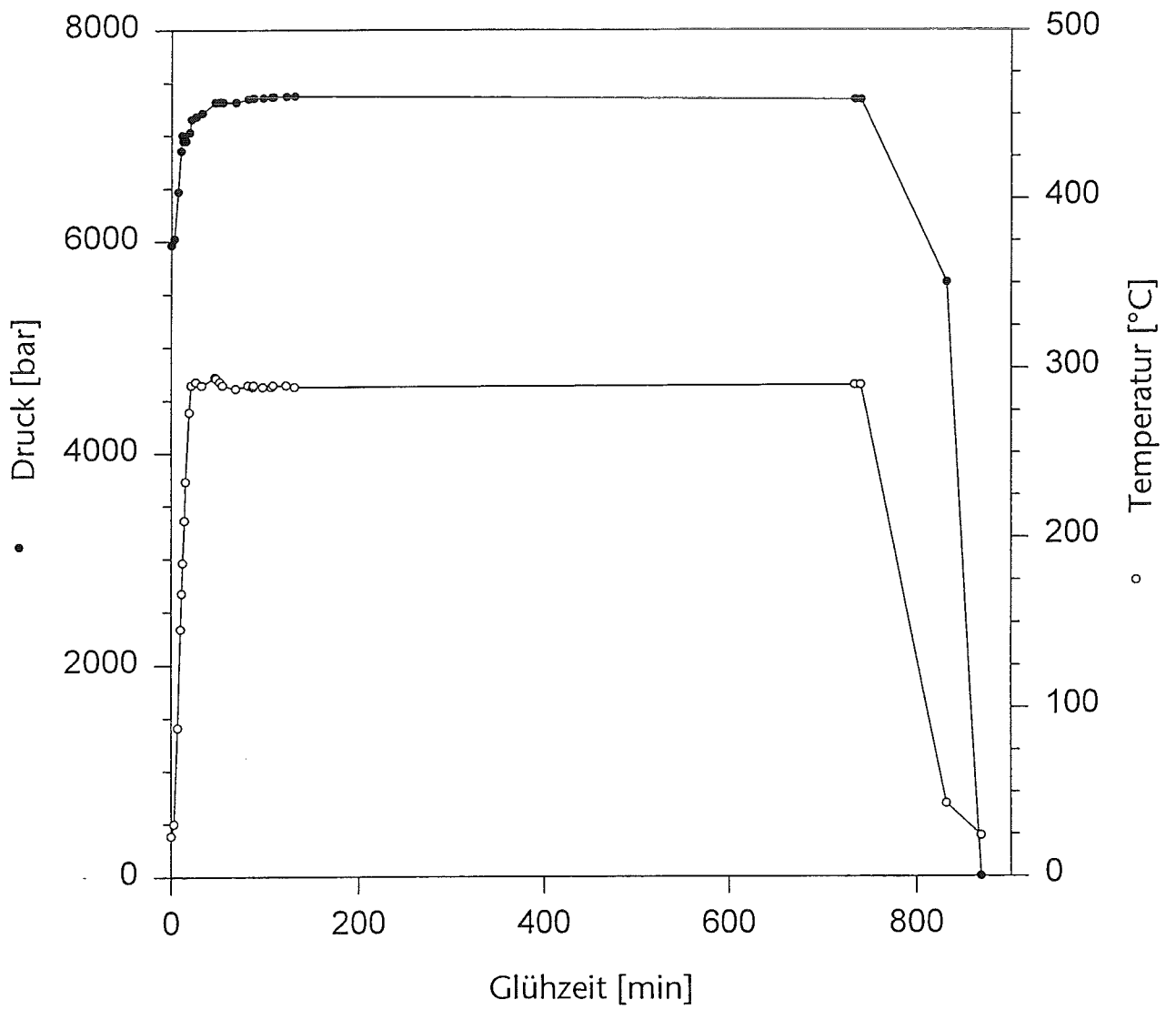
p=0.32 GPa



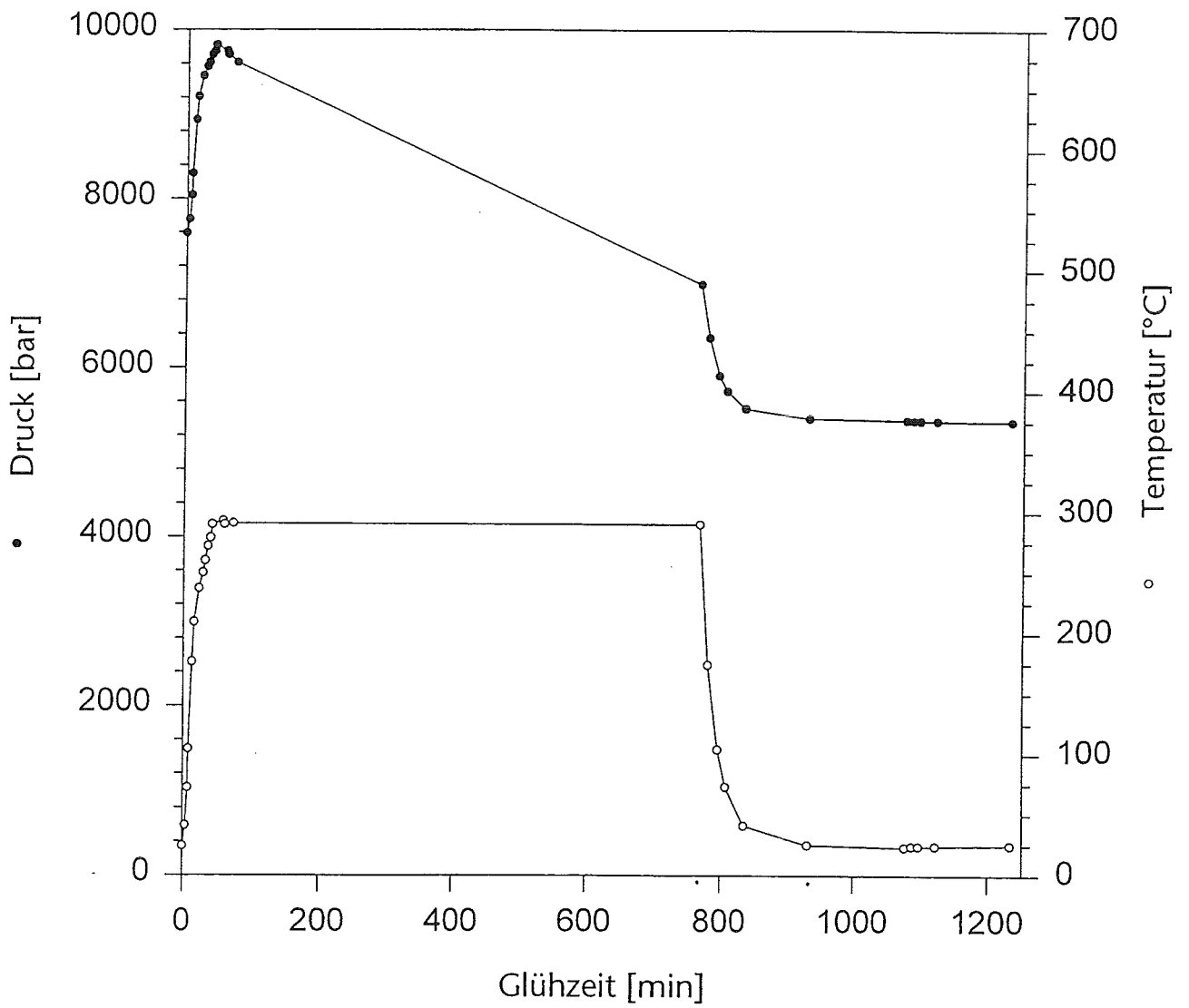
p=0.51 GPa



p=0.74 GPa



p=0.84 GPa



APPENDIX D

The Original DSC Measurements

Pd40Ni40P20-SF2-SR40-ESP42-27.06

Mass = 9.341 mg

Heating Rate = 40.00 K/min

Tmin = 320.0 K

Molweight = 73.466 g/mol

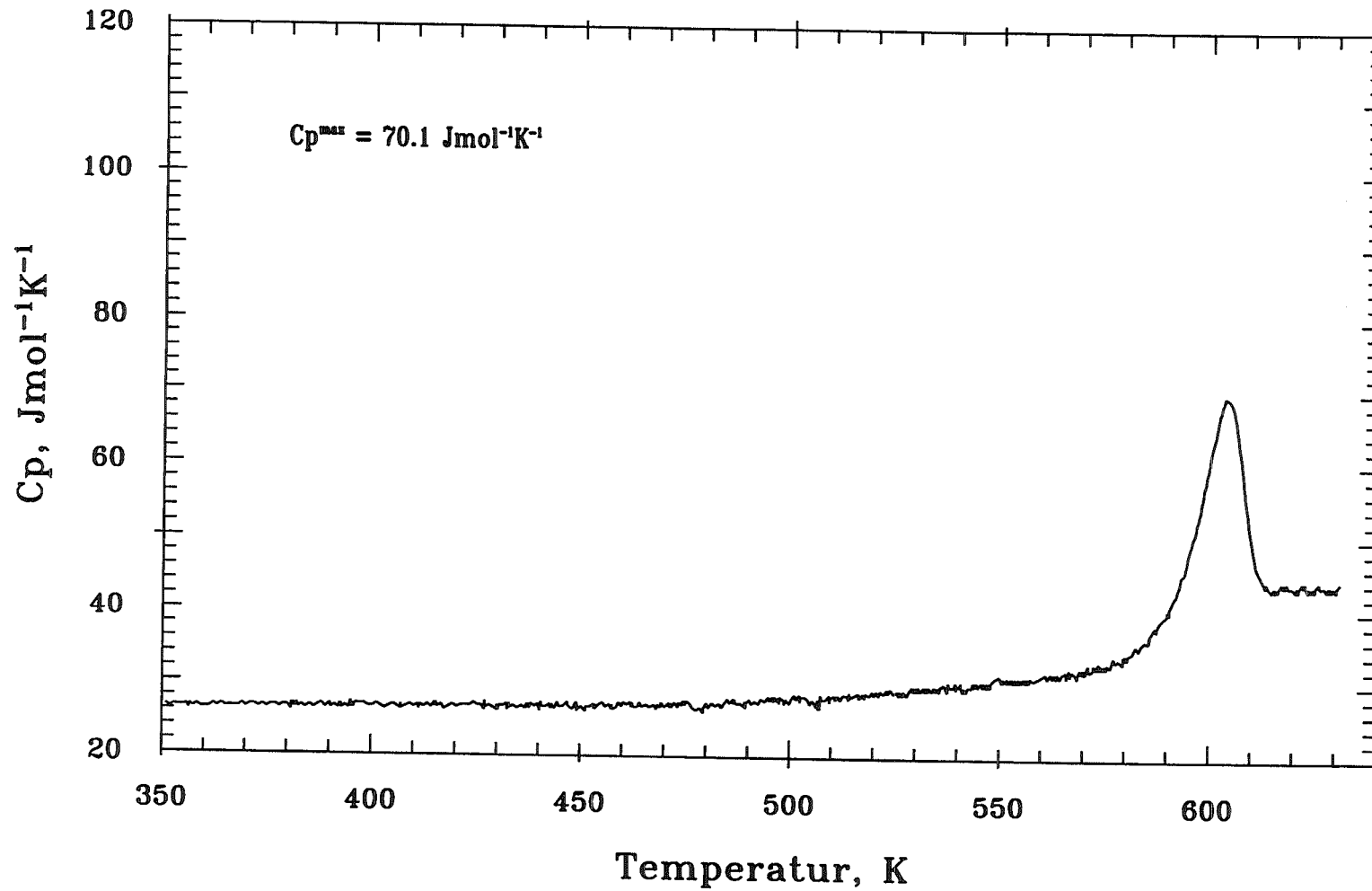
Cooling Rate = 40.00 K/min

Tmax = 640.0 K

Saphir Mass = 33.958 mg

Range = 10.0 mcal/s

$\rho = 0,02 \text{ GPa}$



Pd40Ni40P20-SF2-SR40-ES43-01.07

Mass = 12.830 mg

Heating Rate = 40.00 K/min

Tmin = 320.0 K

Molweight = 73.466 g/mol

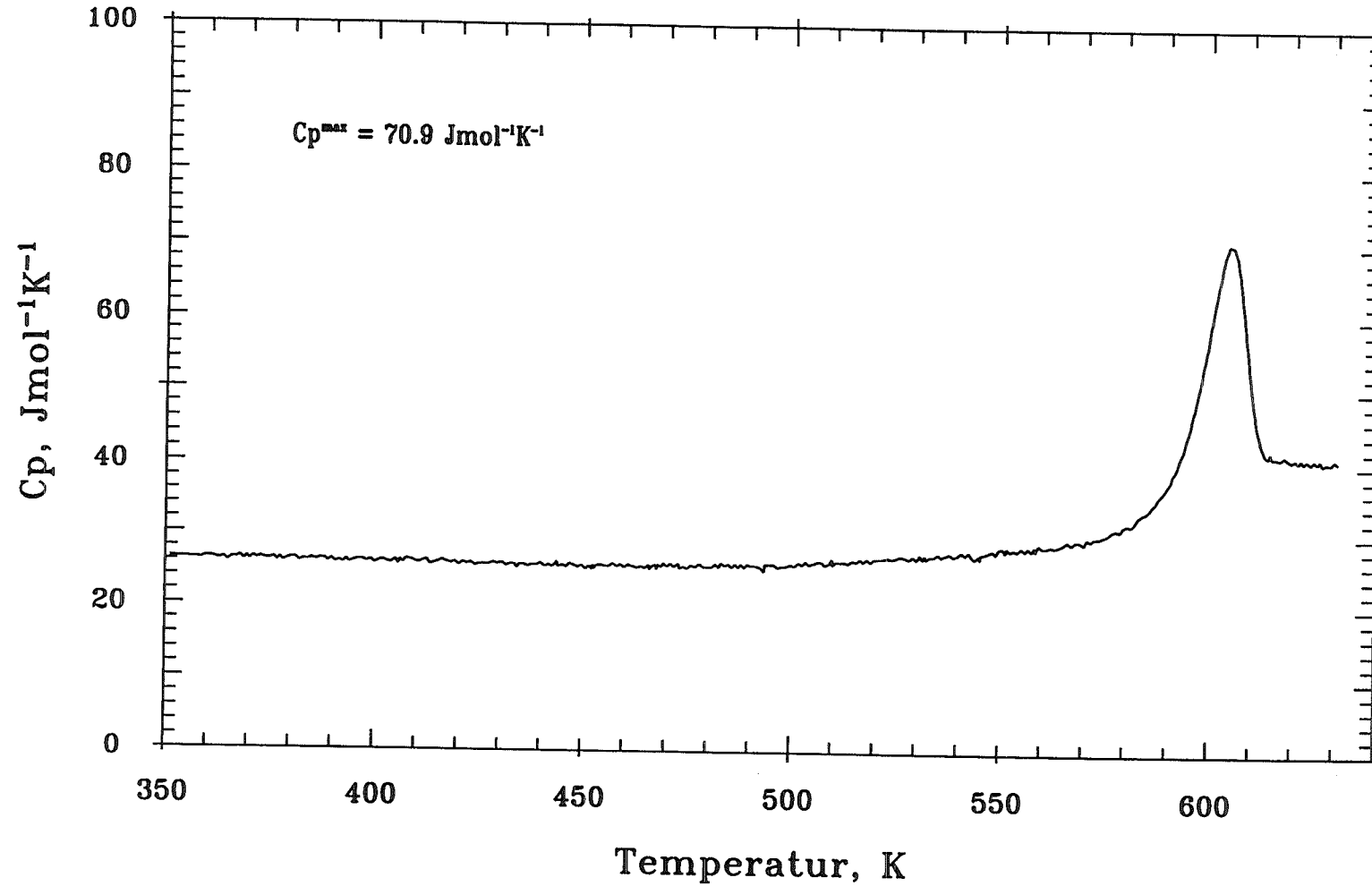
Cooling Rate = 40.00 K/min

Tmax = 640.0 K

Saphir Mass = 33.958 mg

Range = 10.0 mcal/s

$p = 0,23 \text{ GPa}$



Pd40Ni40P20-SF2-SR40-ESP45-28.06

Mass = 6.424 mg

Heating Rate = 40.00 K/min

Tmin = 320.0 K

Molweight = 73.466 g/mol

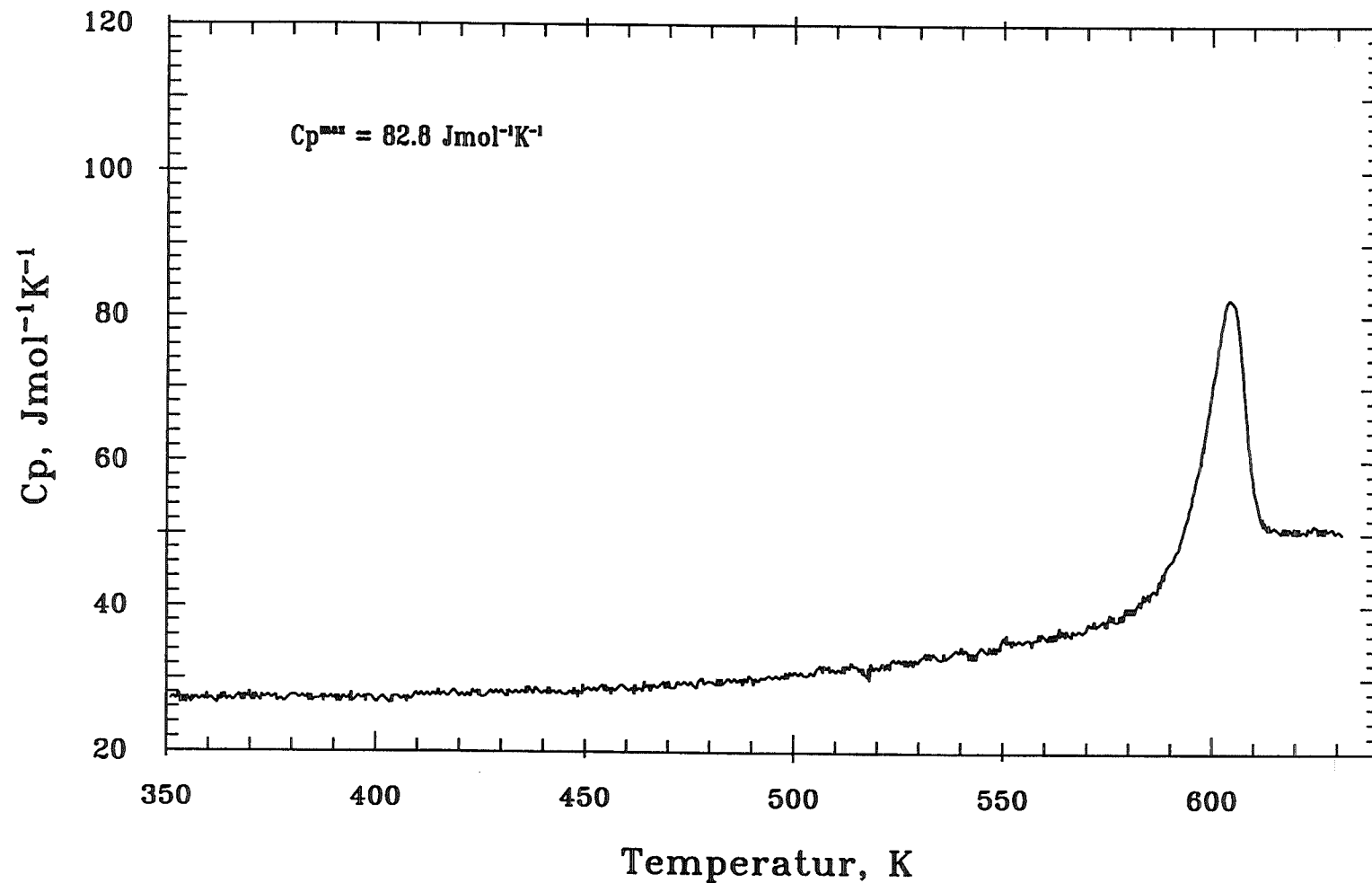
Cooling Rate = 40.00 K/min

Tmax = 640.0 K

Saphir Mass = 33.958 mg

Range = 10.0 mcal/s

$p = 0,43 \text{ GPa}$



Pd40Ni40P20-SF2-SR40-ESP46-28.06

Mass = 14.446 mg

Heating Rate = 40.00 K/min

Tmin = 320.0 K

Molweight = 73.466 g/mol

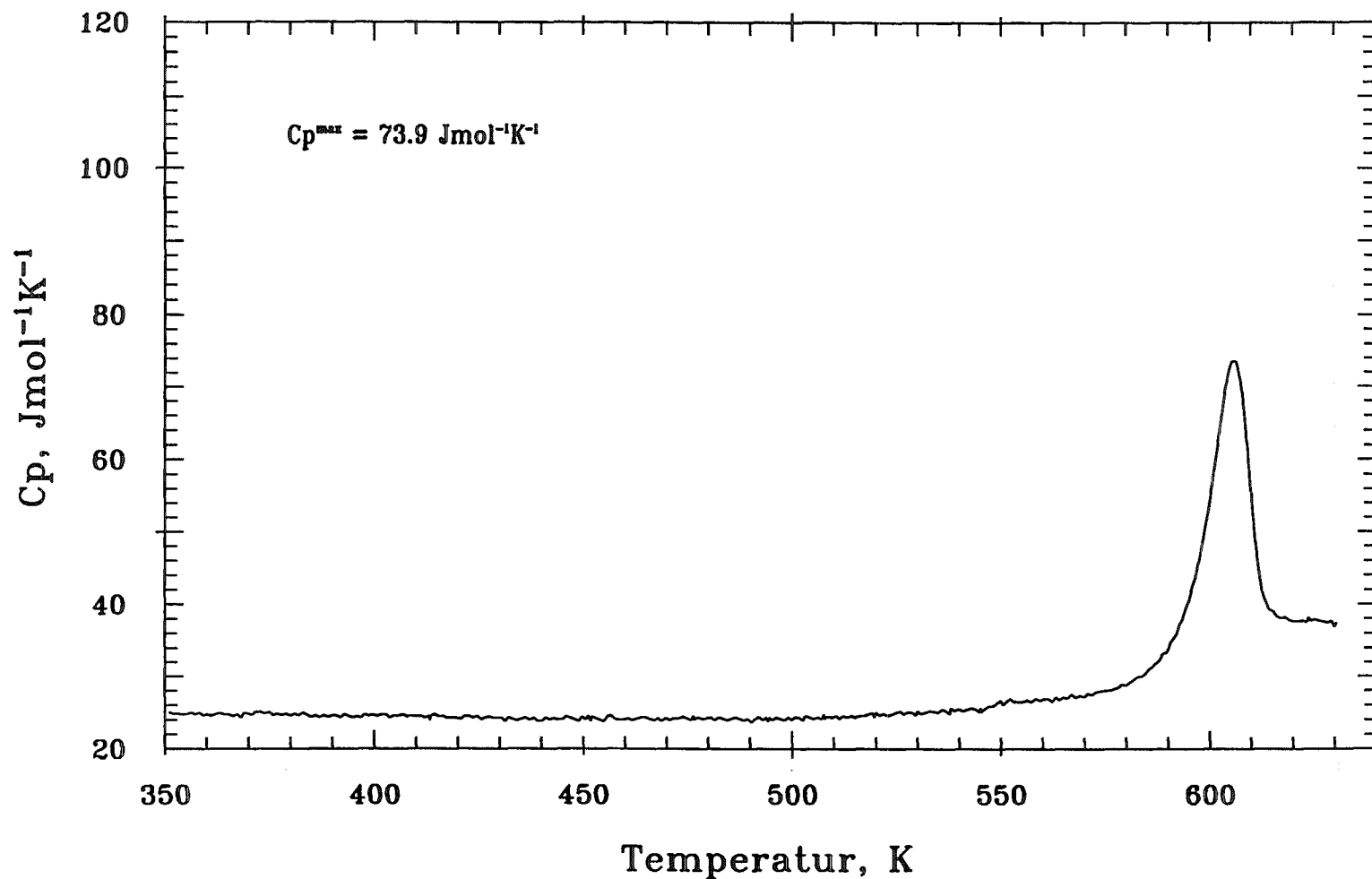
Cooling Rate = 40.00 K/min

Tmax = 640.0 K

Saphir Mass = 33.958 mg

Range = 10.0 mcal/s

$p = 0,75 \text{ GPa}$



Pd40Ni40P20-SF2-SR40-ESP67-27.07

Mass = 19.872 mg

Heating Rate = 40.00 K/min

Tmin = 320.0 K

Molweight = 73.466 g/mol

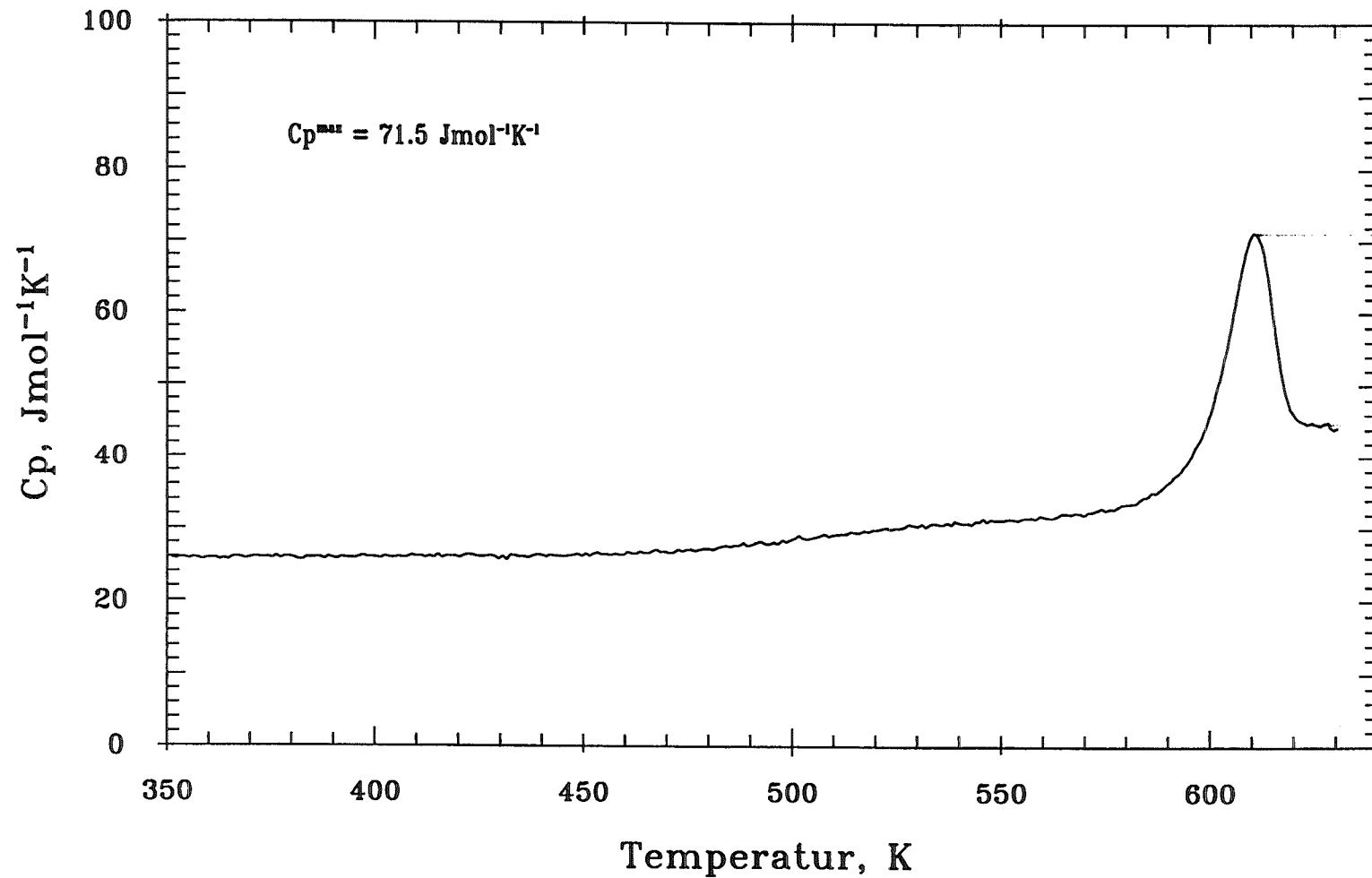
Cooling Rate = 40.00 K/min

Tmax = 640.0 K

Saphir Mass = 33.958 mg

Range = 10.0 mcal/s

p = 61 bar



Pd40Ni40P20-SF2-SR40-ESP68-27.07

Mass = 19.383 mg

Heating Rate = 40.00 K/min

Tmin = 320.0 K

Molweight = 73.466 g/mol

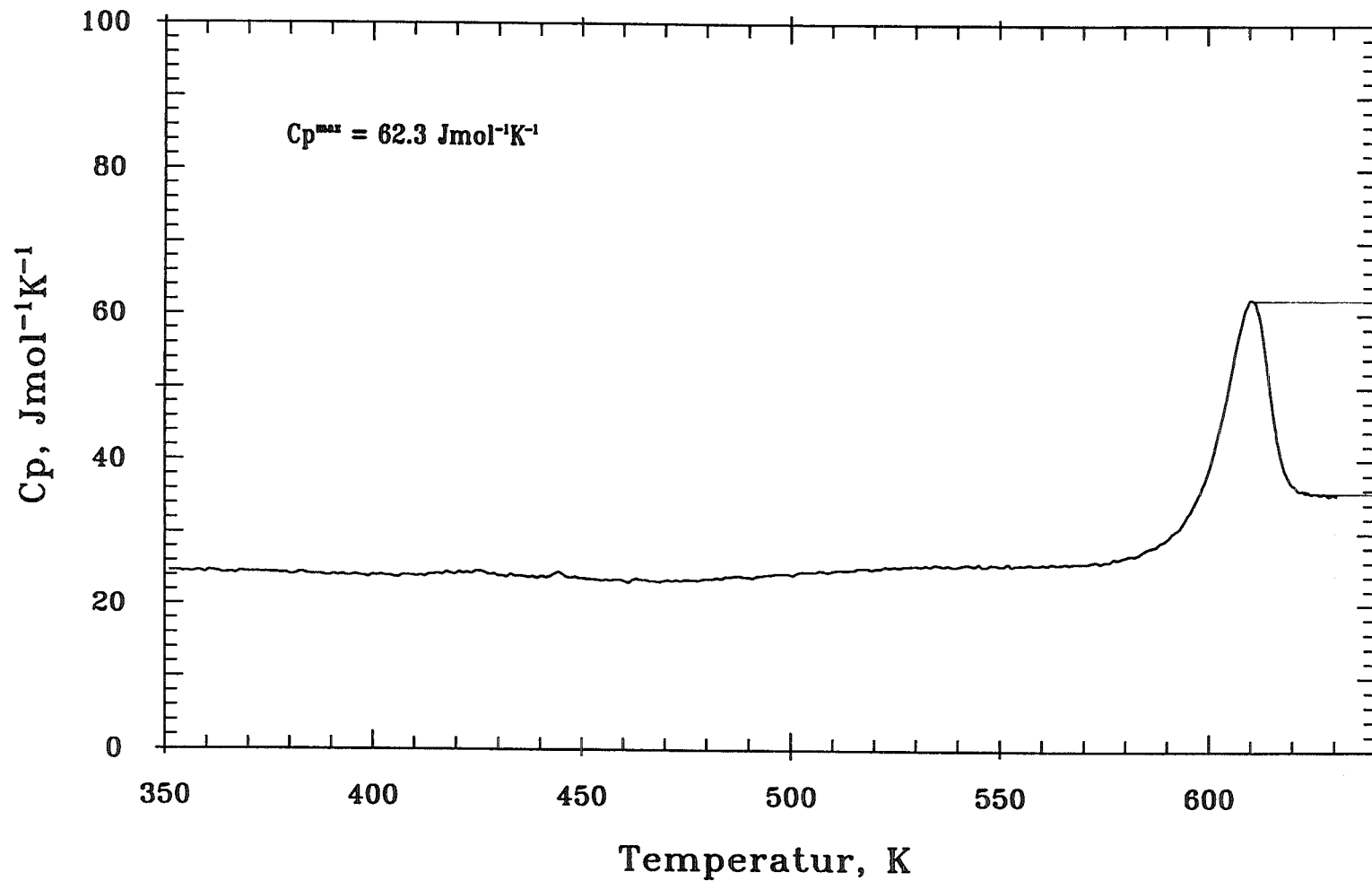
Cooling Rate = 40.00 K/min

Tmax = 640.0 K

Saphir Mass = 33.958 mg

Range = 10.0 mcal/s

p = 61 bar



Pd40Ni40P20-SF2-SR40-ESP62-26.07

Mass = 19.972 mg

Heating Rate = 40.00 K/min

Tmin = 320.0 K

Molweight = 73.466 g/mol

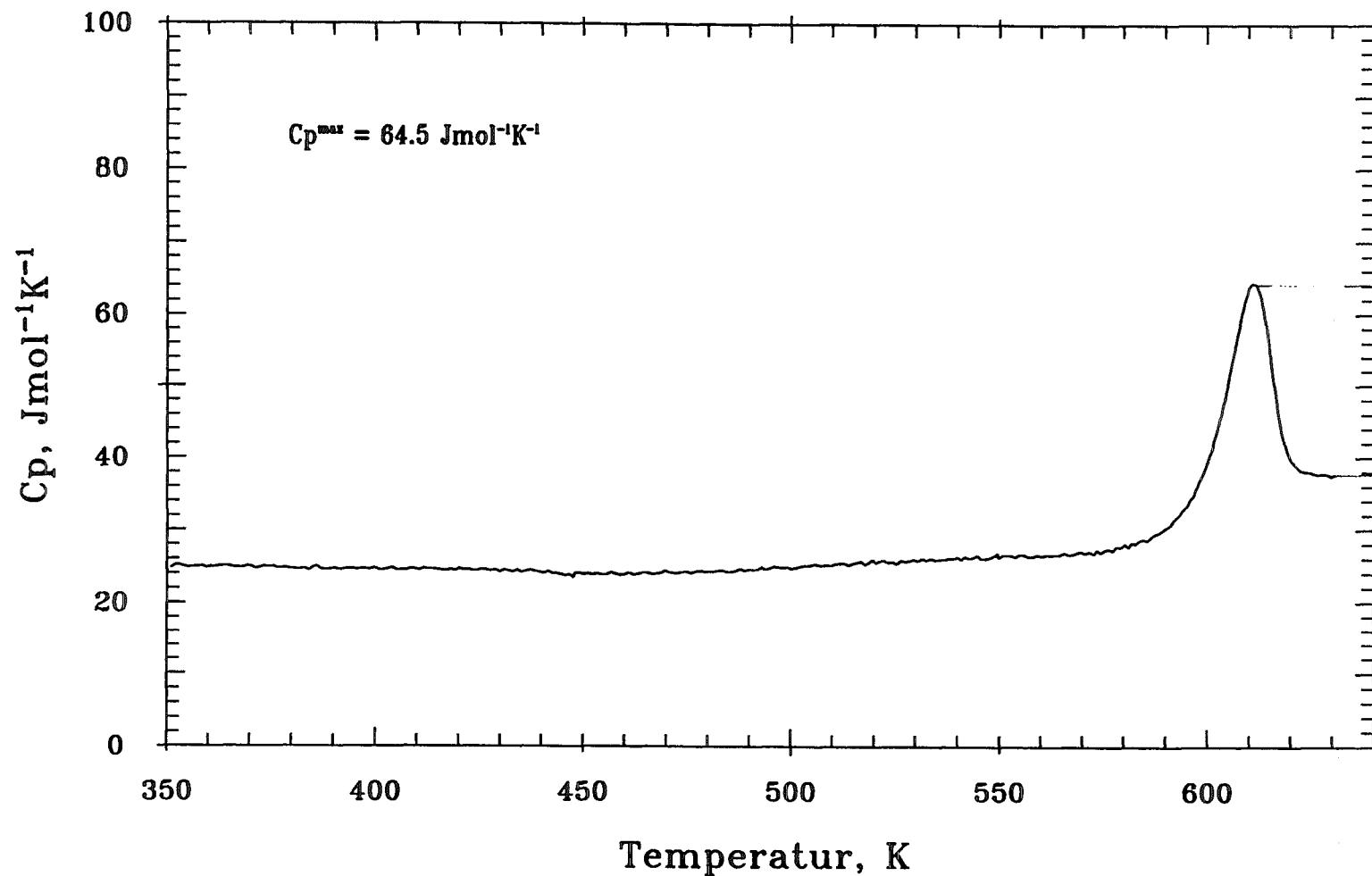
Cooling Rate = 40.00 K/min

Tmax = 640.0 K

Saphir Mass = 33.958 mg

Range = 10.0 mcal/s

p = 1020 bar



Pd40Ni40P20-SF2-SR40-ESP63-26.07

Mass = 21.283 mg

Heating Rate = 40.00 K/min

Tmin = 320.0 K

Molweight = 73.466 g/mol

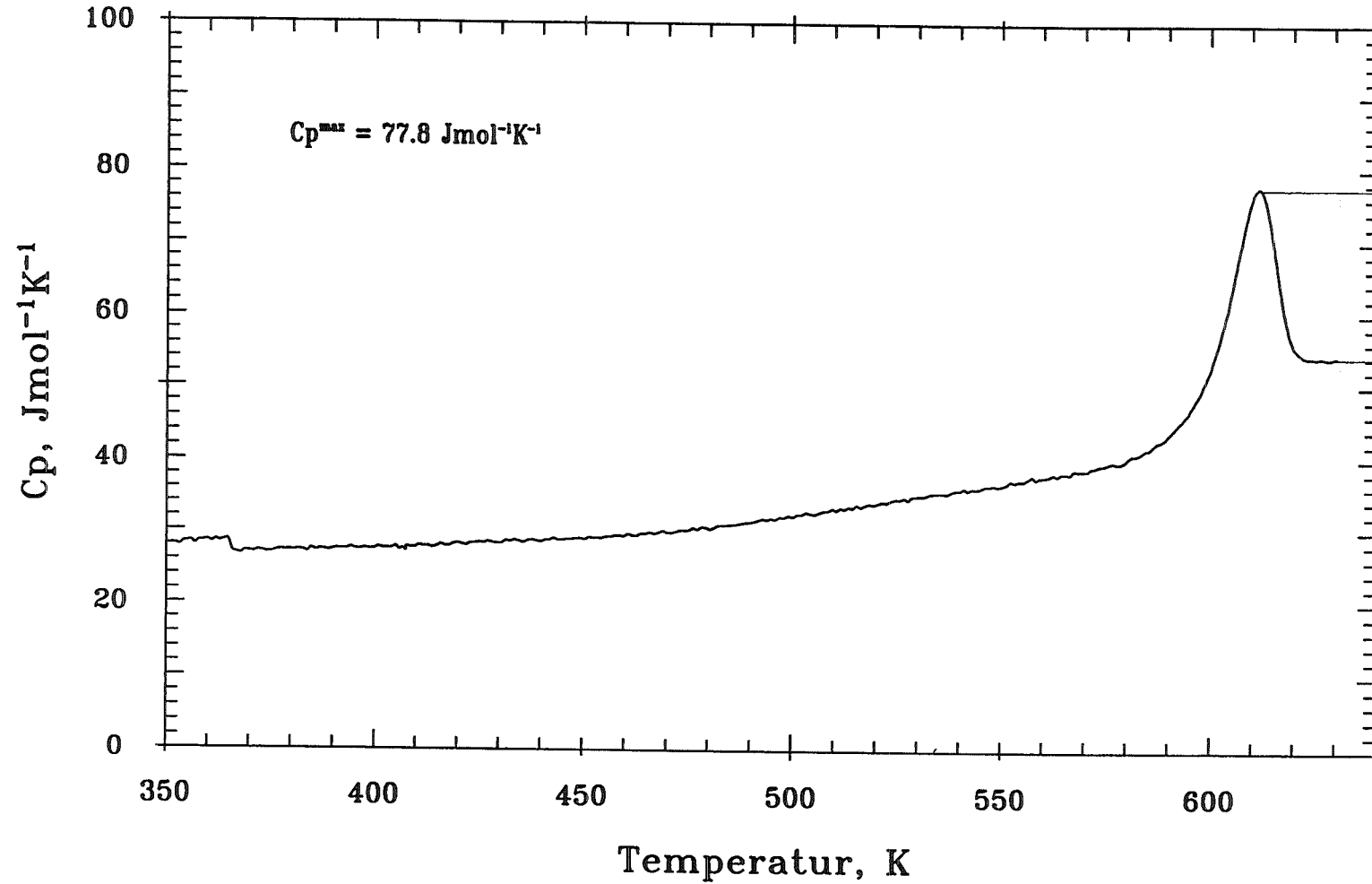
Cooling Rate = 40.00 K/min

Tmax = 640.0 K

Saphir Mass = 33.958 mg

Range = 10.0 mcal/s

p = 1020 bar



Pd40Ni40P20-SF2-SR40-ESP64-26.07

Mass = 24.018 mg

Heating Rate = 40.00 K/min

Tmin = 320.0 K

Molweight = 73.466 g/mol

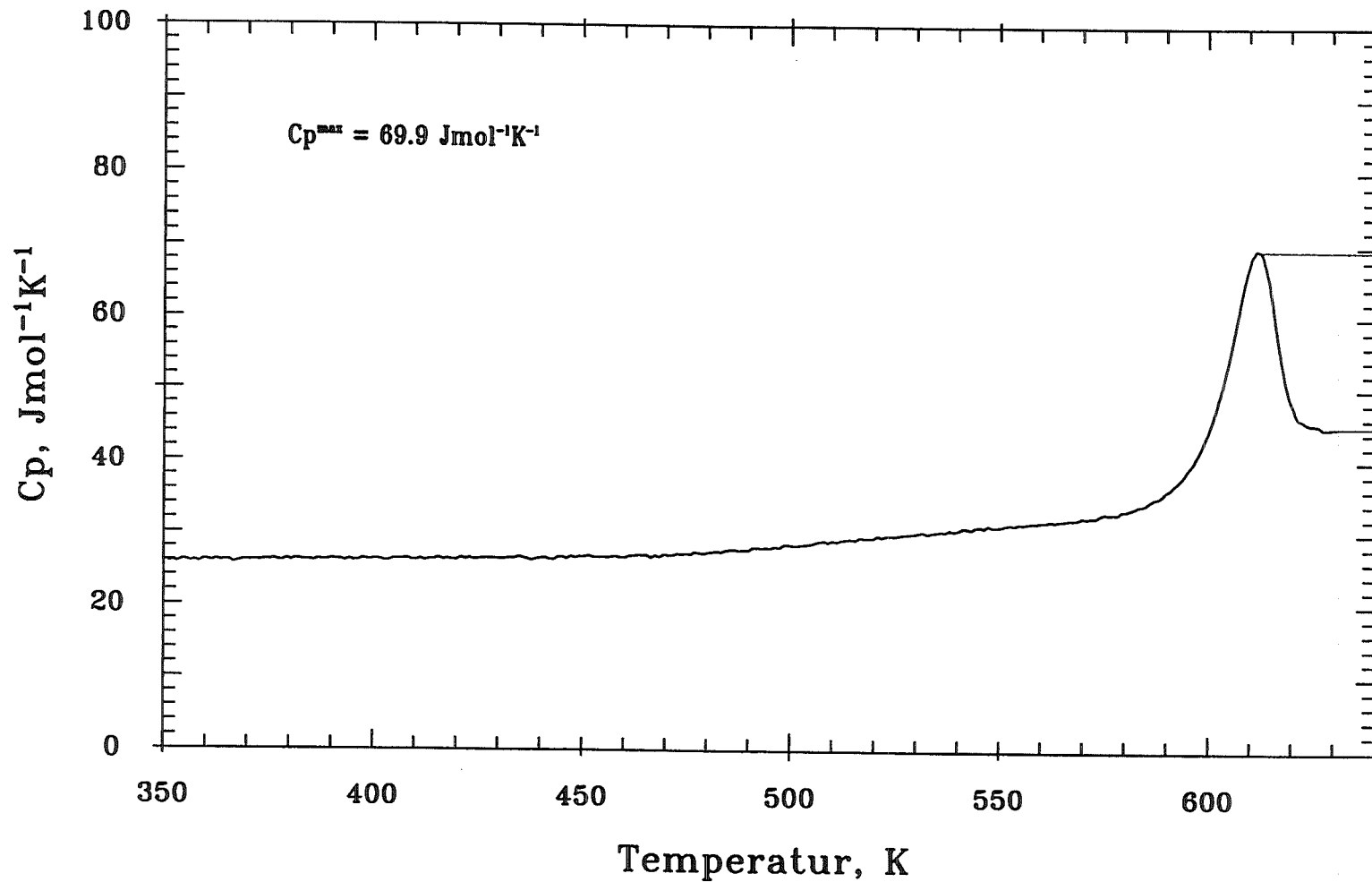
Cooling Rate = 40.00 K/min

Tmax = 640.0 K

Saphir Mass = 33.958 mg

Range = 10.0 mcal/s

p = 1020 bar



Pd40Ni40P20-SF2-SR40-ESP70-05.11

Mass = 22.071 mg

Molweight = 73.466 g/mol

Saphir Mass = 33.958 mg

Heating Rate = 40.00 K/min

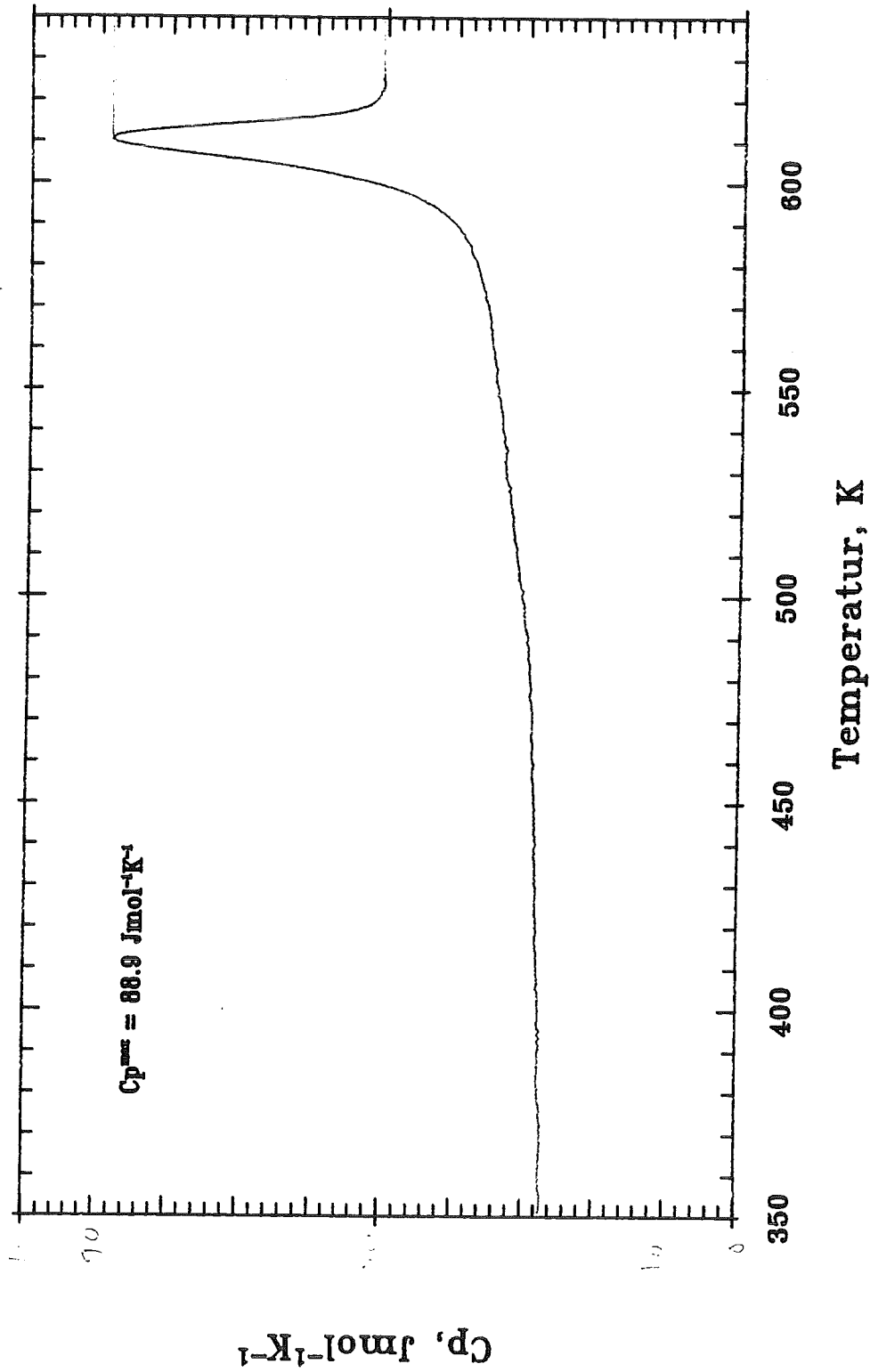
Cooling Rate = 40.00 K/min

Range = 10.0 mcal/s

Tmin = 320.0 K

Tmax = 640.0 K

p = 2100 bar



P440Ni40P20-SF2-SR40-ESP71-05.11

Mass = 21.895 mg

Molweight = 73.466 g/mol

Saphir Mass = 33.958 mg

Heating Rate = 40.00 K/min

Cooling Rate = 40.00 K/min

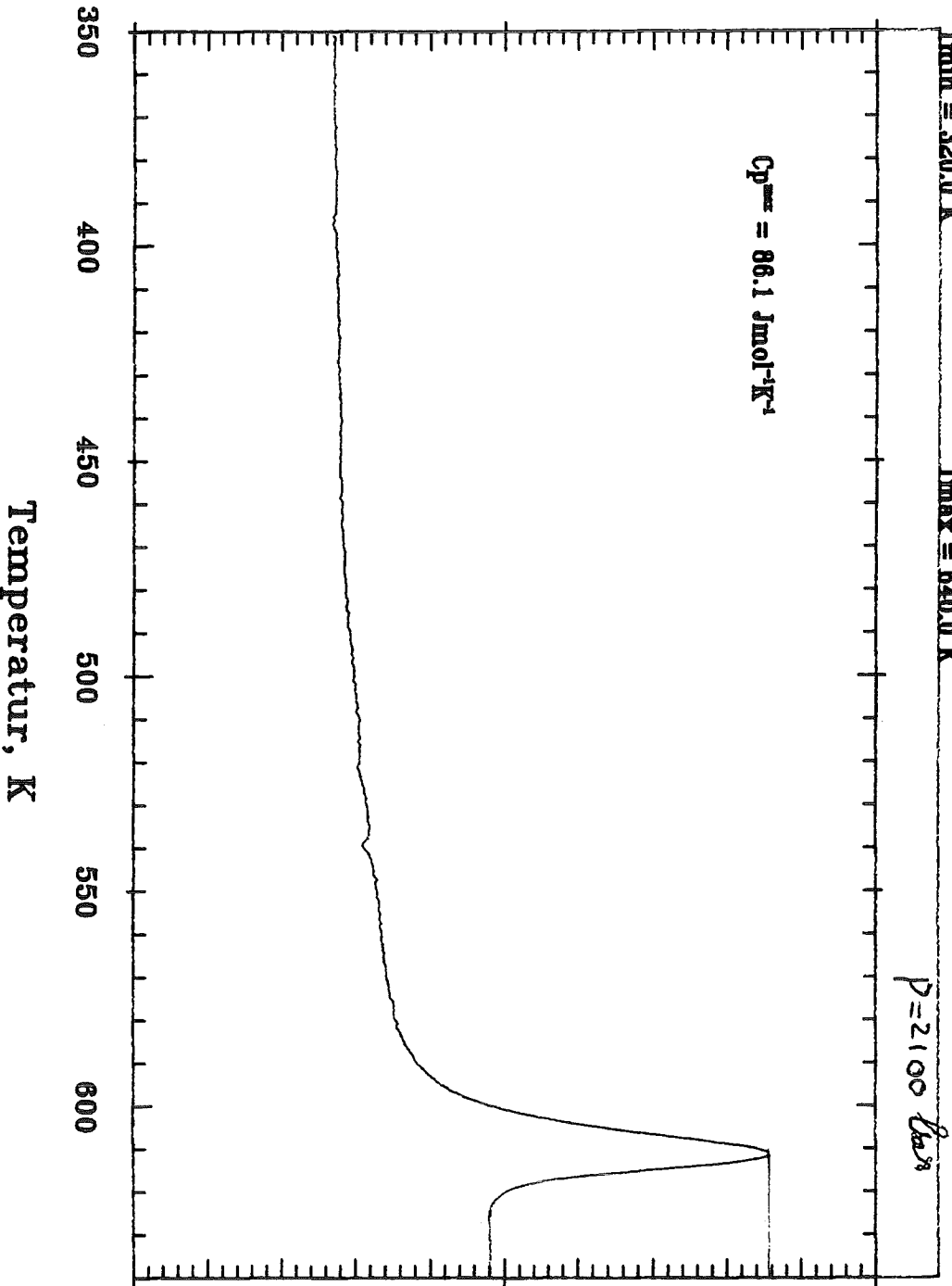
Range = 10.0 mcal/s

Tmin = 320.0 K

Tmax = 640.0 K

P = 2100 bar

Cp, Jmol⁻¹K⁻¹



Pd40Ni40P20-SF2-SR40-ESP72-06.11

Mass = 21.088 mg

Heating Rate = 40.00 K/min

Tmin = 320.0 K

Molweight = 73.486 g/mol

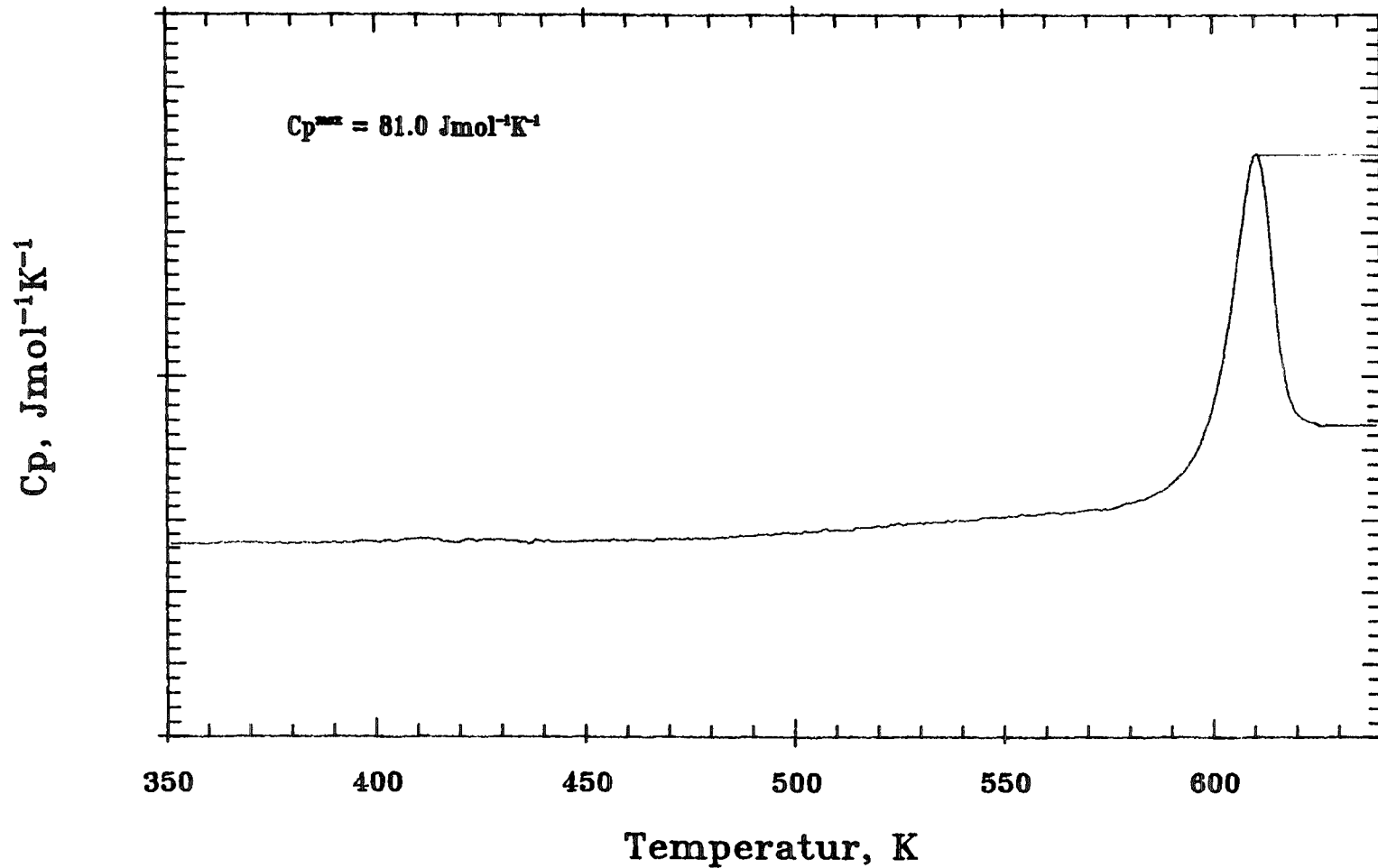
Cooling Rate = 40.00 K/min

Tmax = 640.0 K

Saphir Mass = 33.958 mg

Range = 10.0 mcal/s

p = 2100 bar



Pd40Ni40P20-SF2-SR40-ESP50-22.07

Mass = 19.206 mg

Heating Rate = 40.00 K/min

Tmin = 320.0 K

Molweight = 73.466 g/mol

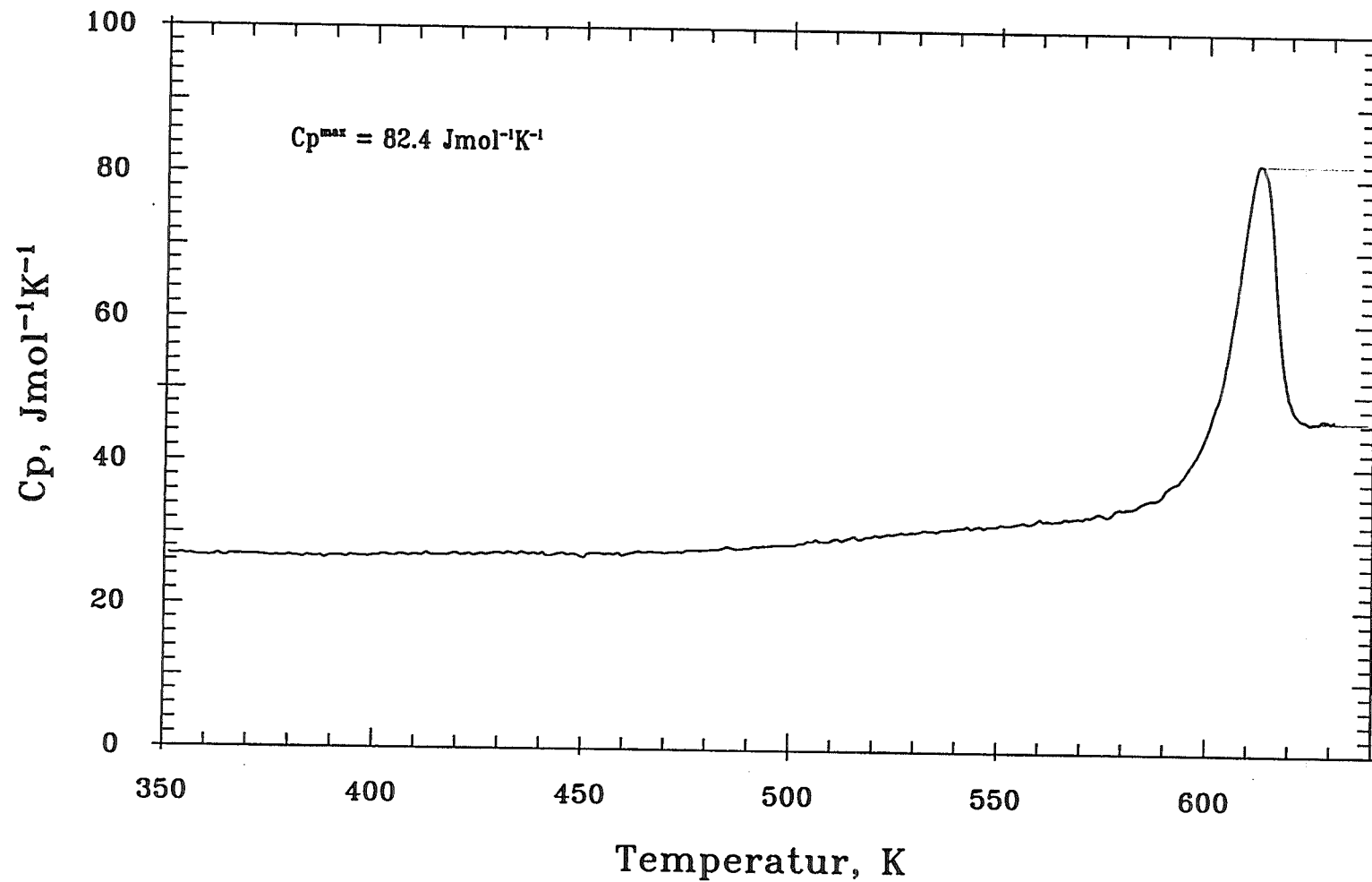
Cooling Rate = 40.00 K/min

Tmax = 640.0 K

Saphir Mass = 33.958 mg

Range = 10.0 mcal/s

p = 3200 bar



Pd40Ni40P20-SF2-SR40-ESP51-22.07

Mass = 20.472 mg

Heating Rate = 40.00 K/min

Tmin = 320.0 K

Molweight = 73.466 g/mol

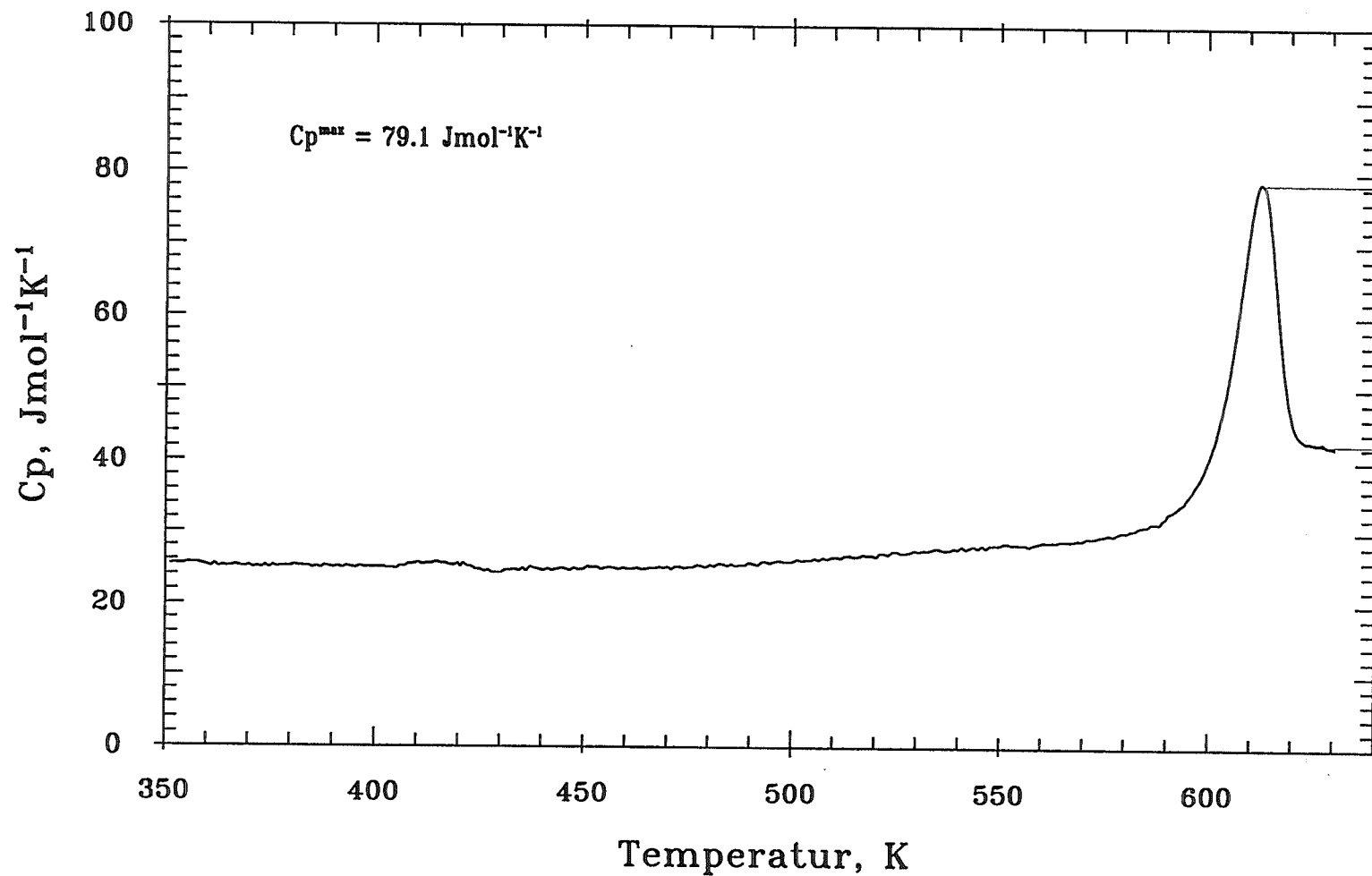
Cooling Rate = 40.00 K/min

Tmax = 640.0 K

Saphir Mass = 33.958 mg

Range = 10.0 mcal/s

$p = 32.00$ bar



Pd40Ni40P20-SF2-SR40-ESP52-23.07

Mass = 21.740 mg

Molweight = 73.466 g/mol

Saphir Mass = 33.958 mg

Heating Rate = 40.00 K/min

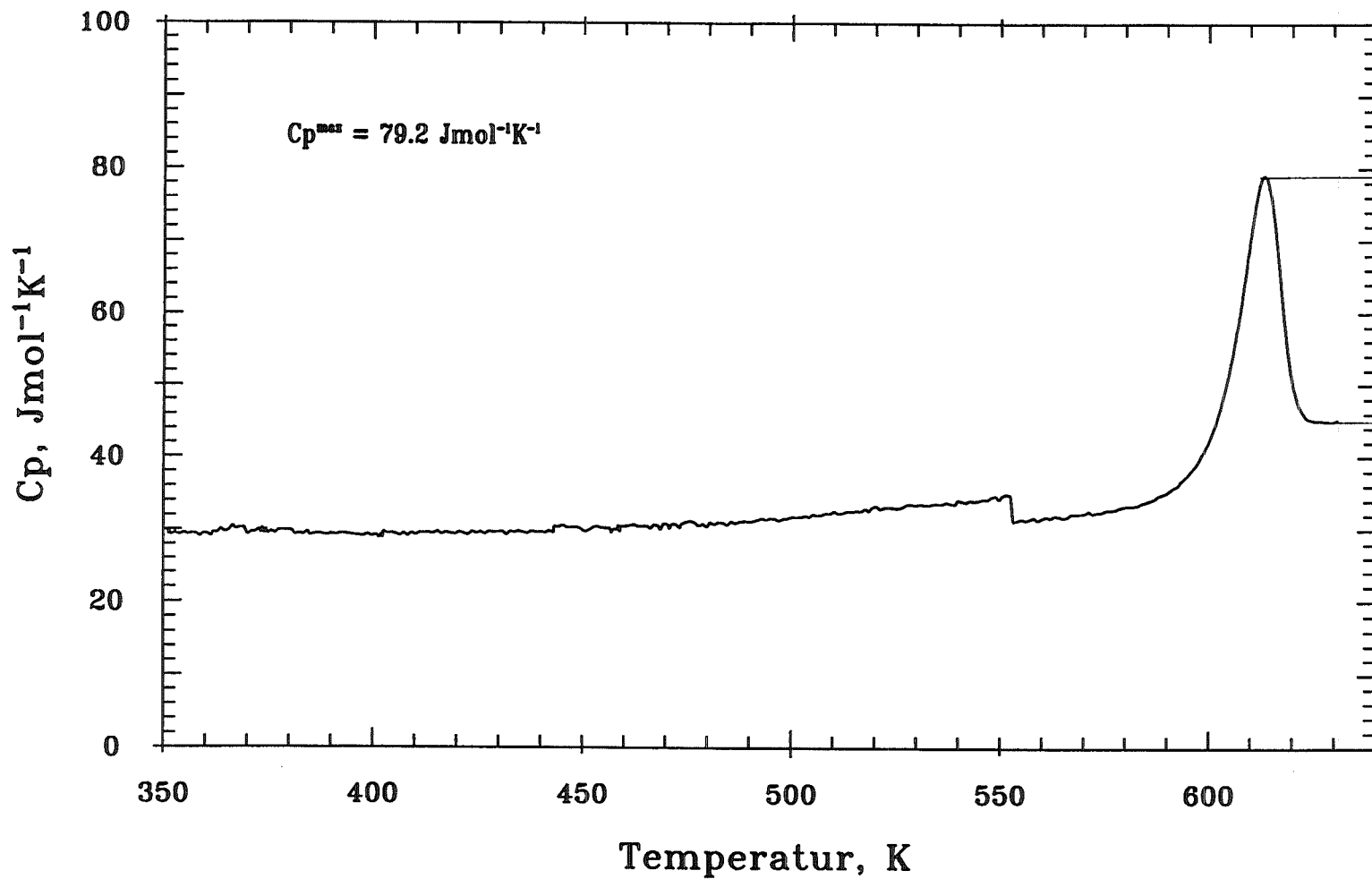
Cooling Rate = 40.00 K/min

Range = 10.0 mcal/s

Tmin = 320.0 K

Tmax = 640.0 K

p = 3200 bar



Pd40Ni40P20-SF2-SR40-ESP59-25.07

Mass = 21.040 mg

Molweight = 73.466 g/mol

Saphir Mass = 33.958 mg

Heating Rate = 40.00 K/min

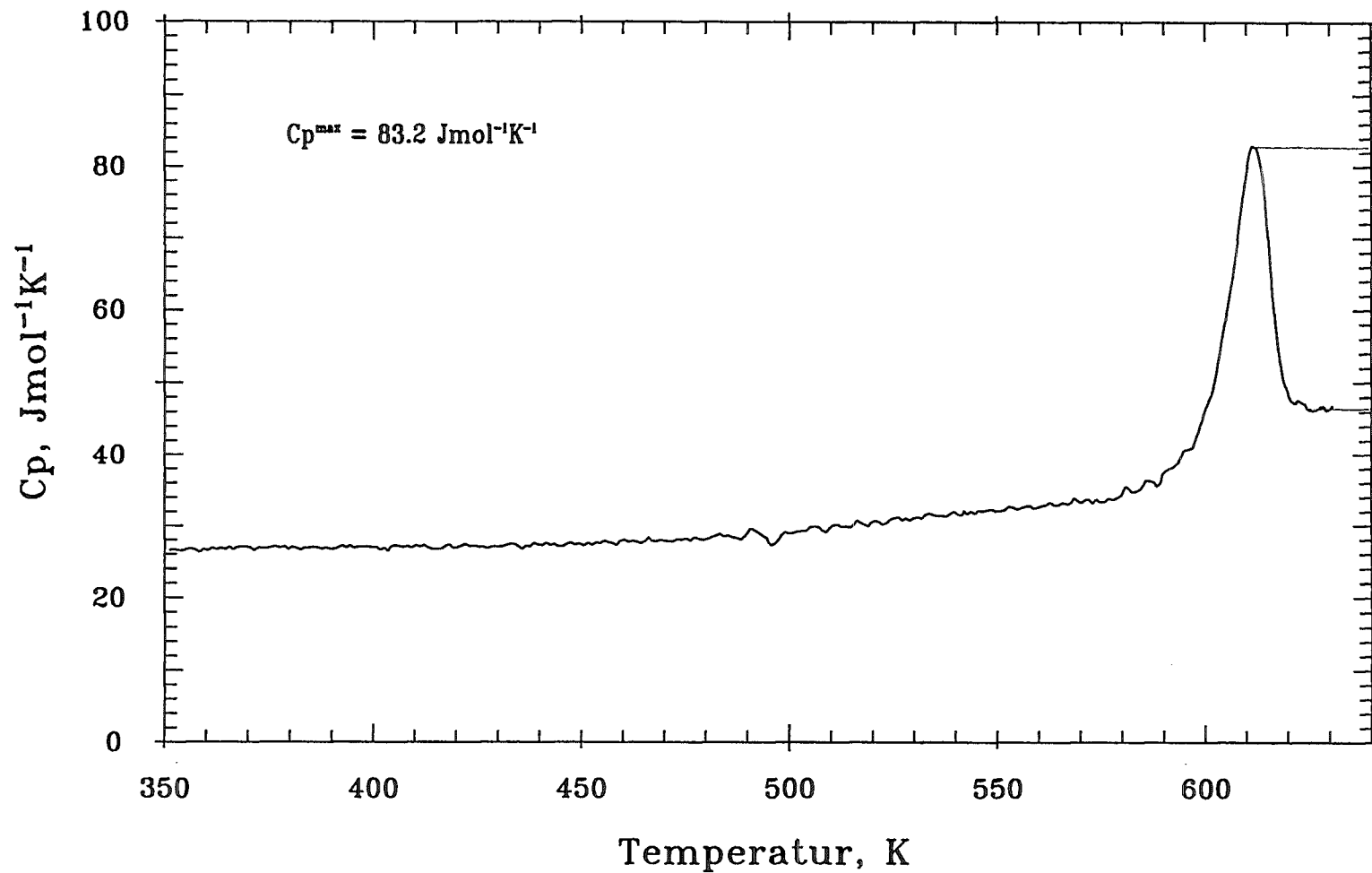
Cooling Rate = 40.00 K/min

Range = 10.0 mcal/s

Tmin = 320.0 K

Tmax = 640.0 K

$p = 5120 \text{ bar}$



Pd40Ni40P20-SF2-SR40-ESP60-25.07

Mass = 20.678 mg

Heating Rate = 40.00 K/min

Tmin = 320.0 K

Molweight = 73.466 g/mol

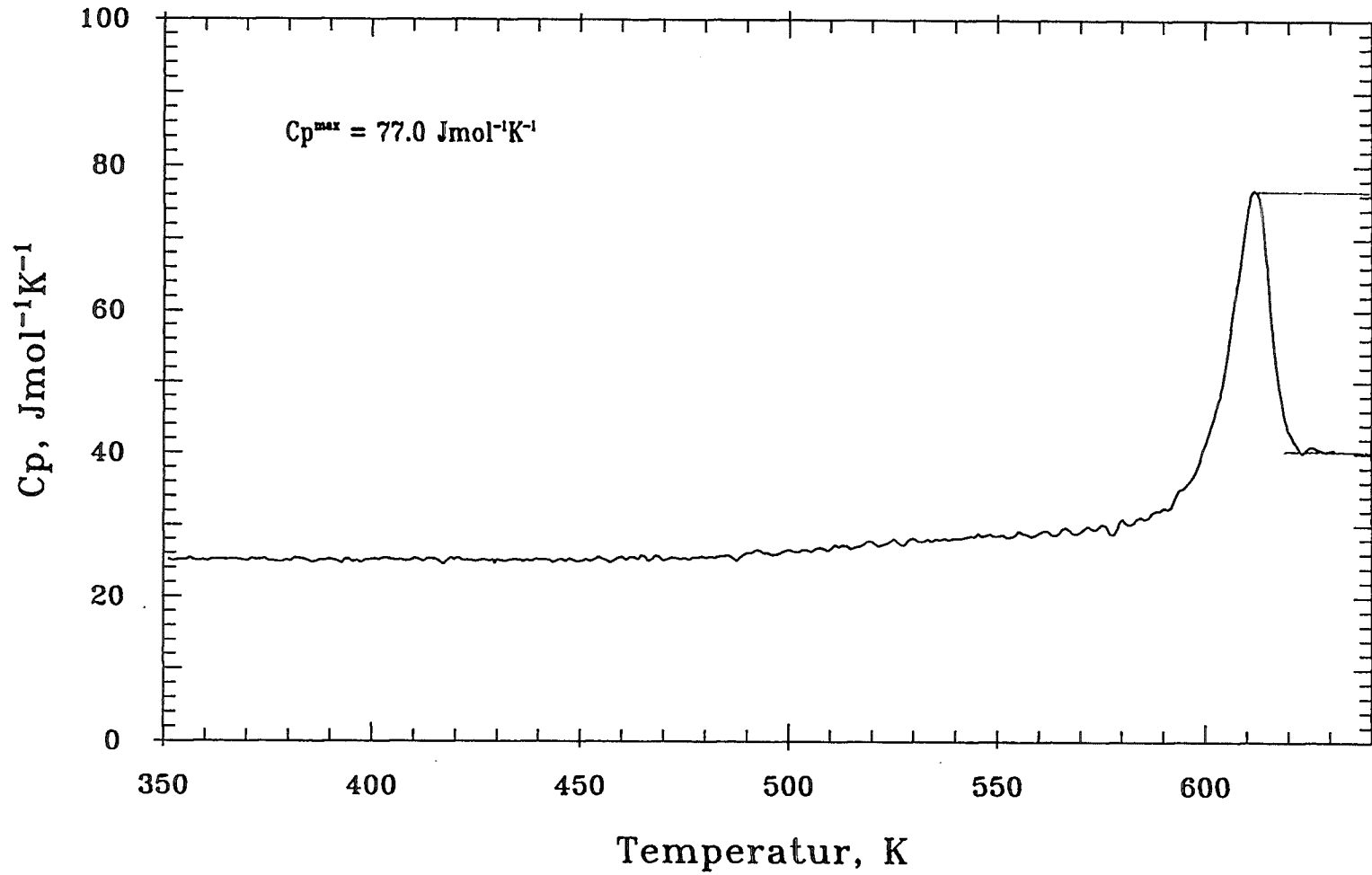
Cooling Rate = 40.00 K/min

Tmax = 640.0 K

Saphir Mass = 33.958 mg

Range = 10.0 mcal/s

p = 5120 bar



Pd40Ni40P20-SF2-SR40-ESP61-26.07

Mass = 17.466 mg

Heating Rate = 40.00 K/min

Tmin = 320.0 K

Molweight = 73.466 g/mol

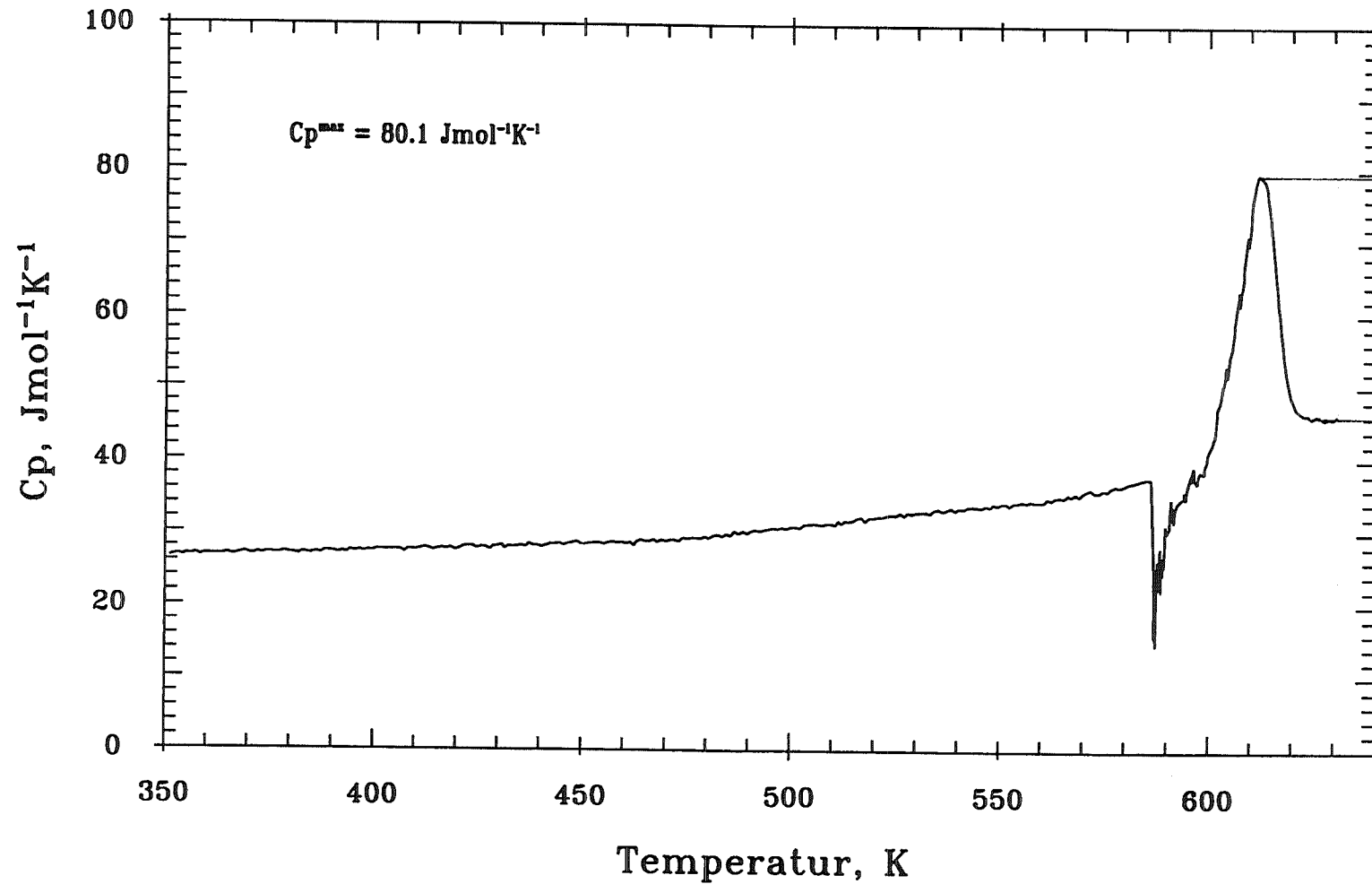
Cooling Rate = 40.00 K/min

Tmax = 640.0 K

Saphir Mass = 33.958 mg

Range = 10.0 mcal/s

$p = 5120 \text{ bar}$



Pd40Ni40P20-SF2-SR40-ESP56-23.07

Mass = 20.055 mg

Heating Rate = 40.00 K/min

Tmin = 320.0 K

Molweight = 73.466 g/mol

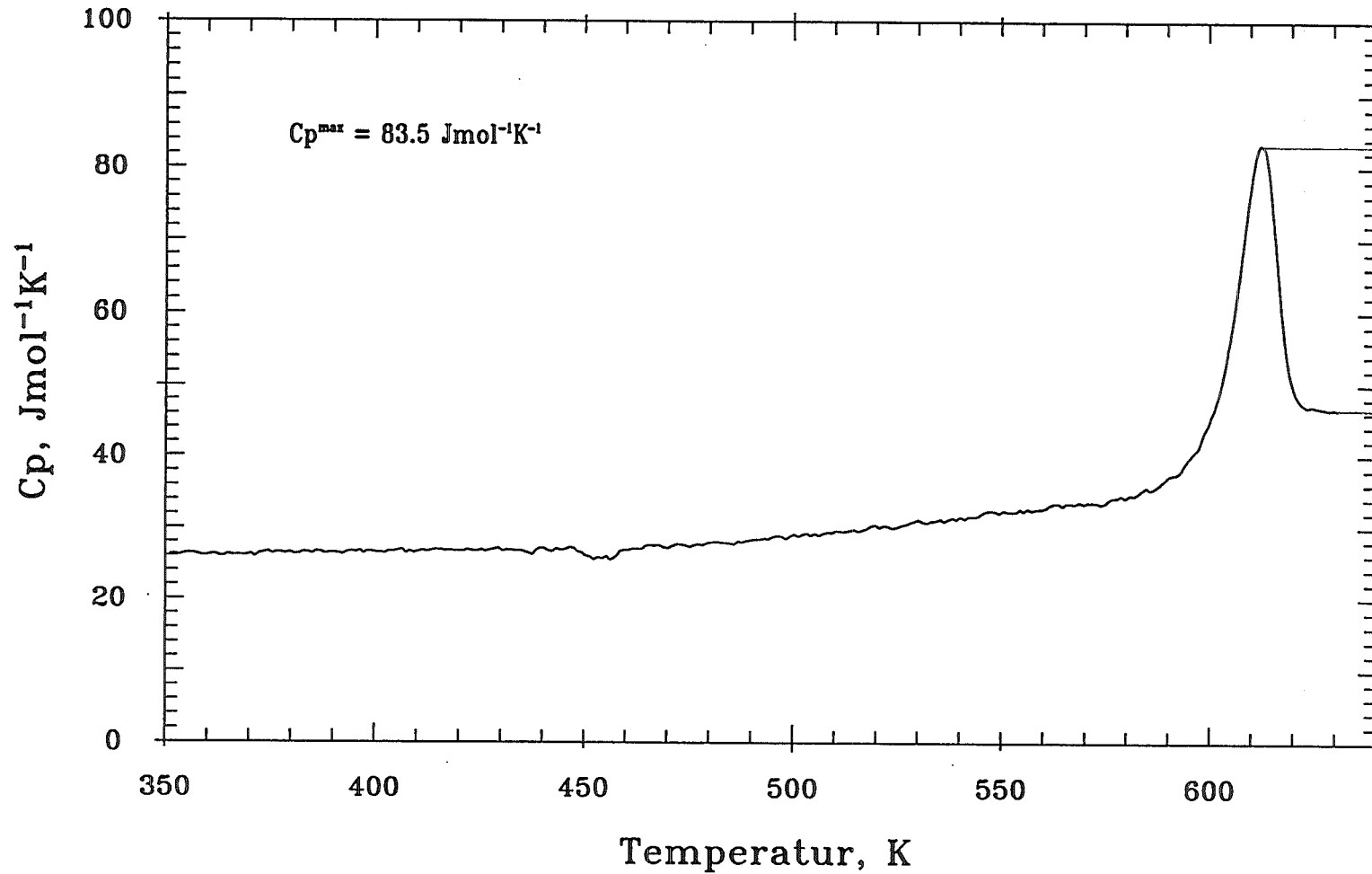
Cooling Rate = 40.00 K/min

Tmax = 640.0 K

Saphir Mass = 33.958 mg

Range = 10.0 mcal/s

$\rho = 7340$ bar



Pd40Ni40P20-SF2-SR40-ESP57-23.07

Mass = 21.167 mg

Molweight = 73.466 g/mol

Saphir Mass = 33.958 mg

Heating Rate = 40.00 K/min

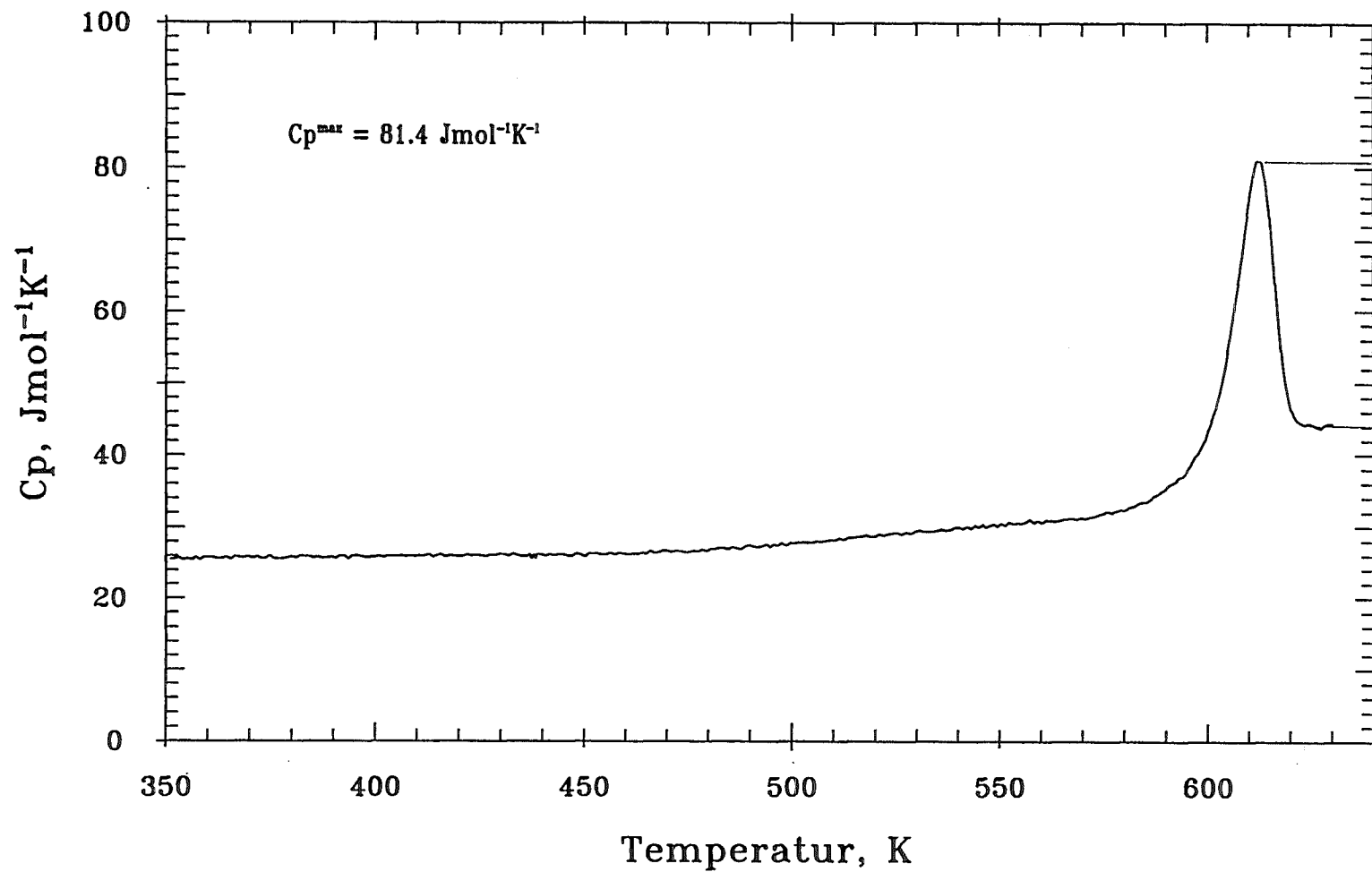
Cooling Rate = 40.00 K/min

Range = 10.0 mcal/s

Tmin = 320.0 K

Tmax = 640.0 K

$p = 7340$ bar



Pd40Ni40P20-SF2-SR40-ESP58-23.07

Mass = 18.846 mg

Heating Rate = 40.00 K/min

Tmin = 320.0 K

Molweight = 73.466 g/mol

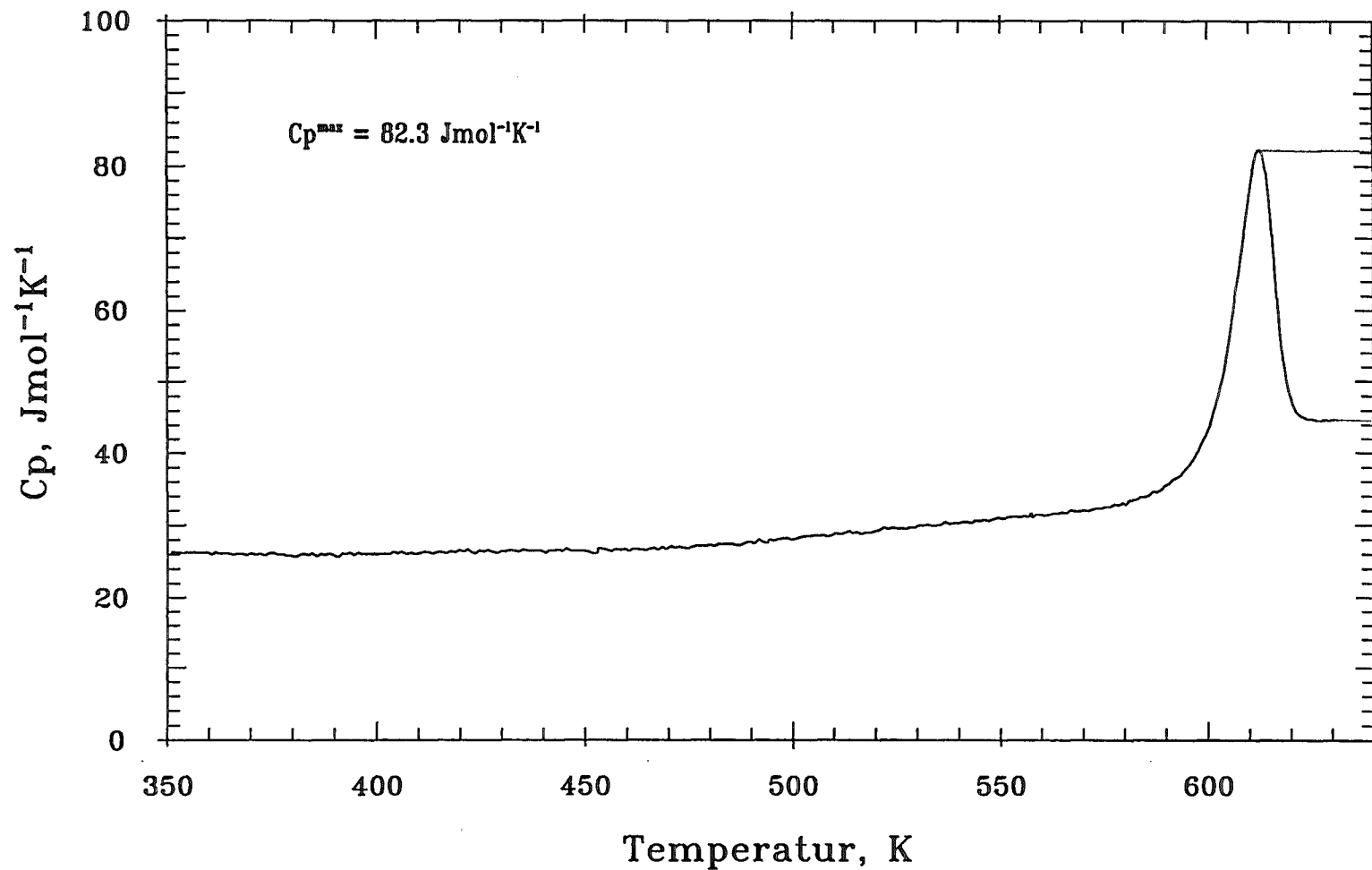
Cooling Rate = 40.00 K/min

Tmax = 640.0 K

Saphir Mass = 33.958 mg

Range = 10.0 mcal/s

p = 7340 bar



Pd40Ni40P20-SF2-SR40-ESP53-23.07

Mass = 22.522 mg

Heating Rate = 40.00 K/min

Tmin = 320.0 K

Molweight = 73.466 g/mol

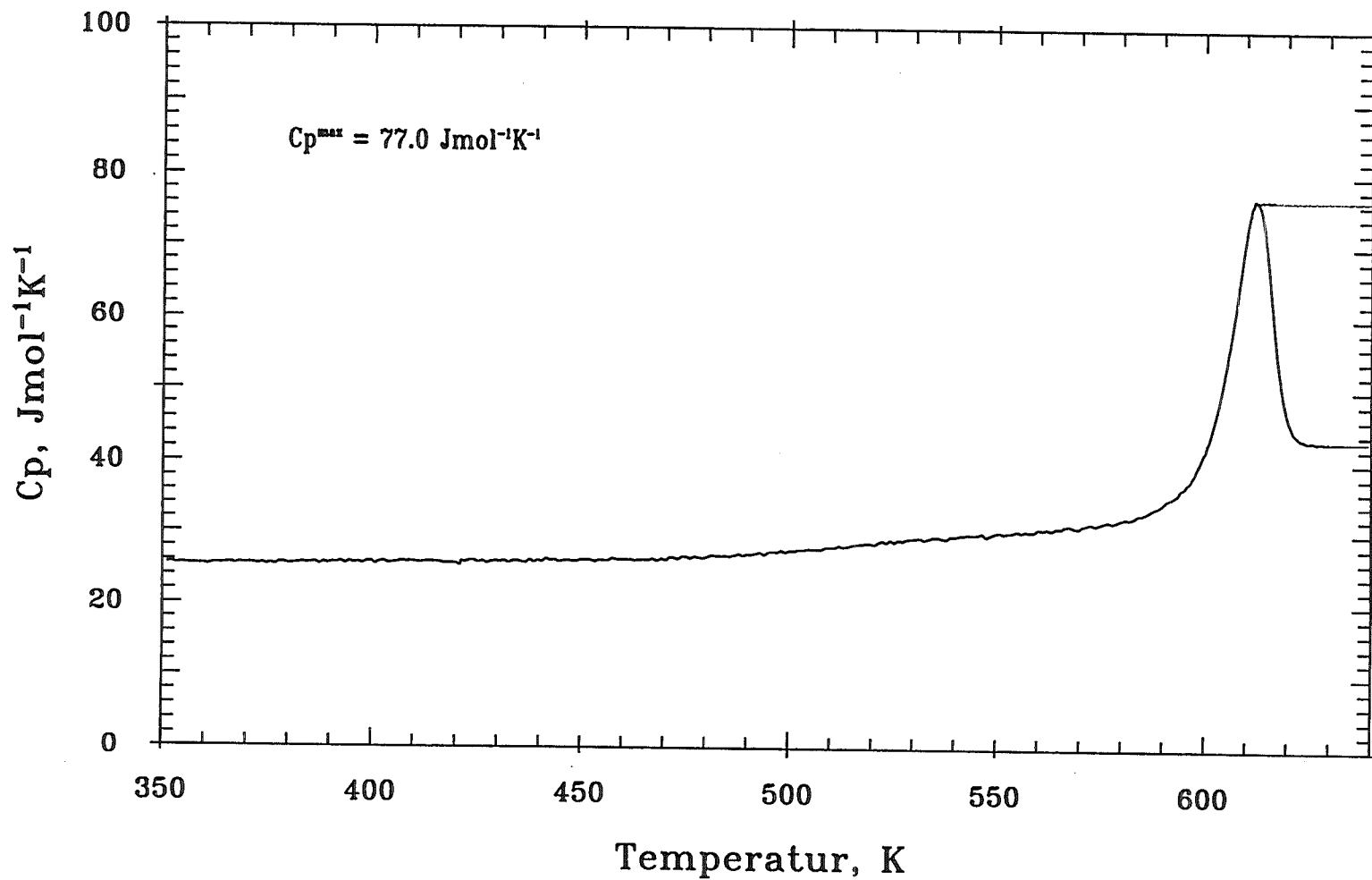
Cooling Rate = 40.00 K/min

Tmax = 640.0 K

Saphir Mass = 33.958 mg

Range = 10.0 mcal/s

$p = 8400 \text{ bar}$



Pd40Ni40P20-SF2-SR40-ESP54-23.07

Mass = 19.938 mg

Heating Rate = 40.00 K/min

Tmin = 320.0 K

Molweight = 73.466 g/mol

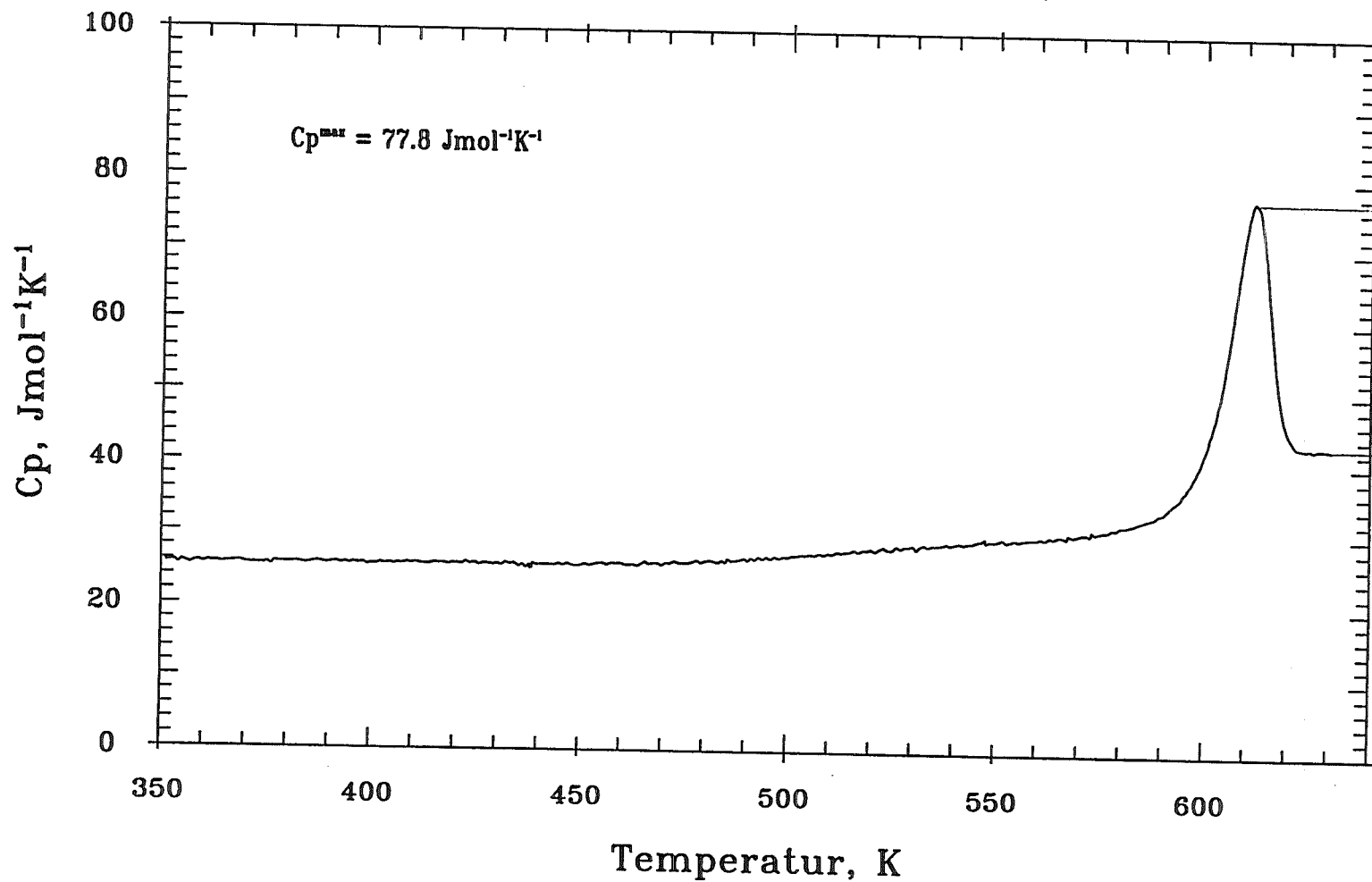
Cooling Rate = 40.00 K/min

Tmax = 640.0 K

Saphir Mass = 33.958 mg

Range = 10.0 mcal/s

p = 8400 bar



Pd40Ni40P20-SF2-SR40-ESP55-23.07

Mass = 20.097 mg

Heating Rate = 40.00 K/min

Tmin = 320.0 K

Molweight = 73.466 g/mol

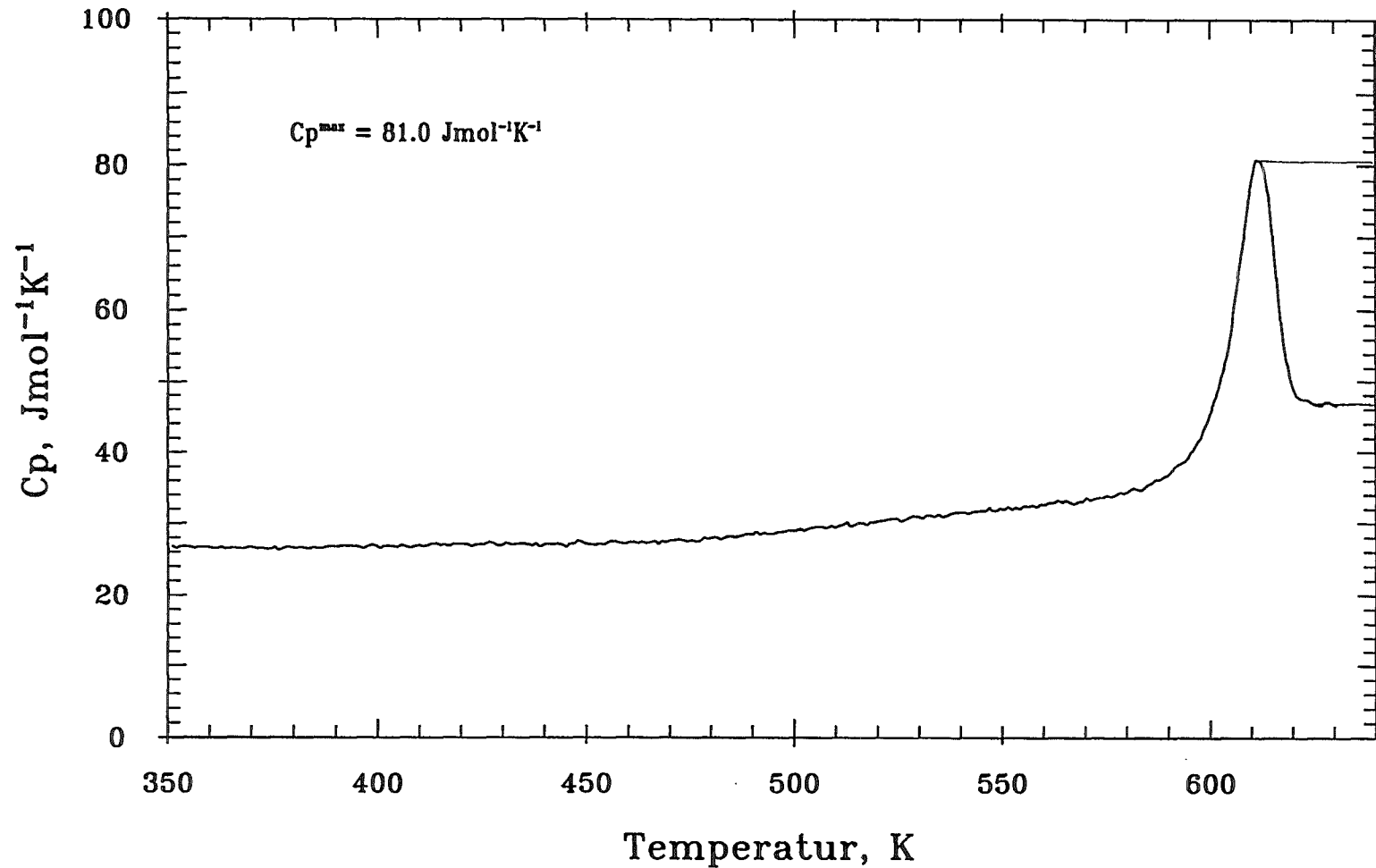
Cooling Rate = 40.00 K/min

Tmax = 640.0 K

Saphir Mass = 33.958 mg

Range = 10.0 mcal/s

p = 8400 bar



APPENDIX E

Estimating χ for Pd₄₀Ni₄₀P₂₀ at room temperature

In order to calculate the compressibility χ for Pd₄₀Ni₄₀P₂₀ at room temperature, we first calculate Young's modulus using the equation

$$E = \rho v_L^2 \quad (\text{E.1})$$

and the previous results $\rho = 9.4 \cdot 10^3 \text{ kg m}^{-3}$ and $v_L = (10.10 \pm 0.09) \text{ m}^2 \text{ s}^{-1}$ [8]. Assuming a 5% relative error in ρ results in $E = (9.5 \pm 0.5) \cdot 10^{10} \text{ Pa}$.

We now calculate the bulk modulus B_T using the equation

$$B_T = \frac{E}{3(1-2\nu)} \quad (\text{E.2})$$

where ν is Poisson's constant. Using $\nu = 0.41$ [33] and assuming a 5% error in ν , we have $B_T = (1.76 \pm 0.40) \cdot 10^{11} \text{ Pa}$, which is in good agreement with the result $B_T = 1.82 \cdot 10^{11} \text{ Pa}$, found for PdCuSi [34]. Finally, we use

$$\chi = B_T^{-1} \quad (\text{E.3})$$

to obtain $\chi = (5.7 \pm 1.3) \cdot 10^{-12} \text{ m}^2 \text{ N}^{-1}$ for Pd₄₀Ni₄₀P₂₀ at room temperature.

Estimating C_V for Pd₄₀Ni₄₀P₂₀ at room temperature

The specific heat at constant volume, C_V [$\text{Jmol}^{-1}\text{K}^{-1}$] is related to the specific heat at constant pressure, C_p [$\text{Jmol}^{-1}\text{K}^{-1}$] by the relation

$$C_p(T) = C_V(T)(1 + \gamma\alpha_V T) \quad (\text{E.4})$$

where α_V [K^{-1}] is the volume expansion coefficient and γ is the Grüneisen constant, for which we can write:

$$\gamma = \frac{\alpha_V V_m}{\chi C_V} \quad (\text{E.5})$$

where V_m [$\text{m}^3 \text{mol}^{-1}$] is the molar volume and χ [$\text{m}^2 \text{N}^{-1}$] the compressibility. From eqn.s (E.4) and (E.5) we can write for C_V at room temperature:

$$C_V(T_R) = C_p(T_R) - T_R \left(\frac{V_m \alpha_V^2}{\chi} \right)_{T_R} \quad (\text{E.6})$$

C_p was measured for Pd₄₀Ni₄₀P₂₀ by Zappel [30] over the temperature range 320 K-490 K and was found to be linearly dependent on temperature:

$$C_p(T) = A + BT \quad (\text{E.7})$$

with $A = (17.456 \pm 0.843) \text{ Jmol}^{-1}\text{K}^{-1}$ and $B = (19.810 \pm 0.854) \cdot 10^{-3} \text{ Jmol}^{-1}\text{K}^{-2}$.

If we assume eqn. (E.7) to be valid at room temperature, we get

$$C_p(293 \text{ K}) = (23.3 \pm 0.9) \text{ Jmol}^{-1}\text{K}^{-1}.$$

With eqn. (E.6) and the values for V_m , α_V and χ from table 4, we obtain

$$C_V(293 \text{ K}) = (22.5 \pm 0.9) \text{ Jmol}^{-1}\text{K}^{-1}.$$

The error will be an underestimation, since eqn. (E.7) at 293 K while it is found for the temperature range 320 K- 490 K. We therefore increase the error from 0.9 to 1.0 (which is rather arbitrary); hence, we have:

$$C_V(293 \text{ K}) = (22.5 \pm 1.0) \text{ Jmol}^{-1}\text{K}^{-1}.$$

APPENDIX F

Let us consider an amorphous structure of N atoms. The number of defects is then given by:

$$Nc_d = N \exp\left(-\frac{\varepsilon v^*}{\langle v_f \rangle}\right) \quad (\text{F.1})$$

To create one extra defect, we need to perform an amount of work against the pressure equal to $p\Delta V_F$, where ΔV_F is equal to the increase in volume on the formation of a defect. Hence, due to this process, the average free volume per atom in the sample increases by $\Delta V_F/N$. This gives:

$$Nc_d + 1 = N \exp\left(-\frac{\varepsilon v^*}{\langle v_f \rangle + \Delta V_F / N}\right) \quad (\text{F.2})$$

Dividing eqn. E.2 by eqn. E.1 gives:

$$\frac{Nc_d + 1}{Nc_d} = \exp\left(\varepsilon v^* \left\{ \frac{1}{\langle v_f \rangle} - \frac{1}{\langle v_f \rangle + \Delta V_F / N} \right\}\right) \quad (\text{F.3})$$

for which we can write:

$$1 + \frac{1}{Nc_d} = \exp\left(\frac{\varepsilon v^* \Delta V_F / N}{\langle v_f \rangle (\langle v_f \rangle + \Delta V_F / N)}\right) \approx 1 + \frac{\varepsilon v^* \Delta V_F / N}{\langle v_f \rangle (\langle v_f \rangle + \Delta V_F / N)} \quad (\text{F.4})$$

where the last step is justified, because $Nc_d \gg 1$, which means that the expression far left is close to zero; the argument of the exponent is then necessarily small. We have:

$$Nc_d = \frac{\langle v_f \rangle (\langle v_f \rangle + \Delta V_F / N)}{\varepsilon v^* \Delta V_F / N} \approx \frac{\langle v_f \rangle^2}{\varepsilon v^* \Delta V_F / N} \quad (\text{F.5})$$

where the last approximation is justified because $\langle v_f \rangle \gg \Delta V_F / N$. Hence, we have:

$$\varepsilon v^* \Delta V_F c_d = \langle v_f \rangle^2 \quad (\text{F.6})$$

which, using eqn.(E.1) and $\langle v_f \rangle = \varepsilon v^* x$, we get:

$$\varepsilon v^* \Delta V_F \exp\left(-\frac{1}{x}\right) = (\varepsilon v^* x)^2 \quad (\text{F.7})$$

or, in terms of v^* :

$$v^* = \frac{\exp(-1/x)}{\varepsilon x^2} \Delta V_F \quad (\text{F.8})$$

which should be independent of x . Since we have calculated our effective value of ΔV_F at $x = x_{eq}(0 \text{ Pa}, 563 \text{ K}) = 0.0629$, we should take this value to check the equation. We have:

$$v^* = 3 \cdot 10^{-5} \Delta V_F \quad (\text{F.9})$$

APPENDIX G

We shall here incorporate the boundary conditions

$$\begin{aligned} S_n &\geq z_x \\ S_n - z_c &< z_n < S_n / n \end{aligned} \quad (G.1)$$

into the expression

$$nd\mu e^{-\mu} \int dz_1 \int dz_2 \cdots \int dz_{n-1} \exp(-S_{n-1}) \quad (G.2)$$

which will give us the concentration distribution $c_n(z_c)$. For S_{n-1} , we have the restriction

$$\lambda - (\mu + d\mu) \leq S_{n-1} \leq (\lambda + d\lambda) - \mu. \quad (G.3)$$

The $d\mu$ term will only give rise to a second order term, so we drop it (we will come back to this later) and hence we have:

$$\lambda - \mu \leq S_{n-1} \leq \lambda - \mu + d\lambda. \quad (G.4)$$

Bearing this condition in mind, we substitute $S_{n-1} = \lambda - \mu$ in eqn. G.2 and get:

$$\begin{aligned} nd\mu e^{-\lambda} \int_{\mu}^{\infty} dz_1 \cdots \int_{\mu}^{\infty} dz_{n-1} \\ (\lambda - \mu \leq S_{n-1} \leq \lambda - \mu + d\lambda) \end{aligned} \quad (G.5)$$

where we have used that $z_1 \dots z_{n-1} < z_n$ and $\mu < z_n < \mu + d\mu$. We can split eqn. G.5 in two parts:

$$\begin{aligned} nd\mu e^{-\lambda} \left\{ \int_{\mu}^{\infty} dz_1 \cdots \int_{\mu}^{\infty} dz_{n-1} - \int_{\mu}^{\infty} dz_1 \cdots \int_{\mu}^{\infty} dz_{n-1} \right\} \\ (S_{n-1} \leq \lambda - \mu + d\lambda) \quad (S_{n-1} \leq \lambda - \mu) \end{aligned} \quad (G.6)$$

Let us concentrate on the second term between braces for a while:

$$\begin{aligned} \int_{\mu}^{\infty} dz_1 \cdots \int_{\mu}^{\infty} dz_{n-1} \\ (S_{n-1} \leq \lambda - \mu) \end{aligned} \quad (G.7)$$

and let us introduce the unit step function $\theta(t)$, defined as:

$$\begin{aligned} \theta(t) &= 0 \quad \text{for } t < 0 \\ &= 1 \quad \text{for } t \geq 0 \end{aligned} \quad (G.8)$$

with eqn. G.8, eqn. G.7 can be written as:

$$\int_{\mu}^{\infty} dz_1 \cdots \int_{\mu}^{\infty} dz_{n-1} \theta(\lambda - \mu - S_{n-1}). \quad (G.9)$$

To get rid of the lower integral boundary, we make the substitutions:

$$\begin{aligned} z_1' &= z_1 - \mu \\ &\vdots \\ z_{n-1}' &= z_{n-1} - \mu \\ S_{n-1}' &= \sum_{i=1}^{n-1} z_i' = S_{n-1} - (n-1)\mu \end{aligned} \quad (G.10)$$

with eqn. G.10, eqn. G.9 can be written as:

$$\int_0^{\infty} dz_1' \cdots \int_0^{\infty} dz_{n-1}' \theta(\lambda - n\mu - S_{n-1}')$$

This integral can be simplified dramatically. To show this, we make a small excursion.

We now calculate the integral

$$\int_0^{\infty} dz_1 \int_0^{\infty} dz_2 \int_0^{\infty} dz_3 \int_0^{\infty} dz_4 \theta(\beta - S_4)$$

bearing in mind the order of integration, we have:

$$S_1 = z_1 \quad \Rightarrow \quad dS_1 = dz_1$$

$$S_2 = z_1 + z_2 \quad \Rightarrow \quad dS_2 = dz_2$$

$$S_3 = z_1 + z_2 + z_3 \quad \Rightarrow \quad dS_3 = dz_3$$

$$S_4 = z_1 + z_2 + z_3 + z_4 \quad \Rightarrow \quad dS_4 = dz_4$$

and hence, we have:

$$\begin{aligned} \int_0^{\infty} dS_1 \int_{S_1}^{\infty} dS_2 \int_{S_2}^{\infty} dS_3 \int_{S_3}^{\infty} dS_4 \theta(\beta - S_4) &= \int_0^{\infty} dS_1 \int_{S_1}^{\infty} dS_2 \int_{S_2}^{\infty} dS_3 \int_{S_3}^{\beta} dS_4 \theta(\beta - S_3) \\ &= \int_0^{\infty} dS_1 \int_{S_1}^{\infty} dS_2 \int_{S_2}^{\infty} dS_3 (\beta - S_3) \theta(\beta - S_3) = \int_0^{\infty} dS_1 \int_{S_1}^{\infty} dS_2 \int_{S_2}^{\beta} dS_3 (\beta - S_3) \theta(\beta - S_2) \\ &= \int_0^{\infty} dS_1 \int_{S_1}^{\infty} dS_2 \left[-\frac{1}{2} (\beta - S_3)^2 \right]_{S_2}^{\beta} \theta(\beta - S_2) = \int_0^{\infty} dS_1 \int_{S_1}^{\infty} dS_2 \frac{1}{2} (\beta - S_2)^2 \theta(\beta - S_2) \\ &= \int_0^{\infty} dS_1 \int_{S_1}^{\beta} dS_2 \frac{1}{2} (\beta - S_2)^2 \theta(\beta - S_1) = \int_0^{\infty} dS_1 \left[-\frac{1}{6} (\beta - S_2)^3 \right]_{S_1}^{\beta} \theta(\beta - S_1) \\ &= \int_0^{\infty} dS_1 \frac{1}{6} (\beta - S_1)^3 \theta(\beta - S_1) = \int_0^{\infty} dS_1 \frac{1}{6} (\beta - S_1)^3 = \left[-\frac{1}{24} (\beta - S_1)^4 \right]_0^{\beta} = \frac{1}{24} \beta^4 = \frac{\beta^4}{4!} \end{aligned}$$

so in general, we have:

$$\int_0^{\infty} dz_1 \cdots \int_0^{\infty} dz_n \theta(\beta - S_n) = \frac{\beta^n}{n!}$$

and hence, we can write for eqn. G.11:

$$\int_0^{\infty} dz_1 \cdots \int_0^{\infty} dz_{n-1} \theta(\lambda - n\mu - S_{n-1}) = \frac{(\lambda - n\mu)^{n-1}}{(n-1)!} \quad (G.11)$$

with which we can write for eqn. G.6:

$$n d\mu e^{-\lambda} \left\{ \frac{(\lambda + d\lambda - n\mu)^{n-1}}{(n-1)!} - \frac{(\lambda - n\mu)^{n-1}}{(n-1)!} \right\} \quad (G.12)$$

which is, in first order, equal to:

$$\begin{aligned} n d\mu e^{-\lambda} \left\{ \frac{1}{(n-1)!} (n-1) (\lambda - n\mu)^{n-2} d\lambda \right\} \\ = \frac{n}{(n-2)!} e^{-\lambda} (\lambda - n\mu)^{n-2} d\lambda d\mu \end{aligned} \quad (G.13)$$

Here, we see that if we would have kept the term $d\mu$ in eqn. G.4, all the way through to eqn.(E.14), it not have changed the first order approach of eqn. G.15.

Finally, we have arrived at a point where we can comfortably incorporate the boundary conditions G.1 and G.2. Doing so, we have:

$$\begin{aligned}
c_n(z_c) &= \int_{z_c}^{\infty} d\lambda \int_{\lambda-z_c}^{\lambda/n} d\mu \frac{n}{(n-2)!} e^{-\lambda} (\lambda - n\mu)^{n-2} \theta\left(\frac{\lambda}{n} - (\lambda - z_c)\right) \\
&= \int_{z_c}^{\infty} d\lambda \int_{\lambda-z_c}^{\lambda/n} d\mu \frac{n}{(n-2)!} e^{-\lambda} (\lambda - n\mu)^{n-2} \theta\left(\frac{n}{n-1} z_c - \lambda\right) \\
&= \int_{z_c}^{\frac{n}{n-1} z_c} d\lambda e^{-\lambda} \int_{\lambda-z_c}^{\lambda/n} d\mu \frac{n}{(n-2)!} (\lambda - n\mu)^{n-2}
\end{aligned} \tag{G.14}$$

Substituting $u = \lambda - n\mu$, we can write:

$$\begin{aligned}
c_n(z_c) &= \frac{n}{(n-2)!} \int_{z_c}^{\frac{n}{n-1} z_c} d\lambda e^{-\lambda} \left\{ \frac{1}{n} \int_0^{nz_c - (n-1)\lambda} du u^{n-2} \right\} \\
&= \frac{1}{(n-2)!} \int_{z_c}^{\frac{n}{n-1} z_c} d\lambda e^{-\lambda} \frac{1}{n-1} (nz_c - (n-1)\lambda)^{n-1}
\end{aligned} \tag{G.15}$$

Finally, we make the substitution $v = nz_c - (n-1)\lambda$, with which we have:

$$c_n(z_c) = \frac{1}{(n-1)(n-1)!} \exp\left(-\frac{n}{n-1} z_c\right) \int_0^{z_c} dv \exp\left(\frac{v}{n-1}\right) v^{n-1} \tag{G.16}$$

which is the expression we were looking for.

APPENDIX H

We shall here analytically solve the integral

$$I = \int_0^{z_c} dv \exp\left(\frac{v}{n-1}\right) v^{n-1} \quad (\text{H.1})$$

Taking the 1st partial derivative of I gives us:

$$I = \left[(n-1) \exp\left(\frac{v}{n-1}\right) v^{n-1} \right]_0^{z_c} - \int_0^{z_c} dv (n-1) \exp\left(\frac{v}{n-1}\right) (n-1) v^{n-2} \quad (\text{H.2})$$

Taking the 2nd partial derivative of I gives us for the integral within I :

$$\left[-(n-1)^2 \exp\left(\frac{v}{n-1}\right) (n-1) v^{n-2} \right]_0^{z_c} + \int_0^{z_c} dv (n-1)^2 \exp\left(\frac{v}{n-1}\right) (n-1)(n-2) v^{n-3} \quad (\text{H.3})$$

the $(n-2)^{\text{th}}$ partial derivative of I adds:

$$\left[(-1)^{n-3} (n-1)^{n-2} \exp\left(\frac{v}{n-1}\right) (n-1)(n-2) \cdots (3) v^2 \right]_0^{z_c} + (-1)^{n-2} \int_0^{z_c} dv (n-1)^{n-2} \exp\left(\frac{v}{n-1}\right) (n-1) \cdots (3)(2) \quad (\text{H.4})$$

the $(n-1)^{\text{th}}$ partial derivative of I adds:

$$\left[(-1)^{n-2} (n-1)^{n-1} \exp\left(\frac{v}{n-1}\right) (n-1)(n-2) \cdots (2) v \right]_0^{z_c} + (-1)^{n-1} \int_0^{z_c} dv (n-1)^{n-1} \exp\left(\frac{v}{n-1}\right) (n-1) \cdots (2)(1) \quad (\text{H.5})$$

and finally, the n^{th} partial derivative of I adds:

$$\left[(-1)^{n-1} (n-1)^n \exp\left(\frac{v}{n-1}\right) (n-1) \cdots (2)(1) \right]_0^{z_c} \quad (\text{H.6})$$

Putting all this together, we have for I :

$$\begin{aligned} I &= \left[\exp\left(\frac{v}{n-1}\right) \left\{ (n-1) v^{n-1} - (n-1)^2 (n-1) v^{n-2} + \cdots + (-1)^{n-2} (n-1)^{n-1} (n-1) \cdots (2) v + (-1)^{n-1} (n-1)^n (n-1) \cdots (2)(1) \right\} \right]_0^{z_c} \\ &= \exp\left(\frac{z_c}{n-1}\right) \left\{ (n-1) z_c^{n-1} - (n-1)^2 (n-1) z_c^{n-2} + \cdots + (-1)^{n-2} (n-1)^{n-1} (n-1) \cdots (2) z_c + (-1)^{n-1} (n-1)^n (n-1) \cdots (2)(1) \right\} \\ &\quad + (-1)^n (n-1)^n (n-1) \cdots (2)(1) \\ &= (n-1)^n (n-1)! \exp\left(\frac{z_c}{n-1}\right) (-1)^n \left\{ \exp\left(-\frac{z_c}{n-1}\right) - \left[1 - \left(\frac{z_c}{n-1}\right) + \cdots + \frac{1}{(n-1)!} (-1)^{n-1} \left(\frac{z_c}{n-1}\right)^{n-1} \right] \right\} \\ &= (n-1)^n (n-1)! \exp\left(\frac{z_c}{n-1}\right) (-1)^n \left\{ \exp\left(-\frac{z_c}{n-1}\right) - \sum_{i=0}^{n-1} \frac{1}{i!} \left(-\frac{z_c}{n-1}\right)^i \right\} \quad (\text{H.7}) \end{aligned}$$

For the defect concentration distribution, we had, in integral form:

$$c_n(z_c) = \frac{1}{(n-1)(n-1)!} \exp\left(-\frac{n}{n-1} z_c\right) \int_0^{z_c} dv \exp\left(\frac{v}{n-1}\right) v^{n-1} \quad (\text{H.8})$$

and after evaluating the integral, we have:

$$c_n(z_c) = (n-1)^{n-1} e^{-z_c} (-1)^n \left\{ \exp\left(-\frac{z_c}{n-1}\right) - \sum_{i=0}^{n-1} \frac{1}{i!} \left(-\frac{z_c}{n-1}\right)^i \right\} \quad (\text{H.9})$$

which is the expression we were looking for.